TU Delft

LUMC Leiden University Medical Center

Erasmus MC Universitair Medisch Centrum Rotterdam

POSITIONING OF CRANIOFACIAL PATIENT-SPECIFIC IMPLANTS & SURGICAL GUIDES

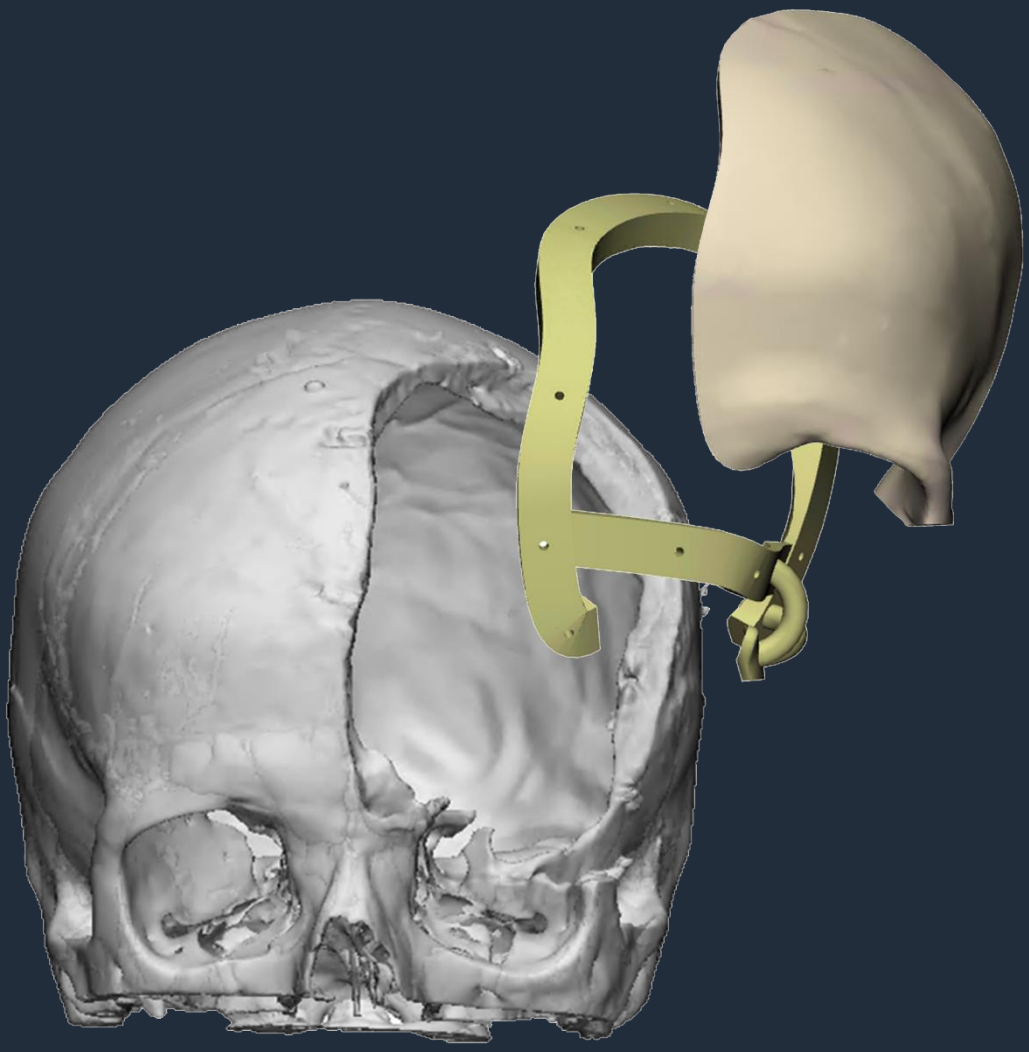

L. NAGTEGAAL

MASTER THESIS TECHNICAL MEDICINE
IMAGING & INTERVENTION
NOVEMBER 2020 - JUNI 2021

Evaluation of the positioning of virtually planned polyetheretherketone patient-specific implants and surgical guides in craniofacial surgery

Thesis in partial fulfilment of the requirements for the joint degree of Master of Science in

Technical Medicine

Delft University of Technology, Leiden University Medical Centre, Erasmus University Medical Centre Rotterdam

Larissa Nagtegaal

Department of Maxillofacial Surgery, Leiden University Medical Center
November 2020 – July 2021

Supervisors
Dr. S.E.C. Pichardo
Dr. R.P.J. van den Ende

Assessment committee members

Chairman	Prof.dr.ir. J. Harlaar[1]
Medical supervisor	Dr. S.E.C. Pichardo[2]
Technical supervisor	Dr. R.P.J. van den Ende[2]

[1]TU Delft, Delft, the Netherlands
[2]Department of Maxillofacial Surgery, Leiden University Medical Center, Leiden, the Netherlands

i. Preface

Eight years ago, I graduated from the Stedelijk Dalton Lyceum in Dordrecht. At that time I could not have guessed where I would be now. Not uncommonly for me, I did not know what I wanted to do then. I liked languages, math but also art and there were a lot of things I did not like either. My love for nature, culture and travelling made me decide to take a gap year which has proven to be the exact right move. When I returned, the Bachelor Clinical Technology was being introduced for the first time. I was interested in the human body and I liked the fact that I would be developing technical skills simultaneously. Not one moment have I regretted this choice.

In the master of Technical Medicine, where I followed the track Imaging & Intervention, courses became more practical. During the clinical internships in year 2 I could imagine myself working as a technical physician in the hospital more and more.

Over the years I developed specific interest in image-guided interventions and patient-specific treatments. During my clinical internship at the department of Maxillofacial surgery in the LUMC, I got introduced with patient-specific implants for craniofacial reconstructions. The interesting technical research and clinical aspects of this internship motivated me to start my graduation project here.

It has been a strange year with COVID-19 changing up the 'normal' of a lot of things. I have spent a great time at home instead of at the hospital. Nevertheless, like everyone, I made the most of it and I have very much enjoyed the days I did spend at the hospital. I am proud of the research I have performed and I am convinced the results will contribute to better patient care eventually.

I want to thank Sarina for really including me in the clinic, inviting me to attend the craniofacial surgeries, for always being open for questions and for her enthusiasm for technical innovations. Many surgeons can learn from this.

Roy, I want to thank you for supervising me on a daily basis, for including me in the planning processes, for sharing two licences of Materialise with me and two others and for the fun conversations we had during the limited times we were both physically present at the department.

Lastly, I want to thank my family and friends and specifically my roommates who were always there (because we were in lockdown).

Larissa Nagtegaal

Delft, June 2021

ii. Summary

Craniofacial reconstructions are performed in case of tumour resection, bone graft removal or trauma. Conventionally, these reconstructions were performed with autologous bone or allografts, but technological innovations have introduced the use of patient-specific implants (PSIs). These patient-specific implants can be designed to the exact shape and size of the defect, decreasing operative time spent on contouring and intraoperative implant modifications. When the reconstruction is preceded by a resection, a surgical guide can additionally be designed.

First, a literature study was conducted to summarize the quantitative outcomes of PSI positioning and the use of surgical guides in craniofacial surgery. Quantitative analysis has only been performed in a small amount of studies, concerning (angular) deviation between postoperative PSI position and planned PSI position, bone-to-implant gap and overlap of the postoperative PSI position with the planned PSI position. Quantitative analysis on the realised osteotomies using surgical guides has not been reported.

Following this, we developed a method to quantitatively evaluate the positioning of craniofacial patient-specific implants and the realised osteotomies and we applied this method to the available patient data from the Maxillofacial department in the LUMC. In conclusion, cranial implants were positioned in good agreement with the planned position, while orbital implants had a higher translational and rotational deviation. Osteotomies were on average created larger than planned. PSI positioning accuracy can be increased by improving the use and positioning of surgical guides and introducing surgical navigation.

iii. Table of contents

iv. List of abbreviations

3D	Three-dimensional
CAD	Computer-assisted/aided design
CAM	Computer-assisted/aided manufacturing
(CB)CT	(Cone-beam) Computed Tomography
CM	Centre of Mass
EBM	Electron Beam Melting
FDM	Fused Deposition Modelling
HA	Hydroxyapatite
ICP	Iterative Closest Point
JPOF	Juvenile Psammomatoid Ossifying Fibroma
LUMC	Leiden University Medical Center
MRI	Magnetic Resonance Imaging
OZC	Orbitozygomatic Complex
PEEK	Polyetheretherketone
PMMA	Polymethylmethacrylate
Post-op	Post-operative
Pre-op	Pre-operative
PSI	Patient-specific Implant
ROI	Region of Interest
SD	Standard Deviation
SDA	Surface Distance Analysis
SLA	Stereolithography
SLM	Selective Laser Melting
SLS	Selective Laser Sintering
STL	Standard Tessellation Language
TBI	Traumatic Brain Injury
XML	Extensible Markup Language

1. General introduction

1.1 Clinical context

Bony craniofacial defects that require reconstructive surgery are usually a result of tumour resection, bone graft removal or trauma. Two main sites for reconstruction include the cranial bones and the orbital bone. Cranioplasty is performed to restore the protection of the underlying brain, whereas reconstruction of the orbital bone aims at retaining symmetrical globe positioning. Besides these functional goals, the other main goal of reconstruction is to improve and recover aesthetics.

Conventionally, craniofacial reconstructions were performed with autologous bone or allografts. Over the years surgeons have started to use alloplastic materials as an alternative. Common alloplastic materials are polymethylmethacrylate (PMMA, a polymer) that is moulded into the defect intraoperatively and titanium mesh that is used for orbital reconstructions.

The last years however, technological innovations have introduced preoperative planning, intraoperative navigation and manufacturing of patient-specific implants (PSIs). These patient-specific implants can be designed to the exact shape and size of the defect, using preoperative imaging. As a result, a decrease in operative time spent on contouring and intraoperative implant modifications is reported in literature [10,15]. Besides PSIs, a surgical guide can be designed to enable a one-stage surgical procedure for resection and reconstruction.

The LUMC has been designing and implanting PSIs with the use of surgical guides for approximately two years now. These PSIs are fabricated from a polymer called polyetheretherketone (PEEK). In literature, the positioning of these PSIs has been assessed by using clinical outcome measures and subjective measures for aesthetics.

However, in order to validate, optimize and improve preoperative planning and placement of PSIs, objective evaluation of the positioning is necessary. Additionally, PSI positioning can be influenced by the positioning and use of a surgical guide whenever the reconstruction is preceded by a resection.

Quantitative analysis on the positioning of PSIs in craniofacial surgeries has only been reported in a small amount of studies, concerning (angular) deviation between the postoperative PSI position and the planned PSI position, bone-to-implant gap and overlap of the postoperative PSI position with the planned PSI position [2, 7, 11-13, 16-18, 23, 26, 27]. Quantitative analysis on the realised resection outlines with the use of surgical guides in craniofacial surgery has not been reported.

1.2 Research purposes

No standard for the assessment of the postoperative PSI position currently exists and objective methods to evaluate the resection outlines created with the use of surgical guides in craniofacial surgery have not been described in literature.

Therefore, the goal of my thesis was to develop a method to evaluate the positioning of craniofacial patient-specific implants and the realised osteotomies and to apply this method to the available patient data. This aim can be translated into two research questions:

1) What are the differences between the realised PSI positions and the planned PSI positions?
2) What are the differences between the realised osteotomies and the planned osteotomies?

Because the design of craniofacial implants depends on the reconstruction site, we were additionally interested in the difference between cranial implants and orbital implants. Whereas cranial implants always attach to adjacent bone edges on the cranium, created by resection or by trauma, orbital

implants contain a segment that extents into the orbit. When it regards a resection, this part is resected manually. Therefore, the following sub question was covered:

a) Is there a difference in deviation from the preoperative PSI position between cranial implants and orbital implants?

The second sub question that we covered was:

b) How does a difference between the realised osteotomy and planned osteotomy influence the positioning of the PSI?

1.3 Thesis outline

The current chapter contains the clinical context of my thesis, the research purposes and the thesis outline. Chapter 2 contains the literature review *Quantitative evaluation of patient-specific implant positioning in craniofacial reconstructive surgery: a literature review*. This review systematically summarizes the literature on objective measures used for the evaluation of craniofacial PSIs and the use of surgical guides for the creation of the osteotomies. Chapter 3 provides background information about subjects that will be discussed in this thesis. In chapter 4, the performed research is reported. Finally, chapter 5 concludes this thesis.

2. Quantitative evaluation of patient-specific implant positioning in craniofacial reconstructive surgery: a literature review

Abstract

Introduction: Bony craniofacial defects require both functional and aesthetic reconstruction. These reconstructions can nowadays be performed using virtually planned patient-specific implants (PSIs), sometimes also making use of a surgical guide in case of a one-stage resection and reconstruction. Most studies report clinical outcomes and subjective measures for aesthetics, while not many evaluate the PSI position quantitatively. Therefore, the objective of this review was to summarize the literature on the quantitative outcomes of PSI positioning and the use of surgical guides in craniofacial surgery.
Methods: A search strategy was performed in the MEDLINE (PubMed) database on 1 December 2020 and was updated on 4 January 2021. Articles were screened on title and abstract and included if they quantitatively compared the postoperative position with the virtually planned position of craniofacial PSIs. Outcomes were systematically summarized and presented.
Results: 11 articles were included, evaluating different craniofacial reconstructions. Five studies calculated the (angular) deviation between postoperative PSI position and planned PSI position, 4 studies calculated the bone-to-implant gap and 3 studies calculated the overlap of the postoperative PSI position with the planned PSI position. All measurements were performed differently. 3 studies made use of a surgical guide, creating adequate osteotomies.
Discussion: Currently, no standard for the assessment of postoperative PSI position exists. In general, a high accuracy of PSI positioning was found in studies using surgical guides and/or surgical navigation, accurately reproducing planned osteotomies and providing intraoperative feedback on PSI positioning. Improving the use of surgical guides could possibly improve postoperative PSI position.

2.1 Introduction

Bony craniofacial defects that require reconstructive surgery can be a result of trauma, tumor resection, infection and congenital anomalies [1, 2]. These defects may result in functional damage and aesthetic deformities and may cause psychological implications [3]. Different sites for reconstructions include the frontal bone, parietal bone, occipital bone, and temporal bone (cranioplasty) and the sphenoidal, orbital and the zygomatic bone [1]. Cranioplasty is performed to restore the protection of the underlying brain and to improve aesthetics [4-8]. Reconstruction of the orbital bone focusses on improving aesthetics as well, but functionally aims at retaining symmetrical globe positioning by restoring the shape and original volume of the orbit in order to avoid enophthalmos (posterior displacement of the eyeball) or diplopia (double vision), caused by muscle entrapment [1, 9-14].

Conventionally, craniofacial reconstructions were done by bone grafting where autologous bone was shaped to fit the defect [12, 15]. Autologous bone is biocompatible, has optimal mechanical properties, is a good substrate for bone ingrowth and revascularization and gives no immunological response [4, 6, 14, 15]. However, this method also causes donor-site morbidity, gives an increased infection risk and when the defects are large or complex, donor-site options may lack [14, 15]. Another option was reconstruction with a bone allograft, having as an advantage no donor-site morbidity, but as a disadvantage the risk of disease transmission [4, 8].
Over the years, surgeons have started to use alloplastic materials as an alternative. An example is intraoperative molding of polymethylmethacrylate (PMMA), which has become one of the most popular materials for cranial reconstruction [16]. For orbital reconstructions, a material that is often used nowadays is titanium mesh. Stock titanium meshes are available, but since the human orbital anatomy is not identical, these meshes require preoperative or intraoperative bending [9, 17, 18].

All aforementioned methods can be difficult and time-consuming, increasing operative time [11]. Especially defects in the cranio-orbital region can be complex, because of their different curvatures and thicknesses [4, 11].

The last years, technological innovations have introduced preoperative planning, intraoperative navigation and manufacturing of patient specific implants (PSIs) [8, 15]. These virtually planned PSIs made of alloplastic materials can be designed to the exact shape and size of the defect, starting with mirroring the contralateral side, followed by manual corrections. The use of PSIs decreases operative time spent on contouring and intraoperative implant modifications and avoids donor-site morbidity [10, 15]. In addition, a surgical guide, or resection template, may be designed to enable a one-stage surgical procedure for resection and reconstruction with a PSI [19].

There are multiple alloplastic materials that are commonly used to manufacture these PSIs, all with their own advantages and disadvantages. Examples are titanium, a metal, hydroxyapatite, a ceramic, and PMMA and polyetheretherketone (PEEK), both polymers. Titanium is biocompatible with a low infection rate. However, it has no protective energy-absorbing properties, it leads to artefacts on postoperative CT images and it is expensive [6, 14]. Hydroxyapatite allows for excellent bone ingrowth, but is very brittle and has a low tensile strength [6, 8]. PMMA has good biocompatibility, strong resistance to functional stress, it is lightweight, radiolucent and low-cost and it can be handled easily. However, there is a risk of fragmentation and lack of incorporation [6, 8, 16]. PEEK is expensive compared to PMMA, but it has several advantages. The elastic modulus and the mechanical strength, or energy absorbing properties, are almost similar to cortical bone [4, 6, 8, 12, 15]. It has excellent biocompatibility, it is radiolucent and non-magnetic so allows for postoperative CT and MRI scans, it is resistant to sterilization procedures by heat or ionizing radiation and it does not release cytotoxic substances [6, 12, 15].

Apart from the multiplicity of PSI materials, there are is also a variety of PSI fabrication techniques. PMMA for example, can be molded pre- or intraoperatively on a patient-specific 3D-printed model or it can be fabricated using additive manufacturing. Titanium and PEEK can be directly fabricated using milling techniques or additive manufacturing. Examples of additive manufacturing are fused deposition modelling (FDM), where a polymer is melted, extruded and deposited layer by layer; laser sintering techniques including selective laser sintering (SLS), selective laser melting (SLM) and electron beam melting (EBM), where a powder is deposited and melted layer after layer; and stereolithography (SLA), where a photo-sensitive liquid resin is solidified using light, every layer [21, 22].

So far, studies have reported multiple outcomes of craniofacial reconstructions with the use of PSIs. These usually include clinical outcomes and subjective measures for aesthetics. However, in order to improve preoperative planning and placement of PSIs, quantitative evaluation of the positioning of PSIs is another important outcome to consider. Besides that, PSI positioning can also be influenced by the positioning and use of a surgical guide whenever the reconstruction is preceded by a resection.
Not many studies have studied these objective outcome measures and there is no clear overview of the studies that have. Therefore, the aim of this review was to summarize the literature on the quantitative outcomes of the positioning of PSIs and the use of surgical guides in craniofacial surgery.

2.2 Methods

a) Search strategy

The search strategy was conducted in the MEDLINE (PubMed) database on 1 December 2020 and was updated on 4 January 2021. Various derivatives or synonyms of the following key terms were inserted: cranial, craniofacial, spheno-orbital, reconstruction, implant, patient-specific, 3D, computer-assisted. The complete search strategy is presented in Appendix A.

b) Inclusion/exclusion criteria

Articles were included if they compared the postoperative position of a craniofacial PSI with its virtually planned position in a quantitative way. Studies regarding the maxilla, mandibula, palatum, nasal bone or chin were excluded, as well as pediatric studies, cadaver or animal studies and studies only describing qualitative outcomes. Only English-written articles, published from 2010 until the end of 2020, were included.

c) Study selection

The resulting articles after conducting the search strategy were screened on title and abstract, based on the predetermined inclusion/exclusion criteria. Potentially relevant articles or articles without available abstract were screened full-text.

d) Data extraction

The following study characteristics were extracted: author, year of publication, study design, number of patients, study period, reconstruction, PSI material and fabrication technique, reconstruction method and software, use of surgical guide or navigation, follow-up and accuracy evaluation method.

e) Outcomes evaluation

The primary outcomes of this study were the quantitative outcomes of PSI positioning and the corresponding evaluation methods. As a secondary outcome, the use of surgical guides was studied. Outcomes were not analysed through meta-analysis, but systematically summarized and presented.

2.3 Results

a) Search results

On 1 December 2020, 1727 articles were identified. After screening of title and abstract, 59 articles were read full-text and 11 were included. The updated search strategy led to 113 new articles, of which 13 were screened full-text and none were included. Eventually, a total of 11 articles were included in the study (Fig. 1). Study characteristics are presented in table 1. Reconstruction types, PSI materials, fabrication methods and PSI positioning evaluation varied between the included studies.

The quantitative outcomes for PSI positioning in the studies can be globally divided into three categories: (angular) deviation of the postoperative PSI position compared to the planned PSI position, bone-to-implant gap and overlap of the postoperative PSI position with the planned PSI position (table 1).

b) (Angular) deviation

There were five studies that evaluated the PSI positioning by determining the (angular) deviation between the virtually planned PSI position and the acquired postoperative PSI position [2, 16-18, 23]. All five studies aligned the postoperative (CB)CT scan with the preoperative (CB)CT scan on which the planning of the PSI was based. The deviation between the actual PSI position and the planned PSI position were evaluated in different ways. Table 2 provides an overview of the evaluation methods per study with corresponding outcomes.

First of all, Kärkkäinen, et al. [17] measured the differences between the aligned postoperative PSI position and the virtually planned PSI position of orbital fracture reconstructions. The authors did this in three sites: anteromedial, anterolateral and posterior, but these sites were not clarified. Measurements were performed in three dimensions (stated as lateral, posterior and superior). 15 patients were included, resulting in a mean difference of 1.8 mm (range 0.4-5.6 mm) anteromedially, 2.0 mm (range 0.6-3.8 mm) anterolaterally and 1.9 mm (range 0.6-5.0 mm) cranially (table 2).

Rana, et al. [18] also evaluated the accuracy of orbital fracture reconstructions, but the method was not presented clearly. They determined the anterior, medial and posterior intraorbital angles in

coronal view between the planned and reconstructed orbits, but no site specifications were given. Over all 17 patients, the mean anterior angle was 4.1º (SD 0.7º), the mean medial angle was 8.2º (SD 1.9º) and the mean posterior angle was 8.2º (SD 1.4º) (table 2).

Schreurs, et al. [23] calculated the deviation for orbital implants regarding secondary orbitozygomatic reconstruction for 2 patients. The deviation was calculated using the Orbital Implant Positioning Frame, that was previously defined by Schreurs, et al. [25]. This reference frame, visualized in figure 1 in appendix B, was set up to quantify rotational and translational deviations. The rotations are expressed in pitch, yaw and roll. Outcomes were -4.5º roll, 2.6 º pitch, 0.8º yaw and 1.5 mm translation for patient 1 and 3.4º roll, -2.3º pitch, 4.5º yaw and 1.6 mm translation for patient 2 (table 2).

Tel, et al. [16] included 9 patients that underwent cranial resection and reconstruction for which they did a surface deviation analysis (SDA), yielding a root-mean-square error (RMSE). The RMSE provided an estimation of how far the error was from 0, with a small value correlating with high accuracy. The RMSE was calculated considering the Euclidean distances between the nodes of the aligned postoperative PSI model and virtually planned PSI model. The minimum, maximum and mean RMSE over all patients were 0.37 mm (SD 0.22 mm), 0.96 mm (SD 0.58 mm) and 0.64 mm (SD 0.49 mm) respectively (table 2).

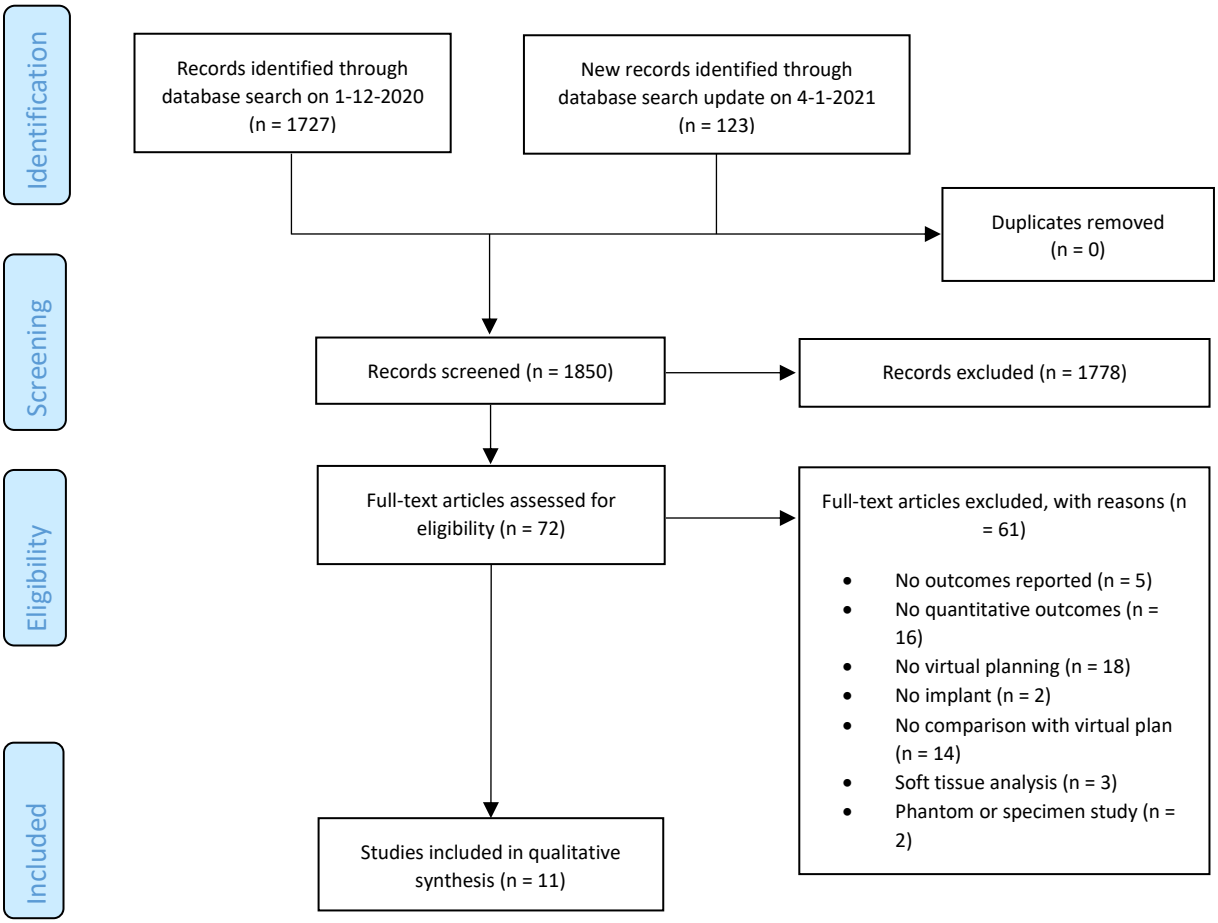

Fig. 1. PRISMA flow diagram of the literature search.

Table 1. Study characteristics.

Author, year	Study design	No. patients	Study period	Reconstruction	PSI material	PSI fabrication	Reconstruction method	Software	Surgical guide/navigation	Follow-up	Accuracy evaluation
Gerbino et al, 2015	CS	13	June 2010-June 2013	Cranio-orbital resection and reconstruction	PEEK	RP	Mirroring, manual alterations	NR	Guide with 7 patients, navigation with 1 patient	CT immediately post-op	Implant-to-bone gap (mm)
Jalbert et al, 2014	CS	5	NR	Fronto-orbital resection and reconstruction	PEEK	NR	NR	NR	Navigation: Brainlab Kolibri	CT post-op	Implant-to-bone gap (mm)
Kärkkäinen et al, 2018	RS	15	Jan 2017-Nov 2017	Orbital fracture reconstruction	Titanium	CNC-milled	Mirroring	Planmeca ProModel	No	CT within 24h post-op	Deviation (mm)
Ming-Chi Hsieh et al, 2020	RS	15	Dec 2015-May 2018	Aesthetic occipital augmentation	PMMA	Moulded	Ideal augmentation lines decided by surgeon	Mimics	No	CBCT 1wk post-op	Overlap (%)
Moser et al, 2017	RS	16	Aug 2012-Dec 2015	Secondary cranial reconstruction	PMMA	Moulded	Mirroring, interpolating	Mimics, Geomagic Studio	No	CT 1 day post-op	Implant-to-bone gap (mm)
Rana et al, 2015	RS	17	June 2010-May 2014	Orbital fracture reconstruction	Titanium	SLS	Mirroring	iPlan CMF 3.0.5, Freeform Plus	Navigation: Kick, Brainlab	CBCT within 24h post-op	Angular deviation
Schreurs et al, 2017	CS	2	NR	Secondary orbitozygomatic reconstruction	NR	NR	Mirroring	iPlan	Guide & navigation	CT/CBCT post-op	Deviation using Orbital Implant Positioning Frame (23)
Stieglitz et al, 2014	RS	19	Feb 2009-March 2012	Secondary cranial reconstruction	PMMA	Moulded	Mirroring, subtraction post-explantation CT from pre-explantation CT	BrainLab iPlan	No	CT only when clinically required	Implant-to-bone gap (mm) & overlap
Stoor et al, 2014	PS	12	NR	Orbital reconstruction	Titanium	EBM	Mirroring	PTC Pro Engineer 3D CAD	No	CT 0-16 days post-op	Overlap (%)
Tel et al, 2020	CS	9	Jan 2019-May 2020	Cranial resection & reconstruction	PMMA	Moulded	Context-driven-reconstruction (CDR)*	Mimics 22.0, 3-Matic 14.0	Guide & navigation: iPlan CMF	CT 48h post-op	Deviation (mm)
Zhang et al, 2015	RS	12	2008-2013	Craniomaxillofacial reconstruction	HA/EAM	SLS	Mirroring	SurgiCase 5.0	Navigation: Accu-Navi system	CT post-op	Deviation (mm)

CS = Comparative Study; RS = Retrospective Study; PS = Prospective Study; NR = not reported; HA/EAM = Hydroxyapatite/Epoxide Acrylate Maleic; RP = Rapid Prototyping; CNC-milled = Computer Numerical Control-milled; SLS = Selective Laser Sintering; EBM = Electron Beam Melting. *In this case, CDR is designing the PSI based on the surrounding cranial vault instead of mirroring or best-matching another subject's CT

Table 2. Evaluation methods and outcomes for studies calculating (angular) deviation of the postoperative PSI position compared to the planned PSI position.

Study	Reconstruction	Accuracy evaluation	Outcomes		
Kärkkäinen, et al.	Orbital fracture reconstruction	Difference in three dimensions: lateral, posterior & superior [mm]	Anteromedial	Mean	1.8 mm (range 0.4-5.6 mm)
			Anterolateral	Mean	2.0 mm (range 0.6-3.8 mm)
			Cranial	Mean	1.9 mm (range 0.6-5.0 mm)
Rana, et al.	Orbital fracture reconstruction	Intraorbital angles between reconstructed and planned orbit in coronal view [º]	Anterior	Mean	4.1º (SD 0.7º)
			Medial	Mean	8.2º (SD 1.9º)
			Posterior	Mean	8.2º (SD 1.4º)
Schreurs, et al.	Secondary OZC reconstruction	Orbital Implant Positioning Frame [25]	Patient 1	Roll	-4.5º
				Pitch	2.6 º
				Yaw	0.8º
				Translation	1.5 mm
			Patient 2	Roll	3.4º
				Pitch	-2.3º
				Yaw	4.5º
				Translation	1.6 mm
Tel, et al.	Cranial resection & reconstruction	Surface deviation analysis (SDA), yielding a root-mean-square error (RMSE) [mm]	Mean		0.64 mm (SD 0.49 mm)
			Minimum		0.37 mm (SD 0.22 mm)
			Maximum		0.96 mm (SD 0.58 mm)
Zhang, et al.	Craniomaxillofacial reconstruction	Surgical discrepancy [mm]	Mean		0.27 mm (SD 0.07 mm)
			Maximum		2.12 mm (SD 0.65 mm)

Finally, Zhang, et al. [2] reported a three-dimensional mean deviation of 0.27 mm (SD 0.07 mm) and a three-dimensional maximum deviation of 2.12 mm (SD 0.65 mm) over 12 patients (table 2). However, the authors do not report the method that was used to calculate the deviation.

c) Bone-to-implant gap

Four of the studies that were included calculated the gaps between the postoperative PSI position and adjacent bone [7, 11, 12, 26]. Outcomes are presented in table 3.

Gerbino, et al. [11] calculated the bone-to-implant gap for cranio-orbital implants in 13 patients and Jalbert, et al. [12] calculated the bone-to-implant gap for fronto-orbital implants in 5 patients. They both reported a maximum spacing of 3 mm around the perimeter of the implant (table 3).

Moser, et al. [7] and Stieglitz, et al. [26] both measured the bone-to-implant gap in the axial plane. Moser, et al. [7] included 16 patients undergoing cranial reconstruction and measured the gaps along the longest diameter of the implant in the frontal, parietal and most superior fronto-parietal area. These areas were not clarified. The mean gap over all patients was 1.8 mm (SD 0.7 mm, range 0.9-3.2 mm) in frontal area, 2.5 mm (SD 1.5 mm, range 0.6-5.8 mm) in parietal area and 1.4 mm (SD 1.3 mm, range 0.3-6.1 mm) in most superior fronto-parietal area. Stieglitz, et al. [26] included 19 patients undergoing secondary cranial reconstruction. They measured the gaps in the frontal, parietal and fronto-orbital area but these areas were not specified. The mean gap was 3.5 mm (SD 5.7 mm, median 1.7 mm) in frontal area, 2.2 mm (SD 2.1 mm, median 1.5 mm) in parietal area and 3.8 mm (SD 2.7 mm, median 3.5 mm) in fronto-orbital area (table 3).

Table 3. Evaluation methods and outcomes for studies calculating bone-to-implant gap.

Study	Reconstruction	Accuracy evaluation	Outcomes		
Gerbino, et al.	Cranio-orbital resection & reconstruction	Bone-to-implant gap [mm]	Maximum		3 mm
Jalbert, et al.	Fronto-orbital resection & reconstruction	Bone-to-implant gap [mm]	Maximum		3 mm
Moser, et al.	Secondary cranial reconstruction	Bone-to-implant gap in axial plane [mm]	Frontal	Mean	1.8 mm (SD 0.7 mm, range 0.9-3.2 mm)
			Parietal	Mean	2.5 mm (SD 1.5 mm, range 0.6-5.8 mm)
			Most superior fronto-parietal	Mean	1.4 mm (SD 1.3 mm, range 0.3-6.1 mm)
Stieglitz, et al.	Secondary cranial reconstruction	Bone-to-implant gap in axial plane [mm]	Frontal	Mean	3.5 mm (SD 5.7 mm, median 1.7 mm)
			Parietal	Mean	2.2 mm (SD 2.1 mm, median 1.5 mm)
			Fronto-orbital	Mean	3.8 mm (SD 2.7 mm, median 3.5 mm)

d) Overlap

Lastly, three studies calculated the overlap of the postoperative PSI position with the planned PSI position (table 4).

Ming-Chi Hsieh, et al. [27] included 15 patients undergoing aesthetic occipital augmentation. They evaluated the PSI accuracy by first aligning the postoperative CBCT with the preoperative model of the virtual planning. They did not specify how. The overlap was defined as the amount of volume overlap between the actual implant and the virtual implant, divided by the volume of the virtually planned implant. The overlap over all patients ranged from 87.8%-99.99%, with a mean of 95.71% (table 4).

Stieglitz, et al. [26] generated a so-called quality grade for evaluation of secondary cranial reconstructions: a 3D reconstruction of the postoperative PSI was subtracted from the 3D model of the planned PSI. In case of a perfectly sized, shaped and implanted PSI, the resulting volume would be 0 cm^3. In case of no overlap at all, the result would be the full volume of the virtually planned PSI. This resulting volume was set in relation to the volume of the virtually planned PSI, to obtain a result independent from the size of the implant. This was then subtracted from 1 and multiplied by 100 to generate the quality grade. This grade could range from 0 (no overlap between the postoperative PSI and planned PSI) to 100 (perfect size, shape and implantation). The mean quality grade over all 19 patients that were included was 73, the median was 80 and the standard deviation was 18 (table 4).

At last, Stoor, et al. [13] included 12 patients requiring orbital reconstruction. They aligned the postoperative 3D model with the preoperative 3D model, using stable anatomical reference points in the frontal bone, maxilla and zygoma, to measure the volumetric surface overlap. The exact method was not reported. Only 3 ranges were given: 1 patient had an overlap of less than 10%, 2 patients had an overlap between 10%-60% and the other 8 patients had an overlap of more than 60% (table 4).

e) Surgical guides

From the eleven studies that were included, only three used a patient-specific surgical guide during surgery (table 1). The studies that did not use a surgical guide either performed reconstruction only (without a preceding resection) [2, 7, 13, 17, 18, 26, 27], or used surgical navigation in order to create the osteotomies [12]. The studies that did use a surgical guide, reported different ways of handling the guide.

Table 4. Evaluation methods and outcomes for studies calculating overlap of the postoperative PSI position with the planned PSI position.

Study	Reconstruction	Accuracy evaluation	Outcomes	
Ming-Chi Hsieh, et al.	Aesthetic occipital augmentation	Overlap [%]	Mean	95.71% (range 87.8%-99.99%)
Stieglitz, et al.	Secondary cranial reconstruction	Quality grade (overlap)	Mean	73 (SD 18, median 80)
Stoor, et al.	Orbital reconstruction	Volumetric surface overlap [%]	1 patient <10%	
			2 patients 10%-60%	
			8 patients >60%	

In seven patients undergoing one-step primary reconstruction of cranio-orbital defects, Gerbino, et al. [11] used virtually planned surgical guides for the exact guidance of the craniotomy and orbital rim resection. These surgical guides were designed with extensions into the orbit for 1 cm around the bony rims, to allow for a precise fit and stability. Intraoperatively, the authors report that only minor adjustments of the implants and bone edges were necessary after performing adequate craniotomies and orbital rim resections with the guide. In one case, extensive adaptation was necessary, which meant that more than 15 minutes and three or more attempts at fitting were required. They reported that the intraoperative resection probably did not match with the planned resection, because of surgical guide malpositioning.

Schreurs, et al. [23] made use of surgical guides for secondary orbitozygomatic reconstructions. These reconstructions consisted of repositioning the orbitozygomatic complex (OZC) to its anatomical position and orbital floor and wall repair with a PSI. In order to reposition the OZC, first an osteotomy was performed using a surgical guide to mobilize the complex. In order to obtain an accurate osteotomy, this surgical guide was designed with screw holes at the location of the screw holes of the previous reconstruction. After the osteotomy, the orbital PSI was positioned using the existing screw hole locations and feedback from surgical navigation and the OZC was repositioned to fit the PSI. Intra-operatively, all screw hole locations matched the screw hole locations in the design and there was no need for creation of new screw holes. Also, surgical navigation revealed accurate repositioning, according to the virtual plan.

In the study of Tel, et al. [16] patients underwent cranial resection and reconstruction, using both a surgical guide and navigation. The surgical guide was designed in such a way to perform a tapered craniotomy. The bony craniotomy, the remaining skull and the virtually planned PSI were loaded into the navigation system for intraoperative navigational feedback. During surgery, the planned craniotomy was first performed using surgical navigation and then refined using the surgical guide. The deviation between these two steps was said to be submillimetric. The cranial PSI that was placed afterwards, fitted the cranial defect precisely in all cases.

2.4 Discussion

Nowadays, more and more craniofacial reconstructions are being performed using virtually planned PSIs, because they can be designed to the exact shape and size of the defect. Whenever these reconstructions regard a one-stage resection and reconstruction, a surgical guide may be designed to guide the planned osteotomy before positioning the PSI. There are numerous articles describing the clinical outcomes and subjective aesthetic outcomes of these reconstructions, but the goal of this review was to summarize existing literature on the quantitative outcomes of craniofacial PSIs.

This review showed that there are many different methods being used to evaluate the postoperative PSI position, with different outcomes. In general, these methods can be divided into three different categories: (angular) deviation of the postoperative PSI position from the virtually planned PSI

position, bone-to-implant gap and overlap between the postoperative PSI position with the virtually planned PSI position.

a) (Angular) deviation

The four studies that reported the deviation in millimeters, showed high accuracy of the PSI positioning. The mean distance between planned PSI and postoperative PSI position, although measured at different locations in different ways, varied between 0.27 mm and 1.9 mm (table 2). These were studies regarding both orbital and cranial reconstructions. Two of these studies (Schreurs, et al. and Tel, et al. [16]) already reported an accurate PSI fitting intraoperatively, with the use of surgical guides and navigation. Zhang, et al. [2] also used surgical navigation to increase accuracy. On the contrary, Kärkkäinen, et al. [17] did not make use of surgical navigation and still reported a low mean deviation. They did however report two patients with a higher deviation (5.0 mm and 5.6 mm). This was assigned to the preoperative planning: in one case the orbital bone was too thin to detect on the preoperative CT and in the other case the contralateral side that was used for mirroring contained a previous fracture, complicating the preoperative planning.
The angular deviation was reported in two studies for orbital implants [18, 23], showing high accuracy as well (table 2). This was most likely caused by the use of surgical guides and navigation for Schreurs, et al. [23] and the use of surgical navigation for Rana, et al. [18].
Four out of five studies fabricated their PSIs using milling techniques or additive manufacturing, accurately reproducing the virtual design.

b) Bone-to-implant gap

The mean bone-to-implant gap was never higher than 3.8 mm, but there was a large spread (table 2). Gerbino, et al. [11] and Jalbert, et al. [12] both reported the same outcome on cranio-orbital reconstructions with PEEK PSIs (maximum gap of 3 mm), but it was unclear whether they performed similar measurements. For Gerbino, et al. [11] this maximum gap was achieved by adequate craniotomy and orbital rim resection using a surgical guide. However, some minor adjustments of the implants and bone edges were still necessary intraoperatively. Jalbert, et al. [12] contributed the small bone-to-implant gap to surgical navigation, accurately reproducing the planned resection. Moser, et al. [7] and Stieglitz, et al. [26] measured the bone-to-implant gaps for secondary cranial reconstructions using PMMA. Here, some outliers were reported, resulting in a larger mean bone-to-implant gap: Moser, et al. [7] found a maximum gap of 6.1 mm and Stieglitz, et al. [26] measured a mean gap of 3.5 mm with a standard deviation of 5.7 mm. One explanation for these outliers could be that PMMA needed to be manually molded on a virtually designed template, decreasing accuracy. Another reason could be the fact that these were secondary reconstructions, where an already existing defect had to be reconstructed. Although the design of the PSI was based on this existing defect, the edges around the defect might have been irregularly shaped, complicating the PSI design or positioning. In addition, no surgical navigation was used to guide the PSI into the correct position.

c) Overlap

Overlap between the postoperative PSI position and virtually planned PSI position was measured for three different kind of reconstructions. The results varied considerably. Ming-Chi Hsieh, et al. [27] reported a high mean percentage overlap for aesthetic occipital augmentations (95.71%), regardless of the fact that PMMA had to be manually moulded on a virtually planned template. Stieglitz, et al. [26] measured the overlap quality grade for cranial reconstructions, using PMMA too. The mean quality grade was 73 and there were four patients with a grade higher than 90, indicating a nearly ideal implanted PSI. On the contrary, 8 patients had a quality grade below 73, which was in most cases said to be caused by a PSI that was moulded too flat or too thin. This can be explained by the fact that they used a 3D model of the skull with planned craniotomy to form the PMMA on, but without taking into consideration the thickness of the skull. Lastly, Stoor, et al. [13] reported a wide range of volumetric surface overlap for titanium orbital PSIs. This wide range suggested inaccurate positioning. They reported that two implants had an incorrect shape because of an incorrect virtual

model. This was caused by the fact that the thinnest parts of the orbital bone were not detectable in the virtual environment and therefore not included in the PSI model. Neither of these three studies used surgical navigation to help steer the PSI into the correct position.

In general, the postoperative PSI positions were accurate, except for a few outliers. These outliers were mainly present in the results of the overlap between postoperative PSI position and virtually planned PSI position. The manual moulding of PMMA could have led to a PSI that did not exactly have the same size and shape as the virtually planned PSI. Thus, the question arises whether this outcome measure should be used to evaluate the postoperative PSI position in these cases. The (angular) deviation between the postoperative PSI position and the virtually planned PSI position, on the other hand, would be a more useful method. It immediately provides feedback in which direction the PSI should have been translated or rotated. The small deviations that were found prove accurate PSI positioning, which was supported by surgical navigation or a surgical guide in almost all cases. Correct preoperative planning does remain very important. Some other outliers in accuracy were found with the evaluation method measuring bone-to-implant gaps. Although gaps between the PSI and adjacent bone do say something about the PSI position, measuring the bone-to-implant gaps does not directly compare the postoperative PSI position with the virtually planned PSI position. These gaps could also be related to the osteotomies or intraoperative adjustments to the PSI. Smaller bone-to-implant gaps suggest better PSI positioning, but this is not always clinically relevant. Moser, et al. [7] reported that, despite the outliers that they found, the mean gaps around sensitive cosmetic and complex anatomical areas such as the pterional region (where the frontal, parietal, temporal and sphenoid bones join together), were smaller than 2 mm.

d) Surgical guides

The three studies that reported the use of surgical guides, all mentioned accurate guide positioning, leading to accurate PSI positioning. Accurate guide positioning was either proven by intraoperative navigational feedback, or by rigid feedback such as corresponding screw hole locations in the guide and skull. In some cases, minor adjustments did have to be made intraoperatively to the PSI or bone edges, and one case required extensive adjustments. This was caused by malpositioning of the surgical guide, but no further reasons were provided. These cases show that there is room for improvement. None of the studies performed an actual quantitative evaluation to verify the intraoperative guide position or the realised osteotomies. Since the use of surgical guides directly influences the PSI positioning, it should be included in future studies that evaluate PSI positioning with preceding resections using guides. Deviations in PSI positioning can be compared with and related to surgical guide positioning, which might help improve the reconstruction.

e) Limitations and future perspective

As mentioned previously, a deviation in PSI positioning does not always have to be clinically relevant. The goal of craniofacial reconstruction is re-establishment of the contour, shape and symmetry to improve aesthetic appearance, but it also has a functional goal. This goal is different for each type of reconstruction. Cranioplasty aims at protecting the underlying brain providing biomechanical stability and facilitating neurological recovery and rehabilitation by improving cerebral haemodynamics and metabolism [7, 12, 16]. Apart from quantitatively evaluating PSI positioning, complications and patient satisfaction about cosmetic outcome are usually recorded for cranioplasty. One thing to consider is that although the bony reconstruction might be accurate, soft tissue changes may be unpredictable and may limit the aesthetic and morphological outcomes.

For orbital reconstructions, the most important goal is to eliminate enophthalmos and diplopia. Different studies have shown that the occurrence of enophthalmos is mainly related to the enlargement of the bony orbit, or increase in orbital volume [11-13, 17, 18, 23]. Cha, et al. [28] reported that the increase in orbital cavity volume was linearly proportional to the amount of enophthalmos and Stoor, et al. [13] reported that an increase of 4-5% of the orbital volume produced an enophthalmos of 3 mm. Therefore, many studies evaluating orbital implant positioning,

include orbital volume measurements. They compare the postoperative orbital volume with the orbital volume of the mirrored unaffected orbit to quantify this functional outcome measure. For this review, these outcomes were not included, because the postoperative PSI position is not directly compared with the virtually planned PSI position in these cases. However, orbital volume is a relevant outcome measure for orbital reconstructions and should definitely be taken into consideration in future research.

This literature review had some limitations. First of all, only the MEDLINE (PubMed) database was consulted and the screening of the articles was performed by one reviewer only. Secondly, the studies that were included regarded different reconstructions and used different materials and fabrication techniques to create the PSIs. In many articles, the measurements of PSI positioning were not explained thoroughly enough to be able to interpret the results completely. This introduced many variables, which complicated the comparison of the outcomes impeding performing a meta-analyses.

All in all, no standard for the assessment of the postoperative PSI position currently exists, which hampers the comparison between studies. Overall, a high accuracy of PSI positioning was found in studies that created accurate osteotomies with surgical guides or navigation and in studies that used surgical navigation for intraoperative feedback on the PSI position. The use of surgical navigation appears essential for accurate PSI positioning. The use of surgical guides provided accurate osteotomies in most cases, but malpositioning of the guide could easily lead to malpositioning of the PSI. Improving the fit of the surgical guide and the way it is handled, could possibly improve the postoperative PSI position. For orbital implants, future research should include orbital volume measurements.

2.5 References

1. Rudman, K., C. Hoekzema, and J. Rhee, *Computer-assisted innovations in craniofacial surgery.* Facial Plast Surg, 2011. 27(4): p. 358-65.
2. Zhang, L., et al., *Computer-Aided Design and Computer-Aided Manufacturing Hydroxyapatite/Epoxide Acrylate Maleic Compound Construction for Craniomaxillofacial Bone Defects.* J Craniofac Surg, 2015. 26(5): p. 1477-81.
3. Scolozzi, P., A. Martinez, and B. Jaques, *Complex orbito-fronto-temporal reconstruction using computer-designed PEEK implant.* J Craniofac Surg, 2007. 18(1): p. 224-8.
4. Alonso-Rodriguez, E., et al., *Polyetheretherketone custom-made implants for craniofacial defects: Report of 14 cases and review of the literature.* J Craniomaxillofac Surg, 2015. 43(7): p. 1232-8.
5. Järvinen, S., et al., *The use of patient specific polyetheretherketone implants for reconstruction of maxillofacial deformities.* J Craniomaxillofac Surg, 2019. 47(7): p. 1072-1076.
6. Jonkergouw, J., et al., *Outcome in patient-specific PEEK cranioplasty: A two-center cohort study of 40 implants.* J Craniomaxillofac Surg, 2016. 44(9): p. 1266-72.
7. Moser, M., et al., *Patient-specific polymethylmethacrylate prostheses for secondary reconstruction of large calvarial defects: A retrospective feasibility study of a new intraoperative moulding device for cranioplasty.* J Craniomaxillofac Surg, 2017. 45(2): p. 295-303.
8. Rammos, C.K., et al., *Patient-specific polyetheretherketone implants for repair of craniofacial defects.* J Craniofac Surg, 2015. 26(3): p. 631-3.
9. Chepurnyi, Y., et al., *Automatic evaluation of the orbital shape after application of conventional and patient-specific implants: Correlation of initial trauma patterns and outcome.* J Oral Biol Craniofac Res, 2020. 10(4): p. 733-737.
10. Gerbino, G., et al., *Single-step resection and reconstruction using patient-specific implants in the treatment of benign cranio-orbital tumors.* J Oral Maxillofac Surg, 2013. 71(11): p. 1969-82.
11. Gerbino, G., et al., *Primary and secondary reconstruction of complex craniofacial defects using polyetheretherketone custom-made implants.* J Craniomaxillofac Surg, 2015. 43(8): p. 1356-63.
12. Jalbert, F., et al., *One-step primary reconstruction for complex craniofacial resection with PEEK custom-made implants.* J Craniomaxillofac Surg, 2014. 42(2): p. 141-8.
13. Stoor, P., et al., *Rapid prototyped patient specific implants for reconstruction of orbital wall defects.* J Craniomaxillofac Surg, 2014. 42(8): p. 1644-9.
14. Tarsitano, A., et al., *Orbital Reconstruction: Patient-Specific Orbital Floor Reconstruction Using a Mirroring Technique and a Customized Titanium Mesh.* J Craniofac Surg, 2016. 27(7): p. 1822-1825.
15. Manrique, O.J., et al., *Craniofacial reconstruction using patient-specific implants polyether ether ketone with computer-assisted planning.* J Craniofac Surg, 2015. 26(3): p. 663-6.
16. Tel, A., et al., *Computer-Guided In-House Cranioplasty: Establishing a Novel Standard for Cranial Reconstruction and Proposal of an Updated Protocol.* J Oral Maxillofac Surg, 2020. 78(12): p. 2297.e1-2297.e16.
17. Kärkkäinen, M., et al., *Primary reconstruction of orbital fractures using patient-specific titanium milled implants: the Helsinki protocol.* Br J Oral Maxillofac Surg, 2018. 56(9): p. 791-796.
18. Rana, M., et al., *Increasing the accuracy of orbital reconstruction with selective laser-melted patient-specific implants combined with intraoperative navigation.* J Oral Maxillofac Surg, 2015. 73(6): p. 1113-8.

19. van de Vijfeijken, S., et al., *The use of cranial resection templates with 3D virtual planning and PEEK patient-specific implants: A 3 year follow-up.* J Craniomaxillofac Surg, 2019. 47(4): p. 542-547.
20. Gordon, C.R., et al., *First-in-Human Experience With Integration of a Hydrocephalus Shunt Device Within a Customized Cranial Implant.* Oper Neurosurg (Hagerstown), 2019. 17(6): p. 608-615.
21. Jindal, S., et al., *3D printed composite materials for craniofacial implants: current concepts, challenges and future directions.* The International Journal of Advanced Manufacturing Technology, 2020.
22. Miljanovic, D., et al., *Design and Fabrication of Implants for Mandibular and Craniofacial Defects Using Different Medical-Additive Manufacturing Technologies: A Review.* Ann Biomed Eng, 2020. 48(9): p. 2285-2300.
23. Schreurs, R., et al., *The orbit first! A novel surgical treatment protocol for secondary orbitozygomatic reconstruction.* J Craniomaxillofac Surg, 2017. 45(7): p. 1043-1050.
24. Tunçbilek, G., et al., *Spring-mediated cranioplasty in patients with multiple-suture synostosis and cloverleaf skull deformity.* J Craniofac Surg, 2012. 23(2): p. 374-7.
25. Schreurs, R., et al., *Quantitative Assessment of Orbital Implant Position--A Proof of Concept.* PLoS One, 2016. 11(3): p. e0150162.
26. Stieglitz, L.H., et al., *Intraoperative fabrication of patient-specific moulded implants for skull reconstruction: single-centre experience of 28 cases.* Acta Neurochir (Wien), 2014. 156(4): p. 793-803.
27. Ming-Chi Hsieh, A., et al., *Esthetic Occipital Augmentation With Computer-Aided Design-Computer-Aided Manufacturing Prefabricated Customized Polymethyl Methacrylate Implant: Comparison of Planned and Final Results.* J Oral Maxillofac Surg, 2020. 78(7): p. 1191.e1-1191.e8.
28. Cha, J.H., et al., *Application of Rapid Prototyping Technique and Intraoperative Navigation System for the Repair and Reconstruction of Orbital Wall Fractures.* Arch Craniofac Surg, 2016. 17(3): p. 146-153.

Appendix

A: Search strategy

("Craniofacial Abnormalities/surgery"[Majr] OR "Skull/surgery"[Majr] OR (“cranial”[ti] OR “cranio*”[ti] OR “cranium”[ti] OR “maxillofacial”[ti] OR “maxillo-facial”[ti] OR "spheno*"[ti] OR "orbit*"[ti] OR "temporal"[ti] OR "frontal"[ti] OR "zygoma*"[ti] OR "occipital"[ti] OR "parietal"[ti]) AND ("Reconstructive Surgical Procedures"[Majr] OR "Prostheses and Implants"[Majr] OR "reconstruct*"[ti] OR "implant*"[ti] OR "prosthes*"[ti] OR "prosthet*"[ti])) AND ("patient-specific"[tiab] OR "patientspecific"[tiab] OR "patient specific"[tiab] OR "PSI"[tiab] OR "PSIs"[tiab] OR "custom*"[tiab] OR "virtually planned"[tiab] OR "virtually-planned"[tiab] OR "virtual*"[tiab] OR "3-D"[tiab] OR "3D"[tiab] OR "3 D"[tiab] OR "3-dimensional"[tiab] OR "3 dimensional"[tiab] OR "threedimensional"[tiab] OR "three-dimensional"[tiab] OR "three dimensional"[tiab] OR "Imaging, Three-Dimensional"[Mesh] OR "Printing, Three-Dimensional"[Mesh] OR "rapid prototyping"[tiab] OR "additive manufacturing"[tiab] OR "Computer-Aided Design"[Mesh] OR "CAD"[tiab] OR "CAM"[tiab] OR "computer-aided"[tiab] OR "computer aided"[tiab] OR "computer-assisted"[tiab] OR "computer assisted"[tiab] OR "computer"[tiab] OR "image processing, computer-assisted"[Mesh]) AND (2010:2020[pdat] AND fft[Filter] AND english[Filter])

B: Orbital Implant Positioning Frame

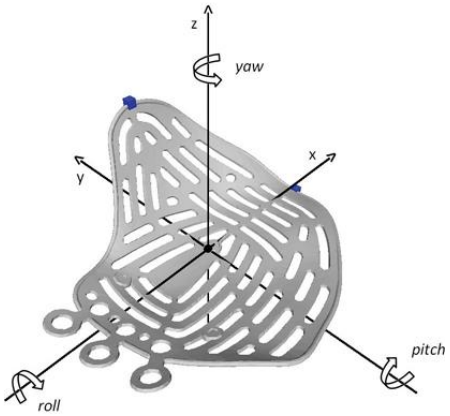

Fig 1. Orbital Implant Positioning Frame, designed by Schreurs, et al. The orientation of the axes that define roll, pitch and yaw are visualized. For right-sided implants, the y-axis is flipped in order to distinguish left and right sided implants. In that case, yaw and roll direction are also opposed [25].

3. Background

3.1 Craniofacial reconstructions

Craniofacial reconstructions are reconstructions of defects in the cranial and/or facial bones. These defects may result in functional damage, aesthetic deformities and psychological implications [3]. Different sites for reconstruction include the frontal bone, parietal bone, occipital bone, temporal bone, sphenoidal bone, zygomatic bone and other orbital bones [1] (figure 1). The goal of craniofacial reconstructions depends on the location. Cranioplasty is performed to restore the protection of the underlying brain, whereas reconstruction of the orbital bones aims at retaining symmetrical globe positioning. This is obtained by restoring the shape and original volume of the orbit in order to avoid enophthalmos (posterior displacement of the eyeball) or diplopia (double vision) [1, 4-14]. Besides these functional goals there is always the goal of aesthetical improvement.

3.1.1 Indications

In the LUMC, common indications for craniofacial reconstructions are tumour resection, bone graft or implant removal and trauma. Other possible indications are congenital anomalies such as fibrous dysplasia or infection.

Tumour resection

Tumour resection generally regards meningioma's and haemangioma's.

Meningioma's are one of the most common primary brain tumours. They arise from the meninges and are usually benign. Only 5-10% behave in an atypical or malignant matter [29]. They grow relatively slowly, but whenever the tumour involves bone, hyperostosis (excessive growth of bone) may occur and result in local mass effect. Possible clinical symptoms include palpable or visible bony mass and proptosis (anterior displacement of the eyeball). The goal for successful treatment is complete tumour removal in order to prevent regrowth [30,31].

Haemangioma's are benign vascular lesions that can occur throughout the whole body, but most frequently in the vertebrae and skull. Haemangioma's of the skull represent 10% of all benign tumours of the skull. They are slowly-growing and usually asymptomatic, unless they exert pressure on surrounding sensitive structures. Resection may be performed whenever this is clinically or cosmetically desirable [32,33]. After tumour resection, reconstruction can take place.

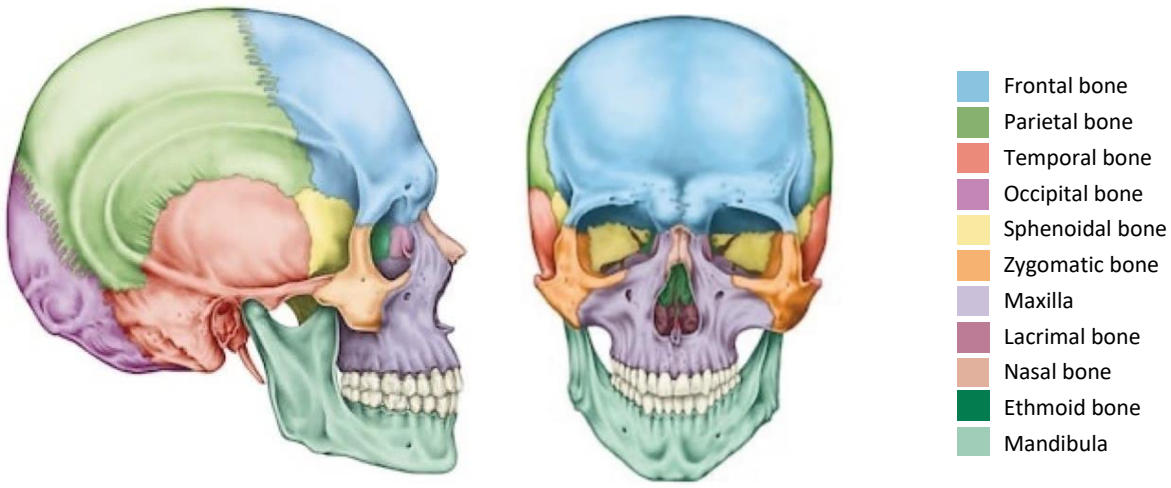

Figure 1. Craniofacial bones. Orbital bones consist of the maxilla, zygomatic bone, lacrimal bone, palatine bone (not visualized), frontal bone, ethmoid bone and sphenoidal bone.

Bone graft or implant removal

Removal of a primary bone graft or implant might be necessary after resorption of a previously implanted bone graft or after infection of the implant. A secondary craniofacial reconstruction can be performed afterwards [8].

Trauma

Traumatic brain injury (TBI) or a stroke are examples of trauma. When trauma increases the intracranial pressure, a decompressive craniectomy can be performed. Part of the cranial vault is removed which can sometimes be reinserted immediately [6]. Whenever this is not possible due to swelling or persistent intracranial pressure, cranial reconstruction takes place at a later stage [19].

3.1.2 Materials

Different materials are used for craniofacial reconstructions. Conventionally, craniofacial reconstructions were done with autologous bone or allografts. Over the years, alloplastic materials have been introduced as an alternative.

Autologous bone

Autologous bone is bone harvested from the patient itself, usually from the iliac crest. Autologous bone is biocompatible and it has optimal mechanical properties. In addition, it is a good substrate for bone ingrowth and revascularization and it evokes no immunological response [4,6]. However, harvesting bone from another location in the patient's body introduces donor-site morbidity with an increased infection risk. There is also the risk of bone resorption and fragmentation and when the defects are large or complex, donor-site options may lack [8,14,15].

Bone allografts

A bone allograft is bone from another human that has been donated. This usually regards cadaveric bone from the bone bank. The advantage of bone allografts over autografts is that there is no donor-site morbidity and therefore less risk of infection. However, tissue from another human introduces the risk of disease transmission [4,8].

Alloplastic materials

Alloplastic materials are materials that have been introduced to use as an alternative for autologous bone and allografts. Large defects can be covered and there is no need for bone harvesting. There are many different materials, all with their own advantages and disadvantages.

Two popular materials are PMMA (polymethylmethacrylate), a polymer, and titanium, a metal. PMMA is one of the most popular materials for cranial reconstruction [16]. This material can be moulded into the defect intraoperatively. Titanium mesh is often used for orbital reconstructions. Stock meshes are available which need preoperative or intraoperative bending to fit the patient's orbital anatomy [9,17,18].

Alloplastic materials can also be used for the fabrication of patient-specific implants. This will be further clarified in the next section (3.2.2).

3.2 Patient-specific implants

The use of autologous bone, allografts or pre- or intraoperative shaping of alloplastic materials can be difficult and time-consuming, increasing operative time [11]. Especially defects in the cranio-orbital region can be complex, because of their different curvatures and thicknesses [4,11]. Patient-specific implants are designed and manufactured outside of the operating room. Therefore, the use of PSIs decreases operative time that is otherwise spent on contouring and intraoperative implant modifications [10,15].

3.2.1 Design

Patient-specific implants are implants that are virtually planned in 3D design software packages, based on preoperative imaging. A CT scan, an MRI scan or a combination of both are used to visualize the patient's anatomy including the defect or tumour. Based on these images a reconstruction is planned.

If needed, resection margins are determined in order to virtually plan the resection. A surgical guide is designed to enable a one-stage procedure for resection and reconstruction. The goal of the surgical guide is to indicate the resection outline, which corresponds to the patient-specific implant outline.

The patient-specific implant is designed to the exact shape and size of the defect, usually starting with mirroring the contralateral side. Another possibility is to use previous imaging of the patient (when available) in order to match the reconstruction with the original anatomy.

After virtually designing the surgical guide and implant, they can be fabricated using different materials and fabrication techniques.

3.2.2 Materials

Patient-specific implants are made from alloplastic materials. Multiple alloplastic materials are used to manufacture PSIs, including titanium, a metal, PMMA and PEEK, polymers, and hydroxyapatite (HA), a ceramic. These materials all have their own advantages and disadvantages.

Titanium

Titanium is biocompatible and has a low infection rate. However, it has no protective energy-absorbing properties, it leads to artefacts on postoperative CT and MRI images and it is expensive [6,14].

Polymethylmethacrylate

Polymethylmethacrylate (PMMA) has good biocompatibility and strong resistance to functional stress. It is lightweight, radiolucent (no artefacts on postoperative CT images), low-cost and it can be handled easily. There is however a risk of fragmentation [6,8,16].

Hydroxyapatite

Hydroxyapatite allows for excellent bone ingrowth, but it is very brittle and has a low tensile strength [6,8].

Polyetheretherketone

Finally, polyetheretherketone (PEEK) is expensive but it has several advantages. The elastic modulus and the mechanical strength, or energy absorbing properties, are almost similar to cortical bone [4,6,8,12,15]. In addition, it has excellent biocompatibility and it is radiolucent and non-magnetic so it allows for postoperative CT and MRI scans [6,12,15]. Most craniofacial reconstructions that require an implant in the LUMC are performed with a patient-specific implant made from PEEK.

3.2.3 Fabrication

Apart from the multiplicity of PSI materials, there are is also a variety of PSI fabrication techniques.

One method is to create a model on which a material, such as PMMA, can be moulded pre- or intraoperatively. The PMMA is initially mouldable but cures to form the patient-specific implant in the desired shape.

Other fabrication techniques are milling or additive manufacturing.

Examples of additive manufacturing are fused deposition modelling (FDM), where a polymer is melted, extruded and deposited layer by layer; laser sintering techniques including selective laser sintering (SLS), selective laser melting (SLM) and electron beam melting (EBM), where a powder is deposited and melted layer after layer; and stereolithography (SLA), where a photo-sensitive liquid resin is solidified using light, every layer [21,22].

The craniofacial PEEK PSIs in the LUMC are fabricated using milling techniques.

3.3 Segmentation

Segmentation partitions a dataset into adjacent regions. Considering image segmentation, these regions consist of pixels or voxels that share common cohesive properties [34]. Examples of segmentation are distinguishing between benign and malign tissue or separating skull from soft tissue.

3.3.1 Thresholding

Thresholding is a segmentation technique that groups all pixels or voxels in an image with an intensity greater than a certain threshold in one class and all other pixels or voxels in another. This class can be called a mask. It is also possible to use multiple thresholds. The optimal threshold is not known beforehand, since it depends on the imaging modality, image acquisition, patient and type of tissue to be segmented. The threshold can be chosen manually by inspecting the image or the histogram of intensity values [34].

3.3.2 Region growing

Region growing is another segmentation technique. It extracts an image region that is connected, based on predefined criteria such as intensity or edges. A so-called seed point is selected, which is compared with neighbouring pixels or voxels with a specific threshold. When these pixels or voxels fall within the predefined threshold they are included in the region, if not they are excluded. The result is dependent on the selected seed point.

3.3.3 Morphological operations

Morphological operations are operations related to the shape (or morphology) of features in an image. A structuring element or kernel, with a certain shape, is positioned at all possible locations in the image and compared with corresponding neighbourhood pixels or voxels.

With dilation, an existing mask is filled up to the structuring element whenever the origin of the structuring element overlaps with the original mask. This operation enlarges the boundaries of foreground pixels or voxels and decreases holes within the region (figure 2).

With erosion, the complete structuring element needs to overlap with the original mask in order to fill up the mask to the origin of the structuring element. This shrinks the boundaries of foreground pixels or voxels and enlarges holes within the region (figure 3). A goal of this operation can be to separate objects or to remove small noisy spots.

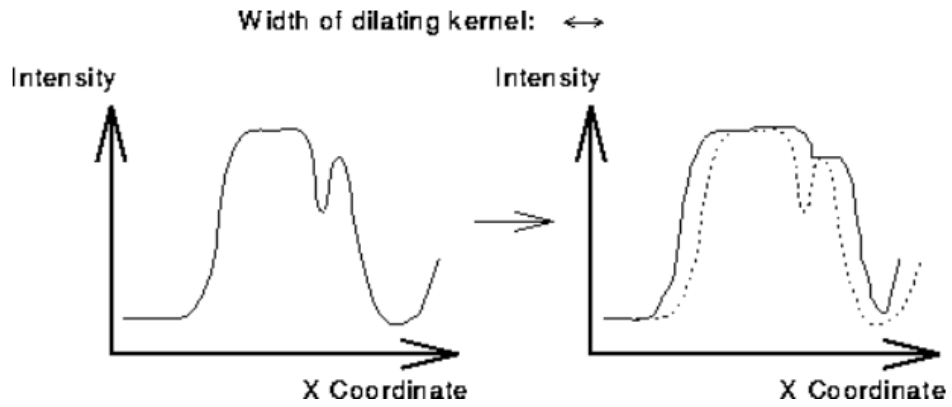

Figure 2. Dilation with a disk-shaped structuring element, or kernel. The graph shows a vertical cross-section of an intensity-based image, the line representing the boundaries of the mask [34].

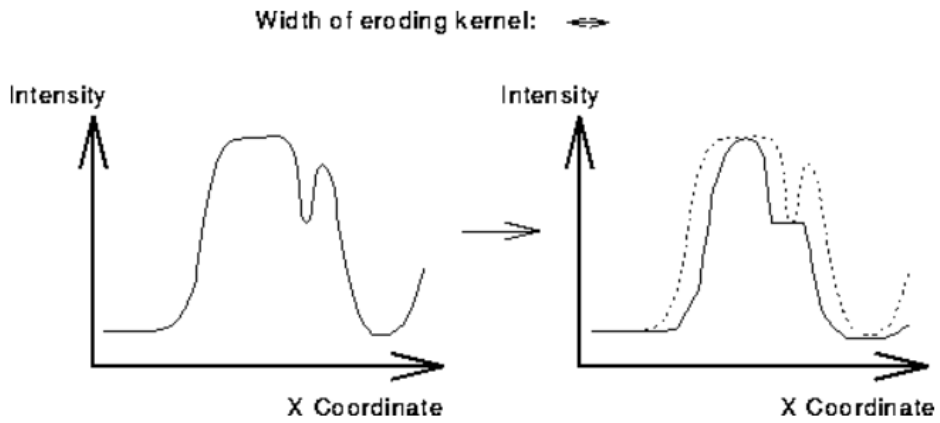

Figure 3. Erosion with a disk-shaped structuring element, or kernel. The graph shows a vertical cross-section of an intensity-based image, the line representing the boundaries of the mask [34].

Dilation and erosion can also be combined: opening is erosion followed by dilation, whereas closing is dilation followed by erosion.

3.4 Registration

3.4.1 Image registration

Image registration spatially aligns two datasets. In the field of medical imaging, this can be useful in order to analyse and compare images from different modalities, such as CT and MRI; from different time-points, to assess treatment progress or disease development; or from different subjects, to determine what is average and what is abnormal.

Registration is an optimization problem where a transformation $T(x)$ is found to spatially align a moving image $I_M(T(x))$ with a fixed image $I_F(x)$. It involves minimizing a cost function or metric which computes the similarity of the images and thereby defines the quality of alignment [34-36]. Other basic registration components include a sampler, an optimizer and an interpolator (figure 4).

In short, a sampler reduces the amount of points that is included in the registration to speed up the process, an optimizer takes steps into the direction of the steepest descent of the metric, reducing the step size with every iteration to reach a minimum and the interpolator interpolates transformed points that are mapped to a non-grid position when these points do not exist in both fixed and moving image.

Since image registration in this thesis was performed using Mimics, where parameters for these basic registration components were pre-set and non-adjustable, only the transform is further described below. This component was used in the method in this thesis.

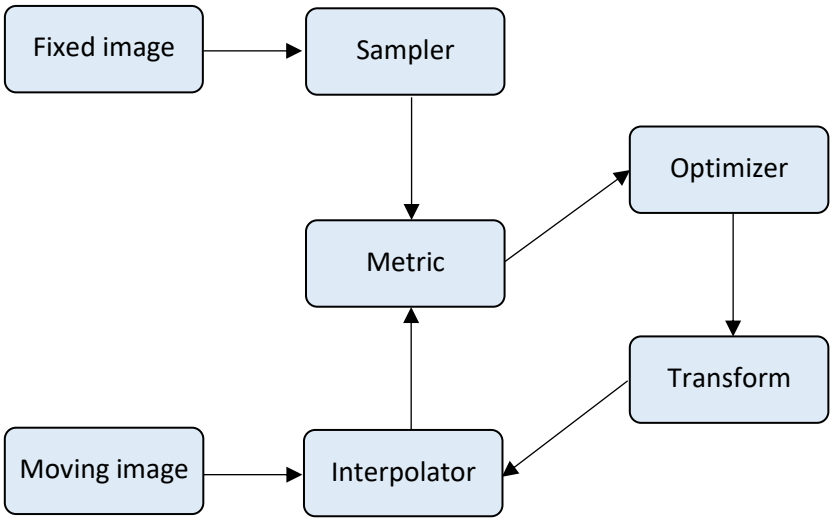

Figure 4. The basic registration components, including a fixed and moving image, sampler, metric, optimizer, interpolator and transform.

Transform

The type of transform determines the possible deformations between the image (figure 5):

1) translation is the simplest form of a transformation, with only a translation vector;
2) rigid transformations allow both translation and rotation, with a translation vector and a rotation matrix that is defined around the centre of rotation;
3) a similarity transform additionally allows scaling with a scaling factor;
4) affine transformations allow translation, rotation, scaling and shearing;
5) non-rigid or deformable transformations allow stretching and shrinking and are usually described by B-splines containing a transformation per pixel or voxel

In this thesis, solely 3D rigid transformations were used. Because a rigid registration only allows translation and rotation, it does not deform features in the image. This allows for accurate comparison of CT scans from two different time-points (preoperative vs. postoperative) of the same patient.

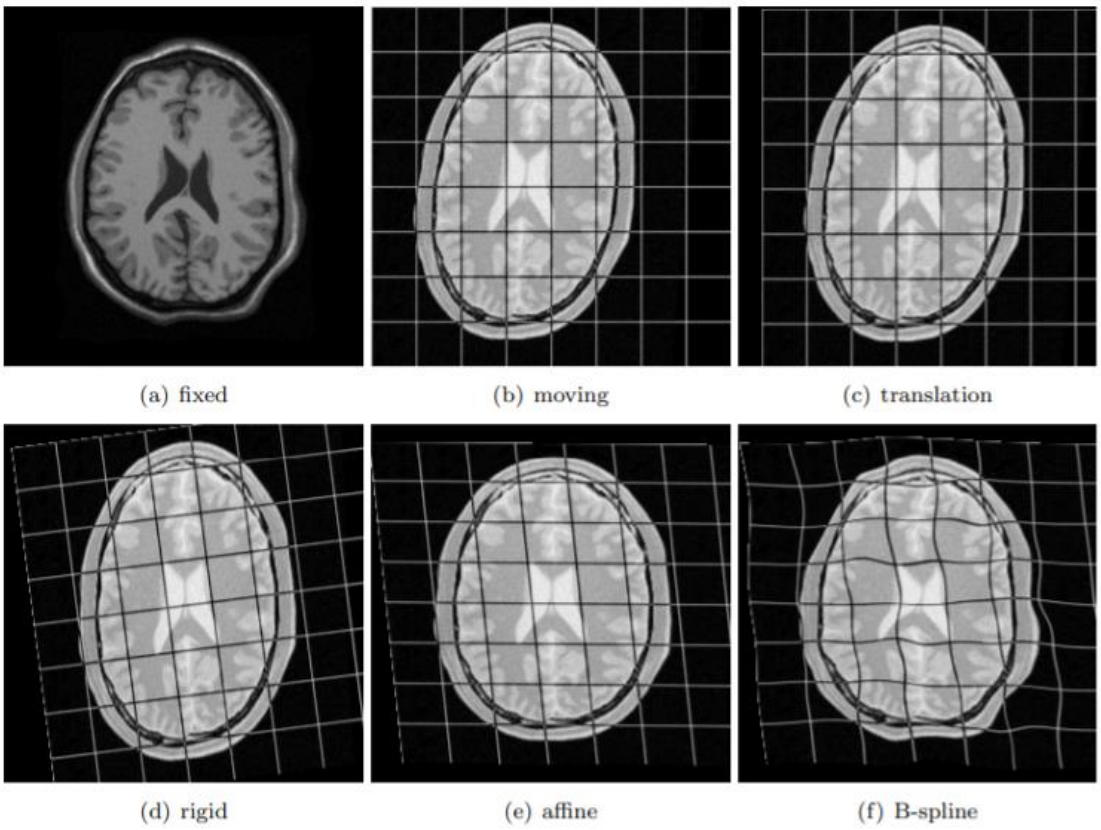

Figure 5. Deformations of the moving image to align with the fixed image using different transformations, including translation (c), rigid transformation (d), affine transformation (e) and non-rigid or deformable transformation (f) [35,36].

Transformation matrices

A 3D rigid transformation consists of a 3D translation vector and a 3D rotation matrix. The rotation matrix can be split up to three different matrices that describe the rotation around the x, y and z-axes. Homogeneous coordinates, representing N-dimensional coordinates with N+1 numbers, are often used for easier computation and to combine translation and rotation. The transformation matrices are specified below.

Translation with vector $t = [t_x\ t_y\ t_z]$:

$$T = \begin{bmatrix} 1 & 0 & 0 & t_x \\ 0 & 1 & 0 & t_y \\ 0 & 0 & 1 & t_z \\ 0 & 0 & 0 & 1 \end{bmatrix}$$

Rotation around the z-axis with angle θ in degrees:

$$R_z(\theta) = \begin{bmatrix} \cos(\theta) & -\sin(\theta) & 0 & 0 \\ \sin(\theta) & \cos(\theta) & 0 & 0 \\ 0 & 0 & 1 & 0 \\ 0 & 0 & 0 & 1 \end{bmatrix}$$

Rotation around the x-axis with angle θ in degrees:

$$R_x(\theta) = \begin{bmatrix} 1 & 0 & 0 & 0 \\ 0 & cos(\theta) & -\sin(\theta) & 0 \\ 0 & \sin(\theta) & \cos(\theta) & 0 \\ 0 & 0 & 0 & 1 \end{bmatrix}$$

Rotation around the y-axis with angle θ in degrees:

$$R_y(\theta) = \begin{bmatrix} \cos(\theta) & 0 & \sin(\theta) & 0 \\ 0 & 1 & 0 & 0 \\ -\sin(\theta) & 0 & \cos(\theta) & 0 \\ 0 & 0 & 0 & 1 \end{bmatrix}$$

Combined translation and rotation:

$$T = \begin{bmatrix} r_{11} & r_{12} & r_{13} & t_x \\ r_{21} & r_{22} & r_{23} & t_y \\ r_{31} & r_{32} & r_{33} & t_z \\ 0 & 0 & 0 & 1 \end{bmatrix}$$

The combined transformation matrix is dependent on the order of translation and rotation.

3.4.2 Surface registration

Surface registration is a similar type of registration as image registration. Instead of aligning images, 3D models are aligned using a certain transformation type.

A 3D model is a collection of points in 3D connected by lines, forming polygons. The points are called vertices and the polygons are called faces. The polygons are usually triangles.

Iterative closest point algorithm

In this thesis, the iterative closest point (ICP) algorithm was used for surface registration of 3D models. In the ICP algorithm a rigid transformation is found to spatially align a moving model with a fixed model and a metric computing the similarity of the models is minimized [34-36].

For each point in the moving model, the closest point in the fixed model is found. Next, a transformation that allows translation and rotation is found using the previously mentioned metric. The transformation is applied and the method is iterated until stopping conditions for registration have been met, such as a minimum residual error or a minimum in the metric.

4 Evaluation of the positioning of virtually planned polyetheretherketone patient-specific implants and surgical guides in craniofacial surgery

Abstract
Purpose: Patient-specific implants (PSIs) and surgical guides are widely used nowadays for the reconstruction of craniofacial defects. In this research, we quantitatively compared the realised position of craniofacial PSIs with the planned position and we calculated the difference between the realised osteotomy and the planned osteotomy if a resection preceded the reconstruction.
Methods: We retrospectively included patients who received a craniofacial polyetheretherketone (PEEK) PSI in the LUMC between February 2019 and January 2021 and had a postoperative CT scan available. Postoperative CT scans were aligned with preoperative CT scans, followed by segmentation of the postoperative PSI position and skull, on which the realised osteotomy was defined by an inner and outer curve. Translation and rotation between the realised PSI position and planned PSI position were calculated as well as the surface distance between the realised osteotomy curves and the planned osteotomy.
Results: 19 patients were included, regarding cranial (n = 11) and orbital (n = 8) implants. The translation vector length ranged from 0.5 mm to 6.7 mm and rotational deviation ranged from 0.9° to 17.4°, both being higher for orbital implants than for cranial implants (U = 3.00, p = .000, U = 15.0, p = .016). 12 patients were included in the osteotomy analysis. Mean distance between realised and planned osteotomy was 1.4 mm (SD 1.6) for outer curves and 0.5 mm (SD 1.7) for inner curves. Absolute mean distances over the two curves ranged from 0.6 mm (SD 0.5) to 4.1 mm (SD 2.6), accurately reproducing the planned osteotomy in most cases.
Conclusion: In this study, there was a large variation in positioning accuracy for craniofacial PSIs. Cranial implants, being in good agreement with the planned PSI positions, were positioned with higher accuracy than orbital implants. In general, realised osteotomies were larger than planned. Better use and positioning of surgical guides could increase the PSI positioning accuracy. Clinical and aesthetical outcomes need to be included in future studies.

4.1 Introduction

Bony craniofacial defects that require reconstructive surgery can be a result of trauma, tumour resection, infection and congenital anomalies [1,2]. Cranioplasty is performed to restore the protection of the underlying brain, whereas reconstruction of the orbital bone aims at retaining symmetrical globe positioning to avoid enophthalmos or diplopia [4-14]. Besides these functional goals, craniofacial reconstructions also serve an aesthetical purpose.

Conventionally, craniofacial reconstructions were performed with autologous bone or allografts but over the years surgeons have started to use alloplastic materials as an alternative. Technological innovations have recently introduced the manufacturing of patient-specific implants (PSIs) that can be designed to the exact shape and size of the defect, using preoperative imaging. As a result, a decrease in operative time spent on contouring and intraoperative implant modifications is reported in literature [10,15]. In addition to PSIs, patient-specific surgical guides can be designed to enable a one-stage surgical procedure for resection and reconstruction.

In order to validate, optimize and improve preoperative planning and placement of PSIs, objective evaluation of the positioning is an important outcome measure. Additionally, PSI positioning can be influenced by the positioning and use of a surgical guide whenever the reconstruction is preceded by a resection.

So far, the positioning of craniofacial PSIs has predominantly been assessed using clinical outcome measures and subjective measures for aesthetics. Quantitative analysis has only been reported in a small amount of studies, concerning (angular) deviation between the postoperative PSI position and the planned PSI position [2,16-18,23], bone-to-implant gap [7,11,12,26] and overlap of the postoperative PSI position with the planned PSI position [13,26,27] but no standard currently exists. Moreover, no quantitative analyses on the osteotomy creation with the use of surgical guides in craniofacial surgery have been reported.

Therefore, the aim of our research was to develop a method to quantitatively evaluate the positioning of craniofacial PSIs and the realised osteotomies and to apply this method to the available patient data from the Department of Maxillofacial surgery at the Leiden University Medical Centre (LUMC).

4.2 Methods

Patients and data collection

Patients who received a craniofacial PSI made from polyetheretherketone (PEEK) in the LUMC in the period of February 2019 to January 2021 and had a postoperative CT scan available were retrospectively included.

For each patient, the STL files of the PSI and the surgical guide, if used, with its osteotomy were available. The osteotomy STL file consists of a curved plane, determining the resection outline.

Data processing

The data processing steps are described below and an overview is presented in figure 1. Appendix I contains the data processing steps in more detail.

a. Image registration

The first step was to align the postoperative CT image with the preoperative CT image. We performed a rigid registration based on the bony anatomy of the skull using Mimics (Materialise, Leuven, Belgium) (figure 1, a).

b. Segmentation

Subsequently, we segmented the skull and the implant on the transformed postoperative CT image using Mimics (figure 1, b). Segmentation techniques that we used include thresholding, region growing, smart fill, erosion and dilation and we performed manual adjustments when necessary. During segmentation of the skull, we paid attention to the edges of the resection to ensure smooth boundaries.

c. Surface registration

In order to account for segmentation inaccuracies or intraoperative adjustments on the implant, we aligned the STL model of the virtually planned implant, or preoperative PSI, with the segmented postoperative PSI using surface registration in 3-Matic (Materialise, Leuven, Belgium) (figure 1, c).

d. *Defining postoperative osteotomy*

For the cases with a resection, we defined two curves on the edges of the bone defect in the postoperative skull to represent the realised osteotomy using 3-Matic (figure 1, d). An outer curve was positioned on the outside of the defect edge, closest to the surface of the skull, and an inner

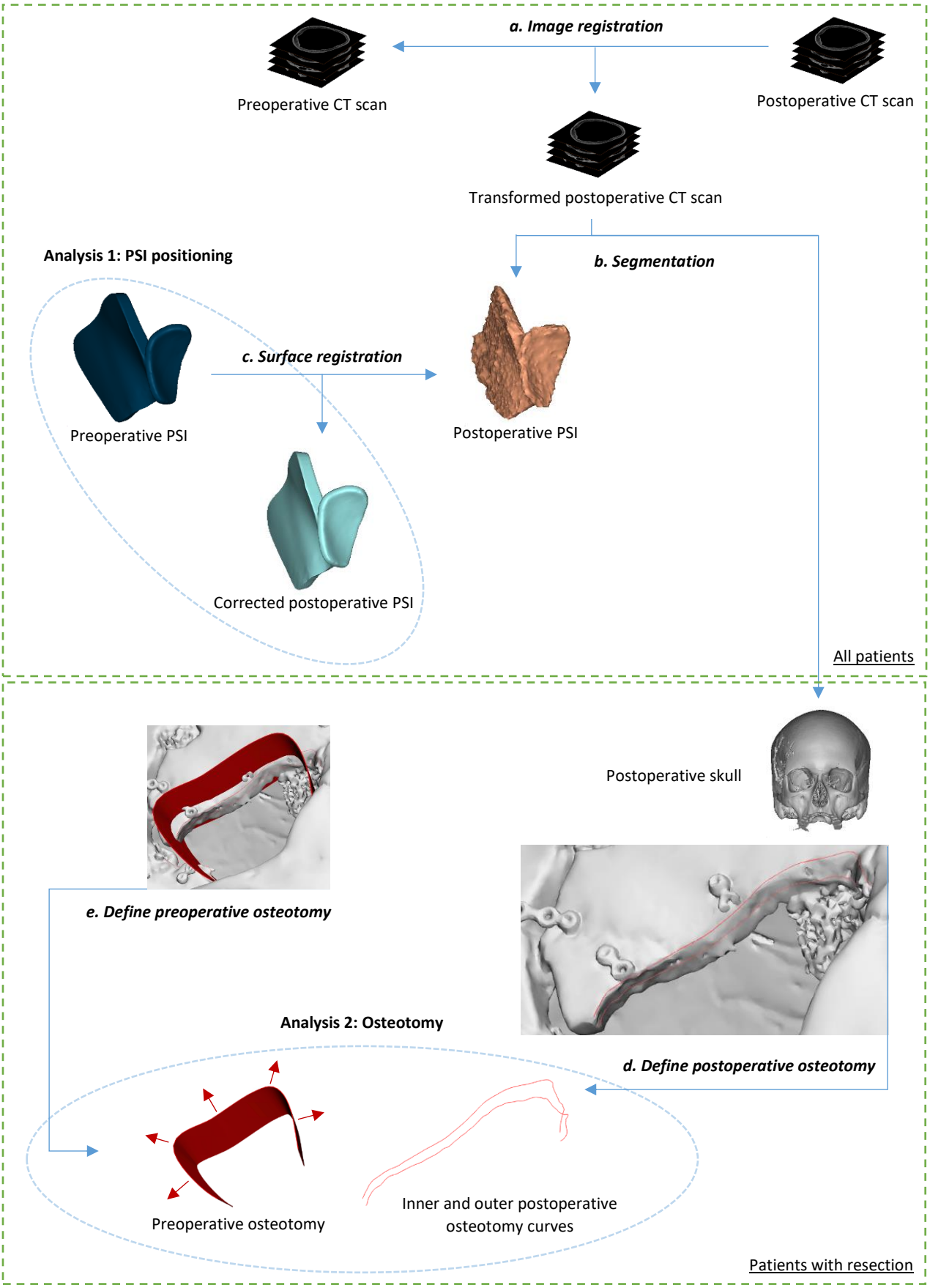

Figure 1. Data processing steps: alignment of postoperative CT scan with preoperative CT scan (a); segmentation of postoperative skull and PSI (b); alignment of preoperative PSI with postoperative PSI (c); creating inner and outer curves that define the postoperative osteotomy (d); defining the preoperative osteotomy (e).

curve was defined on the inside of the defect edge, approximately corresponding to the inner contour of the PSI.

e. Defining preoperative osteotomy

The available osteotomy planes have a thickness of 0.3 mm to be able to perform Boolean operations. For the purpose of this study, we edited the available osteotomy plane in 3-Matic to create an osteotomy surface with no thickness by only including the faces that are located directly adjacent to the surgical guide. In addition, we ensured that the normals of the faces pointed into the direction of the bone edges (figure 1, e).

Analysis

We performed two different analyses. Matlab R2021a (Matworks, Natrick, MA, United States) was used for both analyses. Scripts can be found in Appendix II.

1) PSI positioning

First of all, we calculated the translation and rotation between the corrected postoperative PSI position and the planned PSI position.

For the translation, we used the x, y and z-positions of the vertices of the corrected postoperative PSI and the preoperative PSI to calculate the positions of the centres of mass. Because the models are identical, their centres of mass are in the same position, relative to the model. The following formulas were used (2)(3):

$$\mu_x = \frac{1}{N}\sum_{j=1}^{N} X_j \quad (2.1)$$

$$\mu_y = \frac{1}{N}\sum_{j=1}^{N} Y_j \quad (2.2)$$

$$\mu_z = \frac{1}{N}\sum_{j=1}^{N} Z_j \quad (2.3)$$

with μ being the mean of the x, y or z-coordinates of all vertices that are stored in vector X, Y or Z, made up of *N* vertices.

$$CM_i = [\mu_x\ \mu_y\ \mu_z] \quad (3)$$

The centre of mass (CM) of implant *i,* consisting of an x, y and z-coordinate.

To calculate the translation in millimetres, we subtracted the position of the centre of mass of the preoperative PSI from the position of the centre of mass of the corrected postoperative PSI (4):

$$Translation\ (x, y, z) = CM_{post} - CM_{pre} \quad (4)$$

Translation between the corrected postoperative PSI position and the preoperative PSI position in x, y and z-direction, in millimetres.

In addition, we calculated the length of the translation vector using the following formula (5):

$$|\boldsymbol{u}| = \sqrt{Translation(x)^2 + Translation(y)^2 + Translation(z)^2} \quad (5)$$

with $|\mathbf{u}|$ being the length of the translation vector in millimetres, with a translation *Translation(x,y,z)* in x, y and z-direction.

In order to determine the difference in rotation between the corrected postoperative PSI position and the preoperative PSI position, we repositioned the two models by translating their centres of mass to the origin of the coordinate system (0,0,0).

Subsequently, we performed an iterative closest point (ICP) algorithm on the two models with the preoperative PSI position as fixed model and the corrected postoperative PSI position as moving model. The resulting rotation matrix was converted into Euler angles, providing the angles in radians around the x-axis, y-axis and z-axis. Finally we converted the angles from radians into degrees.

To additionally provide a single rotational deviation for every implant, we calculated the angle around one specific axis through the origin, following Euler's rotation theorem (formula 6):

$$\boldsymbol{\theta} = \theta\, \boldsymbol{v} \qquad (6)$$

with $\boldsymbol{\theta}$ being the axis-angle vector, represented by angle θ in degrees and unit vector **v** [v1, v2, v3] representing the axis.

2) Osteotomy

We used an algorithm from Frisch, D. [41] to compute the shortest distances (surface distances) from the x, y and z-coordinates of the points in the postoperative osteotomy curves to the preoperative osteotomy surface. The points from the inner and outer curves were resampled with an average distance of 0.3 mm between points, to correct for points that were grouped together. The distances were signed according to the normals of the preoperative osteotomy surface to identify on which side of the surface the postoperative points were located. In addition to the distances, the positions of the nearest points on the osteotomy surface were returned (figure 2).

We calculated the mean and the absolute mean over all distances of the inner and outer curves separately: the mean to determine whether the curve was on average realised larger (positive) or smaller (negative) than the planned osteotomy and the absolute mean to determine the overall deviation from the planned osteotomy.

In addition, we calculated the absolute mean distance over the inner and outer curves together to serve as a measure for the average deviation of the realised osteotomy from the planned osteotomy.

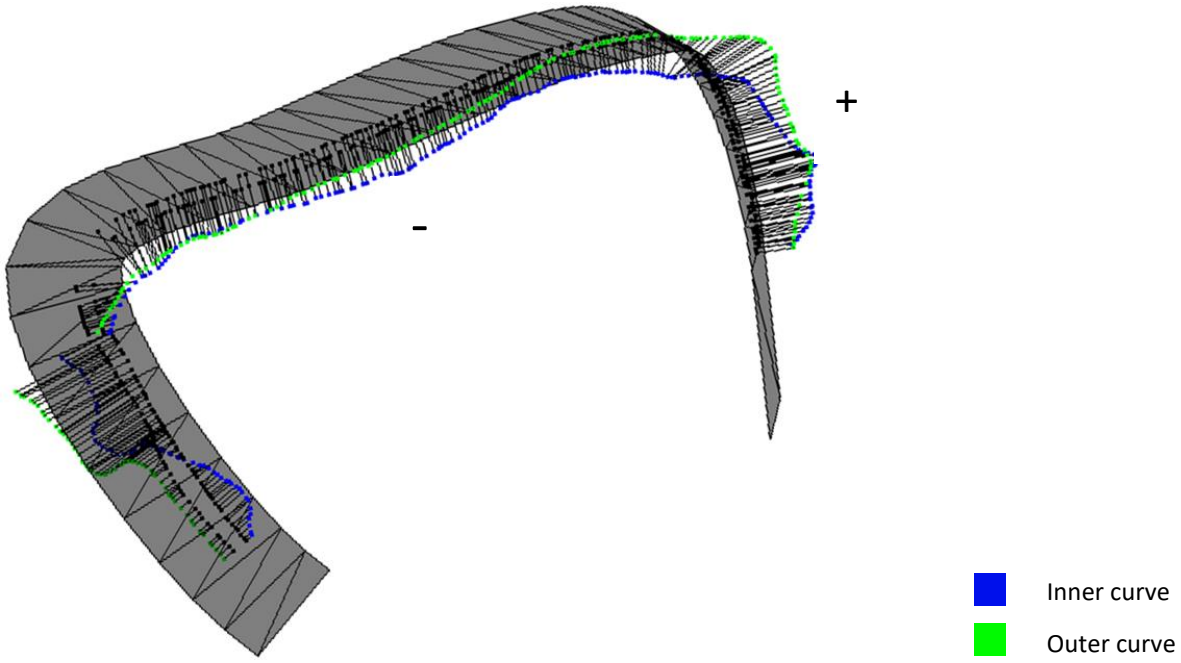

Figure 2. Surface distance calculation between points of the postoperative osteotomy curves (inner curve: blue, outer curve: green) and the preoperative osteotomy surface. The positive sign indicates positive distances (osteotomy realised larger than planned), the negative sign indicates negative distances (osteotomy realised smaller than planned). The black dots are the positions of the nearest points on the osteotomy surface.

Statistical analysis

Statistical analysis was performed using IBM SPSS Statistics 25 (IBM Corp. Released 2017. IBM SPSS Statistics for Windows, Version 25.0. Armonk, NY). We performed a Mann Whitney *U* test to compare the length of the translation vectors and the rotational deviations of the cranial implants with the orbital implants. In addition, we compared the deviation of the inner curve from the planned osteotomy with the deviation of the outer curve from the planned osteotomy. Lastly, we performed a linear regression analysis to determine the relationship between the translational deviation in PSI positioning and the difference between the realised osteotomy and the planned osteotomy. The level of statistical significance was set to 0.05.

4.3 Results

Patient characteristics

In total, we included 19 patients. All 19 patients were available for the PSI positioning analysis. Eight implants concerned the orbit and 11 implants concerned other cranial bones. 13 patients underwent resection before reconstruction. For one patient, no osteotomy model was available and was therefore excluded from the osteotomy analysis. Eventually, 12 patients were available for the osteotomy analysis (5 concerning the orbit, 7 concerning other cranial bones). Median follow-up time was 3.5 months. Patient characteristics, including indication for and location of reconstruction and time to follow-up CT scan are presented in table 1.

Table 1. Patient characteristics including indication for reconstruction, location, whether a planned resection was performed before reconstruction and approximate time to follow-up CT scan in months (m), days (d) or hours (h).

Case	Age	Sex	Indication	Location	Planned resection	Time to follow-up
1	48	F	Hemangioma	Zygoma, left	Yes	10 m
2	59	F	Meningioma	Frontal	Yes	6 m
3	17	M	Meningioma	Frontal	Yes	6 m
4	57	F	Meningioma	Frontal	Yes*	3 m
5	55	F	Squamous cell carcinoma	Maxillary sinus, ethmoid, frontal sinus, right	Yes	1.5 m
6	36	F	Hemangioma	Lateral wall frontal sinus, right	Yes	4.5 m
7	29	M	Juvenile psammomatoid ossifying fibroma (JPOF)	Frontal sinus	Yes	2 m
8	62	F	Meningioma	Frontal, left	Yes	1 h
9	54	F	Hemangioma	Orbit wall, right	Yes	9 m
10	53	F	Meningioma	Spheno-orbital, right	Yes	2 m
11	47	F	Meningioma	Spheno-orbital, left	Yes	4.5 m
12	51	F	Meningioma	Spheno-orbital, left	Yes	5 m
13	48	F	Meningioma	Spheno-orbital, right	Yes	4.5 m
14	25	M	Decompressive craniectomy	Bifrontal	No	2 d
15	63	F	Bone flap removal due to infection	Cranium, right	No	3.5 m
16	44	F	Craniectomy for cerebral infarction	Cranium, left	No	2.5 m
17	48	F	Meningioma	Spheno-orbital, right	No	5 m
18	39	F	Meningioma	Spheno-orbital, left	No	2.5 m
19	44	F	Meningioma	Spheno-orbital, left	No	0.5 m

*osteotomy model not available

Patient-specific implant positioning

The length of the translation vector ranged from 0.5 mm to 6.7 mm over all implants (figure 2). The mean translation vector length for cranial implants (n = 11) was 1.5 mm (SD 0.7) and for orbital implants (n = 8) 4.8 mm (SD 1.5). The mean translation vector length was significantly higher for the orbital implants than for the cranial implants, U = 3.00, p = .000.

The outlier for orbital implants represented the shortest orbital translation vector (1.6 mm).

Figure 3 shows the rotational deviation in angles around a fixed axis, ranging from 0.9° to 17.4°. For cranial implants the mean rotational deviation was 5.0° (SD 4.5). For orbital implants the mean rotational deviation was 10.6° (SD 4.6), significantly higher than for the cranial implants, U = 15.0, p = .016.

Individual translations in x, y and z-direction, lengths of translation vectors, rotational deviations around specific axes and rotations around x, y and z-axes are presented in Appendix III and V.

The realised PSI position and the planned PSI position of cases 16 and 10 are visualized in figures 4 and 5 respectively. The first one is a cranial implant with a translation vector length of 1.1 mm and a rotational deviation of 0.9°. The second one is an orbital implant for which the length of the translation vector was 6.7 mm and the rotational deviation was 17.4°.

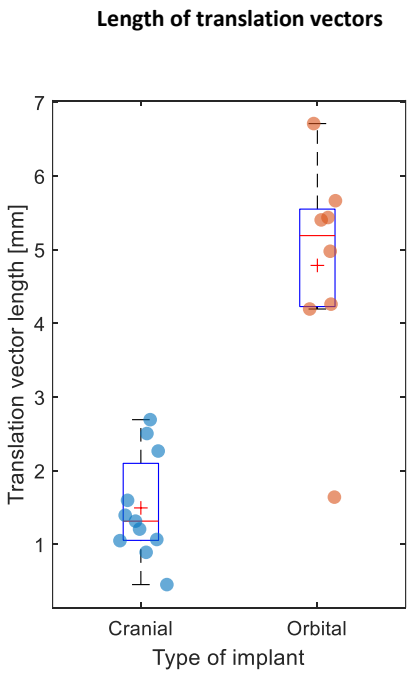

Figure 2. Boxplot of translation vector length in millimetres from the realised PSI position to the planned PSI position, visualized for cranial and orbital implants separately. The red line indicates the median, the red plus indicates the mean and the bottom and top of the boxes represent the 25th and 75th percentiles of the samples.

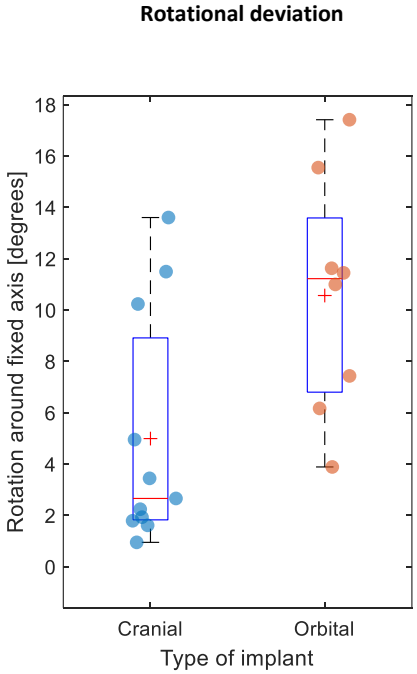

Figure 3. Boxplot of the rotation around a fixed axis in degrees from the realised PSI position to the planned PSI position, visualized for cranial and orbital implants separately. The red line indicates the median, the red plus indicates the mean and the bottom and top of the boxes represent the 25th and 75th percentiles of the samples.

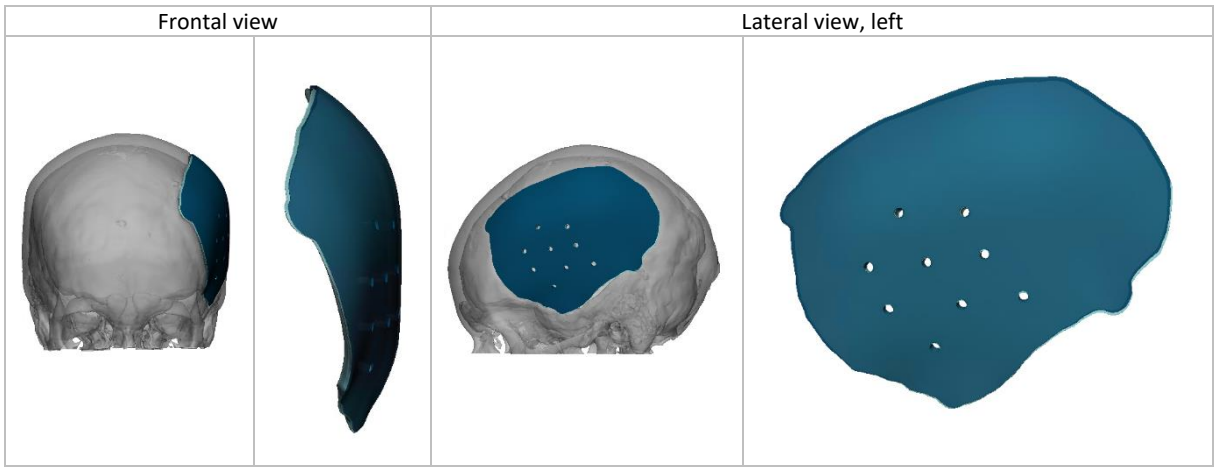

Figure 4. Case 16: cranial implant following craniectomy, left. Dark blue-coloured model represents the planned PSI position, light blue-coloured model represents the realised PSI position.

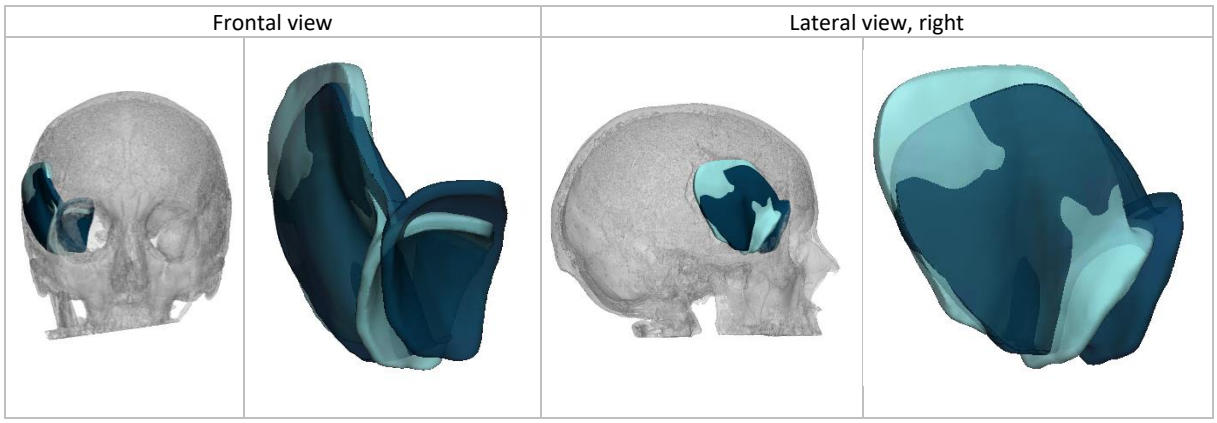

Figure 5. Case 10: spheno-orbital meningioma, right. Dark blue-coloured model represents the planned PSI position, light blue-coloured model represents the realised PSI position.

Osteotomies

Mean distances between the realised osteotomies, represented by the inner and outer curves, and the planned osteotomies are presented in figure 6.

The mean distance between the outer curves and the planned osteotomies over all cases was 1.4 mm (SD 1.6). On average, the realised resections at the outer curves were larger than planned. The mean distance between the inner curves and the planned osteotomies was 0.5 mm (SD 1.7), also indicating that the realised resections were on average larger than planned.

No significant difference was found between the inner and outer curves.

The absolute mean distances between the inner and outer curves and the planned osteotomies are visualized in figure 7. The mean over the two curves is also indicated for every case.

The large standard deviation of the absolute mean for case 2 was caused by a high maximum distance at a certain location of the curves (16.8 mm for the outer curve and 14.1 mm for the inner curve), due to initially wrong use of the surgical guide. However, at other positions of the curves, the realised osteotomy was comparable with the planned osteotomy with a mean distance of 2.7 mm.

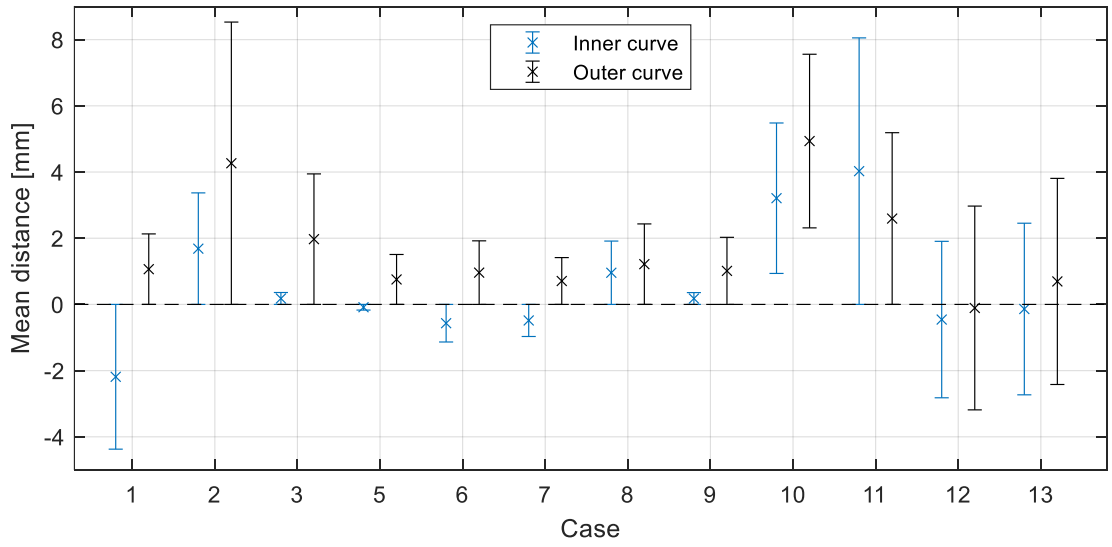

Figure 6. Mean distances in millimetres between the inner (blue) and outer (black) curves, representing the realised osteotomies, and the planned osteotomies. Crosses indicate the mean, error bars represent the standard deviation in positive and negative direction from the mean. A dashed line displays the division between positive and negative mean distances.

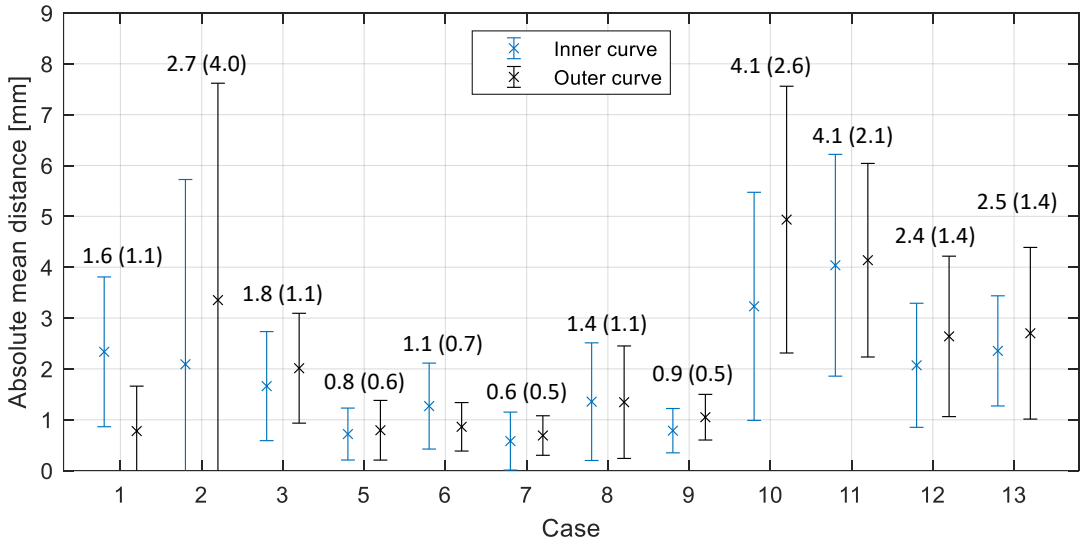

Figure 7. Absolute mean distances in millimetres between the inner (blue) and outer (black) curves, representing the realised osteotomies, and the planned osteotomies. The crosses indicate the mean, the error bars represent the standard deviation in positive and negative direction from the mean. The absolute mean distances (SD) of the inner and outer curves together are specified above the error bars.

Absolute mean distances of 4.1 mm (SD 2.6) and 4.1 mm (SD 2.1) were found for cases 10 and 11 respectively. For these cases, and for case 12 (absolute mean distance = 2.4 (SD 1.4)), no surgical guide was used to create the resection outline, for surgical and logistic reasons (figure 8).

Appendix IV and V contain all individual numbers for the (absolute) mean, minimum and maximum distances between the outer/inner curves and the planned osteotomies.

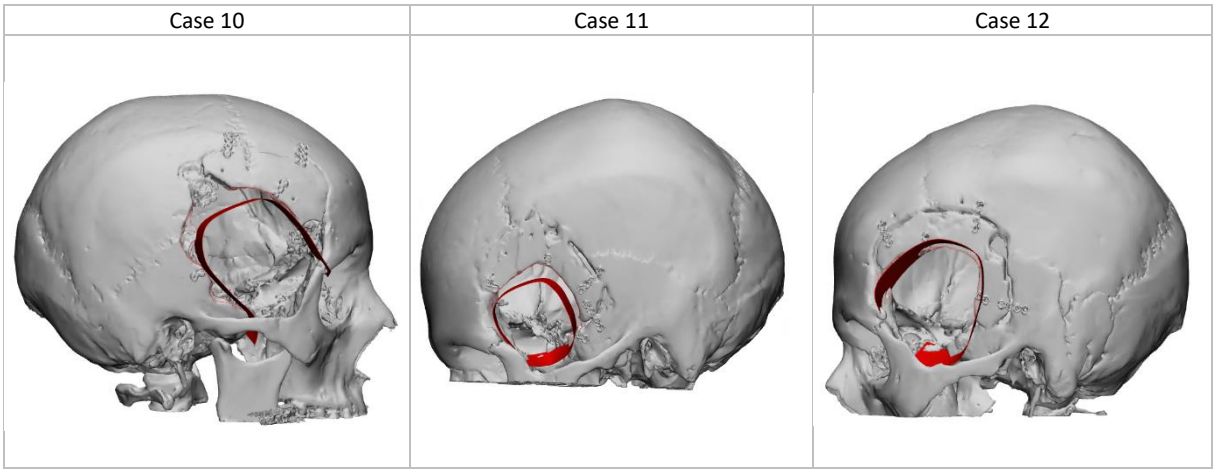

Figure 8. Planned osteotomy visualized in red and realised osteotomy visualized in red lines for inner and outer curves on the postoperative skull, for cases 10, 11 and 12.

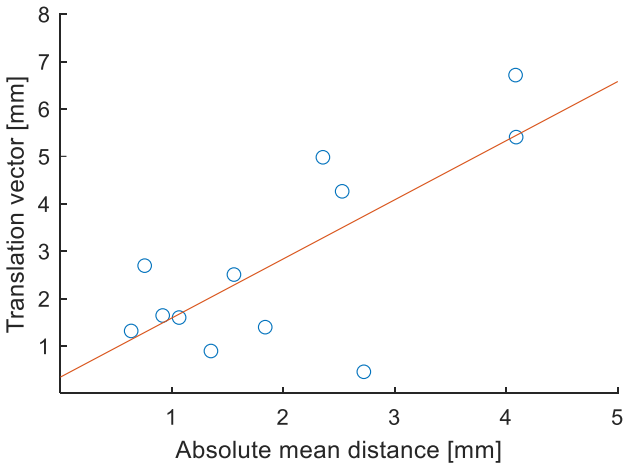

Figure 9. Scatter plot of the relation between the absolute mean distance of the realised osteotomy from the planned osteotomy and the translation vector from the realised PSI position and the planned PSI position. The regression line is represented by y = 0.343 + 1.247x.

We found a significant positive relationship between the absolute mean deviation from the planned osteotomy and the length of the translation vector from the realised PSI position to the planned PSI position (R^2 = 0.537, F(1.10) = 11.587, p = .007). Figure 9 shows the relation between the two variables.

4.4 Discussion

The aim of this study was to calculate the difference between the realised position of craniofacial patient-specific implants and the planned position and in addition determine the deviation of the realised osteotomy from the planned osteotomy when a resection preceded the reconstruction.

In this study of 19 patients, the translational and rotational deviation between the realised and planned PSI positions ranged from 0.5 mm to 6.7 mm and 0.9° and 17.4° respectively. This shows a large variation in positioning accuracy. The realised osteotomies in the 12 patients who underwent resection before reconstruction were on average larger than planned. The absolute mean deviation ranged from 0.6 mm (SD 0.5 mm) to 4.1 mm (SD 2.6 mm), accurately reproducing the planned osteotomies in most cases.

A significant positive relationship was found between the absolute mean deviation from the planned osteotomy and the translational deviation in PSI positioning ($R^2 = 0.537$, $F(1.10) = 11.587$, $p = .007$). The low determination coefficient however warns for a bad fit of the regression line, which can be explained by the small sample size. Nevertheless it is intuitively expected that correct osteotomy creation is necessary to obtain PSI position according to plan.

Within our study, patients had varying indications for reconstruction, regarding different parts of the skull. Because orbital implants not only regard the cranium but also extent into the orbit, these implants are usually more difficult to reach. In line with that, we found that the translational and rotational deviations were higher for orbital implants than for cranial implants ($p = .000$ and $p = .016$ respectively). Cranial implants had a mean translation vector length of 1.5 mm (SD 0.7 mm) and rotational deviation of 5.0° (SD 4.5°), while this was 4.8 mm (SD 1.5 mm) and 10.6° (SD 4.6°) for orbital implants.

The translational deviations that we found for cranial implants are not entirely consistent with previous studies. Zhang, et al. [2] reported higher accuracy of cranial implant positioning in 12 patients with a mean 3D deviation of 0.27 mm (SD 0.07 mm) and Tel, et al. [16] produced a mean Euclidean distance of 0.64 mm (SD 0.49 mm) between nodes of 9 cranial implants. A possible explanation can be the use of surgical navigation in both studies, to accurately position the implant intraoperatively.

Additionally, Kärkkäinen, et al. [17] and Schreurs, et al. [23] both showed lower translational deviations than we did for orbital implants. Kärkkäinen, et al. measured mean deviations of 1.8 mm, 2.0 mm and 1.9 mm anteromedially, anterolaterally and cranially for 15 implants following orbital fractures. Schreurs, et al. [23] found translations of 1.5 mm and 1.6 mm for two patients receiving an orbital implant. Additionally, a roll, pitch and yaw of -4.5°, 2.6°, 0.8° for patient 1 and 3.4°, -2.3°, 4.5° for patient 2 were calculated, which were smaller angular deviations than we found. Another study from Rana et, al. [19] reported mean angles for orbital implants that were more comparable to our findings. They measured a mean anterior, medial and posterior angle of 4.1° (SD 0.7°), 8.2° (SD 1.9°) and 8.2° (SD 1.4°) respectively. Similarly to us, Rana, et al. did not use surgical navigation. It must be mentioned however, that the orbital implants in these studies regarded reconstructions that were restricted to the orbital walls and floor. These are different orbital implants than the implants in this study, which impedes direct comparison with our results.

To the best of our knowledge, this is the first study to publish quantitative results on the realisation of osteotomies created with a surgical guide in craniofacial reconstructions. Studies that have performed quantitative analyses are mainly studies on the use of resection templates for mandibular reconstructions. These are, however, straight resections instead of curved [39].

Other studies regarding craniofacial reconstructions have only mentioned guide positioning without performing a quantitative analysis. Scheurs, et al. [23] proved accurate guide positioning during orbitozygomatic reconstructions by navigational feedback or rigid feedback such as matching screw hole locations in the guide and skull. Tel, et al. [16] reported a submillimetric difference between creation of the cranial osteotomy using surgical navigation and refinement of the osteotomy with the surgical guide. In one cranio-orbital case, reported by Gerbino, et al. [11], extensive adaptation of the implant and bone edges were necessary, because the intraoperative resection did not match the planned resection due to malpositioning of the surgical guide. This supports the relationship between the absolute mean deviation from the planned osteotomy and the translational deviation in PSI positioning that we found in this study.

One of the weaknesses of this study is that we calculated translation and rotation with respect to the x, y and z-axes of the patient coordinate system. These axes however, are not consistent throughout all patients due to different positioning in the CT scanner. This hampers the possibility to compare the translations and rotations of all patients. Along with that, the axes are not always in line with the natural head position and a translation in x, y and z-direction does not directly correspond to a left/right, anterior/posterior and inferior/superior translation respectively. Providing immediate anatomical feedback on the direction the PSI should have been translated or rotated is therefore difficult.

Secondly, lack of contrast between the implant and surrounding tissue and metal artefacts from screws and plates securing the implant sometimes complicated the segmentation of the postoperative implant and skull. The segmentation was a manual operation which might have caused inter and intra-observer variability. Although the effect of this variability on our results is expected to be limited, segmentation could be repeated using multiple observers to exclude this factor.

We minimized the implant segmentation errors by aligning the virtually planned PSI model with the segmented postoperative PSI, finding the optimal overlap and with that the assumed postoperative PSI position. In the analysis, we used this assumed postoperative position for comparison with the planned PSI position. However, intraoperative alterations to the implants could have caused inaccurate surface registration, leading to inaccurate translational or rotational deviations in the analysis. We primarily noticed this potential inaccuracy in cases 1 and 6 which were small implants without substantial curvature, and we expect this effect to be minimal in the other cases.

The main issue with the analysis of the osteotomies, was defining the postoperative osteotomy. Postoperative bone edges were generally not smooth and straight-cut due to segmentation errors or ossification of bone edges or surfaces. The latter can be explained by the median follow-up time of 3.5 months. The curves had to be defined manually, which undoubtedly has introduced random measurement errors. Once more, repeating the creation of curves by multiple observers might reduce these errors.

We have seen a large variation in implant positioning accuracy. In general, cranial implants have been positioned with higher accuracy than orbital implants. A possible explanation for this is that orbital implants extent into the skull where they cannot easily be visualized or reached intraoperatively. When the reconstruction regards a resection, the interior part of the resection is performed manually. In such cases, surgical navigation could provide essential anatomical feedback. In addition, the positioning partially depends on the placement of the cranial part of the implant, which requires accurate bone edges or resection outlines according to the virtual plan. Alternatively, orbital implants are usually positioned in close proximity of the temporal muscle. This is an anatomical structure that commonly complicates PSI positioning.

The high translational and rotational deviations that were found for case 10 (6.7 mm and 17.4°) can be explained by the fact that no surgical guide was used to create the planned resection outline. This caused high deviations from the planned osteotomy with a maximum of 10.2 mm for the outer curve and 9.4 mm for the inner curve. Similar maximum deviations from the planned osteotomy were found for cases 11 and 12 in which the resection was also performed without surgical guide (8.3 mm and 8.8 mm for the outer curve and 8.4 mm and 6.8 mm for the inner curve respectively). Finally, no surgical guide was designed for the resection in case 17, which resulted in a high rotational deviation of 15.5°.

Rotational deviations that were substantially higher than average for cranial implants were noticed in cases 1, 3 and 7 (10.2°, 13.6° and 11.5°). Difficulties regarding surgical guide positioning were reported in the first two cases. For cases 1 and 7, intraoperative modifications on the implant were performed due to suboptimal design or intraoperative adjustment of the resection for clinically relevant reasons. These are potential contributors to an increased angular deviation.

For the majority of implants, intraoperative adjustments were negligible. In three cases we noticed however, that implant alterations were performed at the location where the realised PSI position deviated from the planned PSI position. This indicates that malpositioning of the PSI can increase operative time spent on intraoperative modifications, while a decrease in operative time is supposed to be one of the main advantages of patient-specific implants. Alterations around the nasal bone and the temporal muscle were identified in four cases, accentuating the anatomical structures to take into consideration during the design of the implant.

Case 9 showed the lowest translational deviation for orbital implants (1.6 mm), but the rotational deviation was 11.0°. We noticed that the rotational deviation was in accordance with the deviation from the planned osteotomy. This suggests that the surgical guide was malpositioned with a rotational component. We found similar results for case 3, where an inaccurate fit of the guide was reported intraoperatively and a rotational deviation from the planned osteotomy corresponded to the rotational deviation of the PSI postoperatively. These cases emphasize the importance of accurate surgical guide positioning.

To obtain accurate guide positioning, the guide should be compact, not interfering with soft tissue. At the same time, it must be thick enough around the edges to create a resection outline with an angular offset. Moreover, the guide should fit the patient's anatomy in one specific position. Apart from guide positioning, correct use of the surgical guide should not be underestimated. This was proven by the wrongly created outline of the resection in case 2.

Finally, it appeared that the inner curves of the osteotomies were frequently created smaller than the outer curves. This suggests that the resection outline might be created cautiously, being too superficial or with a different angular offset than the surgical guide provides. As a result, multiple adjustments to the bone edges or implant subsequently have to be made in order to fit the implant, increasing operative time.

Taking into consideration the main goals for cranial reconstruction, a translational and a rotational deviation of 1.5 mm (SD 0.7 mm) and 5.0° (SD 4.5°) are only clinically relevant when the underlying brain is left unprotected or the contour, shape and symmetry of the skull is substantially interrupted. Naturally, lower deviations decrease the chance of implant-to-bone gaps and therewith the interruption of the skull. For orbital implants, the functional goal includes retaining symmetrical globe positioning in order to eliminate enophthalmos and diplopia. Incorrect positioning of the orbital implant can cause an enlargement in orbital volume, which can increase the chance of these clinical complications. The translational deviation of 4.8 mm (SD 1.5 mm) and the rotational deviation

of 10.6° (SD 4.6°) show that improvement of orbital implant positioning is necessary, but including measurements on the orbital volume may provide additional clinical feedback in future studies.

It is important to consider that although bony reconstruction might be accurate, soft tissue changes may be unpredictable and may limit aesthetic and morphological outcomes. Because this was a quantitative analysis study, we did not include clinical or aesthetical outcomes. In future research this quantitative data should be expanded with clinical outcomes, such as complication rate and operative time. The latter might increase when intraoperative implant modifications are necessary. Most importantly, aesthetic appearance can be researched by patient and surgeon satisfaction.

A deviation from the planned osteotomy is clinically relevant when this leads to inaccurate PSI positioning, but more essentially when this regards tumour resection. Although resection is always performed by experienced surgeons that have the ability to distinguish tumour tissue from healthy tissue, wrong placement of the surgical guide can subsequently alter the resection margins of the tumour. Fortunately, all tumours that were included in this study were benign, but incomplete removal can ultimately lead to recurrence of the tumour.

In this study, we found a large variation in positioning accuracy of craniofacial patient-specific implants. The realised position of cranial implants were in good agreement with the planned position, whereas orbital implants had a higher translational and rotational deviation. Realised osteotomies were generally larger than planned.

Positioning accuracy of craniofacial patient-specific implants could potentially increase by better use and positioning of surgical guides and introduction of surgical navigation. Future research should additionally include clinical and aesthetic outcomes.

5 Conclusion

To conclude my thesis, I have provided an answer to my main research questions and sub questions.

1) What are the differences between the realised PSI positions and the planned PSI positions?

A method has been developed to calculate the translational and rotational deviation between realised PSI positions and planned PSI positions. For the 19 patients that were included in the study, the translational deviation ranged from 0.5 mm to 6.7 mm and the rotational deviation ranged from 0.9° to 17.4°, showing a large variation in positioning accuracy. Different reasons for high deviations have been addressed, including implant design, reconstruction site and the use of surgical guides.

2) What are the differences between the realised osteotomies and the planned osteotomies?

To the best of our knowledge, we are the first to have developed a method to calculate the difference between realised osteotomies and planned osteotomies for craniofacial reconstructions. In general, realised osteotomies were larger than planned for the 12 patients undergoing resection before reconstruction. The absolute mean deviation ranged from 0.6 mm (SD 0.5 mm) to 4.1 mm (SD 2.6 mm), accurately reproducing the planned osteotomies in most cases. Cases with the highest deviation were cases where the surgical guide was not used correctly, or not used at all.

a) Is there a difference in deviation from the preoperative PSI position between cranial implants and orbital implants?

In accordance with the fact that orbital implants extent into the orbit and are therefore more difficult to reach than cranial implants, both translational and rotational deviation from the planned PSI position were significantly larger for orbital implants than for cranial implants ($p = .000$ and $p = .016$). A mean translational deviation of 1.5 mm (SD 0.7 mm) and a mean rotational deviation of 5.0° (SD 4.5°) were measured for cranial implants, while this was 4.8 mm (SD 1.5 mm) and 10.6° (SD 4.6°) for orbital implants.

b) How does a difference between the realised osteotomy and planned osteotomy influence the positioning of the PSI?

A significant positive relationship was found between the absolute mean deviation from the planned osteotomy and the translational deviation in PSI positioning ($R^2 = 0.537$, $F(1.10) = 11.587$, $p = .007$). The sample size however was low, so more data is needed to support this statement. Nevertheless there were a number of cases that demonstrated the importance of accurate osteotomy creation in order to obtain accurate PSI positioning.

6 References

1. Rudman, K., C. Hoekzema, and J. Rhee, *Computer-assisted innovations in craniofacial surgery.* Facial Plast Surg, 2011. **27**(4): p. 358-65.
2. Zhang, L., et al., *Computer-Aided Design and Computer-Aided Manufacturing Hydroxyapatite/Epoxide Acrylate Maleic Compound Construction for Craniomaxillofacial Bone Defects.* J Craniofac Surg, 2015. **26**(5): p. 1477-81.
3. Scolozzi, P., A. Martinez, and B. Jaques, *Complex orbito-fronto-temporal reconstruction using computer-designed PEEK implant.* J Craniofac Surg, 2007. **18**(1): p. 224-8.
4. Alonso-Rodriguez, E., et al., *Polyetheretherketone custom-made implants for craniofacial defects: Report of 14 cases and review of the literature.* J Craniomaxillofac Surg, 2015. **43**(7): p. 1232-8.
5. Järvinen, S., et al., *The use of patient specific polyetheretherketone implants for reconstruction of maxillofacial deformities.* J Craniomaxillofac Surg, 2019. **47**(7): p. 1072-1076.
6. Jonkergouw, J., et al., *Outcome in patient-specific PEEK cranioplasty: A two-center cohort study of 40 implants.* J Craniomaxillofac Surg, 2016. **44**(9): p. 1266-72.
7. Moser, M., et al., *Patient-specific polymethylmethacrylate prostheses for secondary reconstruction of large calvarial defects: A retrospective feasibility study of a new intraoperative moulding device for cranioplasty.* J Craniomaxillofac Surg, 2017. **45**(2): p. 295-303.
8. Rammos, C.K., et al., *Patient-specific polyetheretherketone implants for repair of craniofacial defects.* J Craniofac Surg, 2015. **26**(3): p. 631-3.
9. Chepurnyi, Y., et al., *Automatic evaluation of the orbital shape after application of conventional and patient-specific implants: Correlation of initial trauma patterns and outcome.* J Oral Biol Craniofac Res, 2020. **10**(4): p. 733-737.
10. Gerbino, G., et al., *Single-step resection and reconstruction using patient-specific implants in the treatment of benign cranio-orbital tumors.* J Oral Maxillofac Surg, 2013. **71**(11): p. 1969-82.
11. Gerbino, G., et al., *Primary and secondary reconstruction of complex craniofacial defects using polyetheretherketone custom-made implants.* J Craniomaxillofac Surg, 2015. **43**(8): p. 1356-63.
12. Jalbert, F., et al., *One-step primary reconstruction for complex craniofacial resection with PEEK custom-made implants.* J Craniomaxillofac Surg, 2014. **42**(2): p. 141-8.
13. Stoor, P., et al., *Rapid prototyped patient specific implants for reconstruction of orbital wall defects.* J Craniomaxillofac Surg, 2014. **42**(8): p. 1644-9.
14. Tarsitano, A., et al., *Orbital Reconstruction: Patient-Specific Orbital Floor Reconstruction Using a Mirroring Technique and a Customized Titanium Mesh.* J Craniofac Surg, 2016. **27**(7): p. 1822-1825.
15. Manrique, O.J., et al., *Craniofacial reconstruction using patient-specific implants polyether ether ketone with computer-assisted planning.* J Craniofac Surg, 2015. **26**(3): p. 663-6.
16. Tel, A., et al., *Computer-Guided In-House Cranioplasty: Establishing a Novel Standard for Cranial Reconstruction and Proposal of an Updated Protocol.* J Oral Maxillofac Surg, 2020. **78**(12): p. 2297.e1-2297.e16.

17. Kärkkäinen, M., et al., *Primary reconstruction of orbital fractures using patient-specific titanium milled implants: the Helsinki protocol.* Br J Oral Maxillofac Surg, 2018. **56**(9): p. 791-796.

18. Rana, M., et al., *Increasing the accuracy of orbital reconstruction with selective laser-melted patient-specific implants combined with intraoperative navigation.* J Oral Maxillofac Surg, 2015. **73**(6): p. 1113-8.

19. van de Vijfeijken, S., et al., *The use of cranial resection templates with 3D virtual planning and PEEK patient-specific implants: A 3 year follow-up.* J Craniomaxillofac Surg, 2019. **47**(4): p. 542-547.

20. Gordon, C.R., et al., *First-in-Human Experience With Integration of a Hydrocephalus Shunt Device Within a Customized Cranial Implant.* Oper Neurosurg (Hagerstown), 2019. **17**(6): p. 608-615.

21. Jindal, S., et al., *3D printed composite materials for craniofacial implants: current concepts, challenges and future directions.* The International Journal of Advanced Manufacturing Technology, 2020.

22. Miljanovic, D., et al., *Design and Fabrication of Implants for Mandibular and Craniofacial Defects Using Different Medical-Additive Manufacturing Technologies: A Review.* Ann Biomed Eng, 2020. **48**(9): p. 2285-2300.

23. Schreurs, R., et al., *The orbit first! A novel surgical treatment protocol for secondary orbitozygomatic reconstruction.* J Craniomaxillofac Surg, 2017. **45**(7): p. 1043-1050.

24. Tunçbilek, G., et al., *Spring-mediated cranioplasty in patients with multiple-suture synostosis and cloverleaf skull deformity.* J Craniofac Surg, 2012. **23**(2): p. 374-7.

25. Schreurs, R., et al., *Quantitative Assessment of Orbital Implant Position--A Proof of Concept.* PLoS One, 2016. **11**(3): p. e0150162.

26. Stieglitz, L.H., et al., *Intraoperative fabrication of patient-specific moulded implants for skull reconstruction: single-centre experience of 28 cases.* Acta Neurochir (Wien), 2014. **156**(4): p. 793-803.

27. Ming-Chi Hsieh, A., et al., *Esthetic Occipital Augmentation With Computer-Aided Design-Computer-Aided Manufacturing Prefabricated Customized Polymethyl Methacrylate Implant: Comparison of Planned and Final Results.* J Oral Maxillofac Surg, 2020. **78**(7): p. 1191.e1-1191.e8.

28. Cha, J.H., et al., *Application of Rapid Prototyping Technique and Intraoperative Navigation System for the Repair and Reconstruction of Orbital Wall Fractures.* Arch Craniofac Surg, 2016. **17**(3): p. 146-153.

29. Blumenfeld, H. *Neuroanatomy Through Clinical Cases*. 2nd ed. Sunderland, (MA): Sinauer Associates, Inc; 2010. 157-158 p.

30. Marbacher, S. et al. *Intraoperative patient-specific reconstruction of partial bone flap defects after convexity meningioma resection.* World Neurosurgery, 2013; **79**(1):124-30.

31. Fisher, F.L., et al. *Surgery as a safe and effective treatment option for spheno-orbital meningioma: a systematic review and meta-analysis of surgical techniques and outcomes.* Acta Ophthalmol. 2021 Feb;**99**(1):26-36.

32. Reis B.L., et al. *Primary hemangioma of the skull*. Arq Neuropsiquiatr. 2008 Sep;66(3A):569-71.

33. Politi, M., et al. *Intraosseous hemangioma of the skull with dural tail sign: radiologic features with pathologic correlation.* AJNR Am J Neuroradiol. 2005 Sep;26(8):2049-52.

34. Yoo, T.S. *Insight into images. Prinicples and practice for segmentation, registration, and image analysis.* Wellesey (MA): A K Peters, Ltd; 2004. 119-128 p.

35. S. Klein, M. Staring, K. Murphy, M.A. Viergever, J.P.W. Pluim, "elastix: a toolbox for intensity based medical image registration," IEEE Transactions on Medical Imaging, vol. 29, no. 1, pp. 196 - 205, January 2010.

36. D.P. Shamonin, E.E. Bron, B.P.F. Lelieveldt, M. Smits, S. Klein and M. Staring, "Fast Parallel Image Registration on CPU and GPU for Diagnostic Classification of Alzheimer's Disease", Frontiers in Neuroinformatics, vol. 7, no. 50, pp. 1-15, January 2014.

37. Keklikoglou, K., et al. *Micro-computed tomography for natural history specimens: a handbook of best practice protocols.* European Journal of Taxonomy. 2019: 522. 1-55. 10.5852/ejt.2019.522.

38. Rohner, D., et al. *Importance of patient-specific intraoperative guides in complex maxillofacial reconstruction.* J Craniomaxillofac Surg. 2013 Jul;41(5):382-90. doi: 10.1016/j.jcms.2012.10.021. Epub 2012 Dec 8. PMID: 23228282.

39. Weijs, W.L., et al. *Accuracy of virtually 3D planned resection templates in mandibular reconstruction*. J Craniomaxillofac Surg. 2016 Nov;44(11):1828-1832. doi: 10.1016/j.jcms.2016.08.024. Epub 2016 Sep 9. PMID: 27713052.

40. Mascha, F., et al. *Accuracy of computer-assisted mandibular reconstructions using patient-specific implants in combination with CAD/CAM fabricated transfer keys*. J Craniomaxillofac Surg. 2017 Nov;45(11):1884-1897. doi: 10.1016/j.jcms.2017.08.028. Epub 2017 Sep 5. PMID: 28965991.

41. Daniel Frisch (2021). point2trimesh( ) — *Distance Between Point and Triangulated Surface* (https://www.mathworks.com/matlabcentral/fileexchange/52882-point2trimesh-distance-between-point-and-triangulated-surface), MATLAB Central File Exchange. Retrieved June 15, 2021.

42. Caiti, G., et al. *Positioning error of custom 3D-printed surgical guides for the radius: influence of fitting location and guide design*. Int J CARS 13, 507–518 (2018). https://doi.org/10.1007/s11548-017-1682-6

43. Van den Broeck, J., et al. *Preoperative analysis of the stability of fit of a patient-specific surgical guide*. Computer Methods in Biomechanics and Biomedical Engineering, 2015;18:1, 38-47, DOI: 10.1080/10255842.2013.774383

44. Damstra, J., et al. *Simple technique to achieve a natural position of the head for cone beam computer tomography.* British Journal of Oral and Maxillofacial Surgery, 2010;48:3, p236-238.

45. James, J., et al. *A new method to orient 3-dimensional computed tomography models to the natural head position: a clinical feasibility study.* Oral and Maxillofacial surgery, 2011;68:3, p584-591.

7 Appendices

7.1 Appendix I: Data processing steps

Data processing steps performed in Mimics/3-Matic (Materialise, Leuven, Belgium), according to figure 1 in the methods section (chapter 4.2).

Mimics

a) Image registration

1) Import anonymised DICOM files of preoperative and postoperative CT scans
2) Automatic Registration:
    a. Fixed image: preoperative CT scan
    b. Moving image: postoperative CT scan
    c. Define region of interest (ROI) and perform initial alignment
3) Apply transformation to postoperative CT scan → **transformed postoperative CT scan**

b) Segmentation

1) Choose suitable thresholds for skull and implant (figure 1)
2) Improve segmentation by using region grow, smart fill, erosion, dilation and manual adjustments
3) Calculate parts and smooth if necessary → **Postop_Skull & Postop_Implant**
4) Export STL files

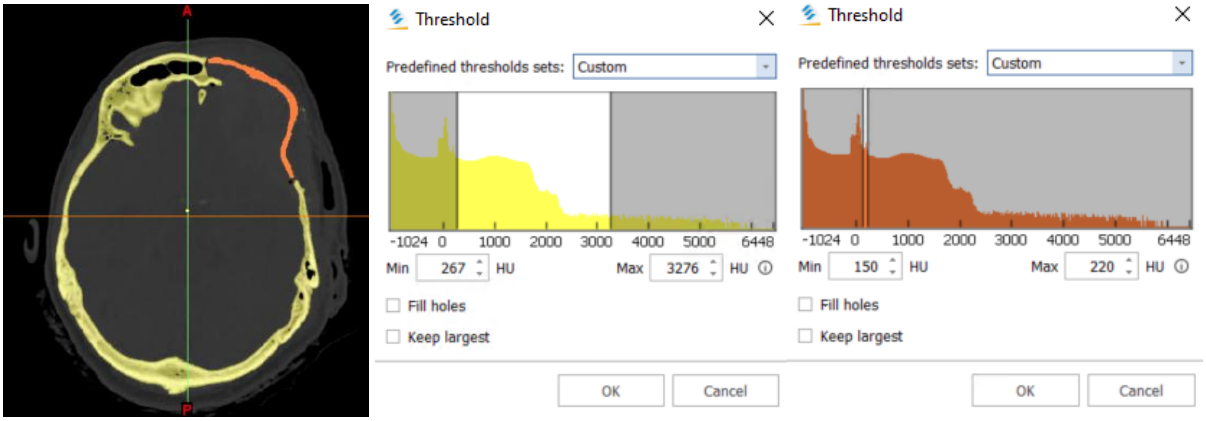

Figure 1. Choosing threshold for segmentation of postoperative skull (yellow) and postoperative implant (orange) in Mimics.

Figure 2. Surface registration of planned PSI (dark blue) to segmented postoperative PSI (orange) in 3-Matic, anterior view.

3-Matic

Import STL files: Preop_Implant, Osteotomy, Guide, Postop_Implant, Postop_Skull (reduce and wrap to speed up process).

c) Surface registration

1) Global registration: repeat until minimum average distance error is reached (figure 2) → **Postop_Implant_corr**
    a. Fixed entity: Postop_Implant
    b. Moving entity: (duplicate of) Preop_Implant
    c. Parameters:
        i. Distance threshold method: manual
        ii. Distance threshold: vary between 1 to 5
        iii. Number of iterations: 100
        iv. Subsample percentage: 40%
2) Export STL file

d) Define postoperative osteotomy

1) Select faces of side of Preop_Implant & copy to new surface (figure 3A)
2) Select surface subcontours, following the guide outline → one for the inner curve, one for the outer curve (figure 3B) & copy to new curves
3) Attract curves to Postop_skull (figure 3C)
    a. Entities: Inner_curve, Outer_curve
    b. Target entities: Postop_Skull
    c. Parameters:
        i. Distance threshold: 5.0
        ii. Attach curve
4) Improve curves by smoothing and editing manually → **Inner_curve & Outer_curve** (figure 4)
5) Export XML files

e) Define preoperative osteotomy

1) Select faces of Osteotomy that are directly adjacent to the surgical guide & copy to new part (figure 5)
2) Ensure that normals point in direction of bone edges, otherwise invert normals
3) Export STL file

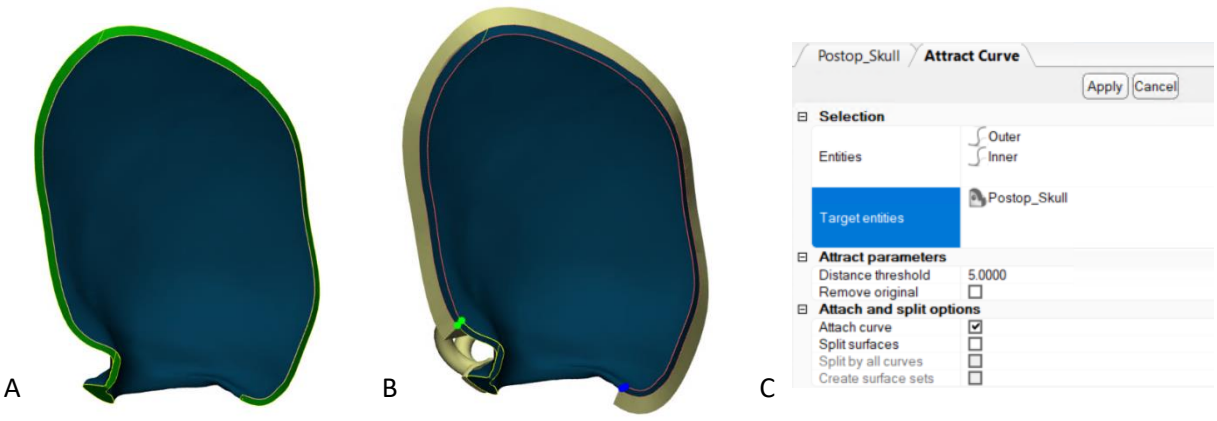

Figure 3. Defining inner and outer curve for resection outlines on postoperative skull in 3-Matic, posterior view.

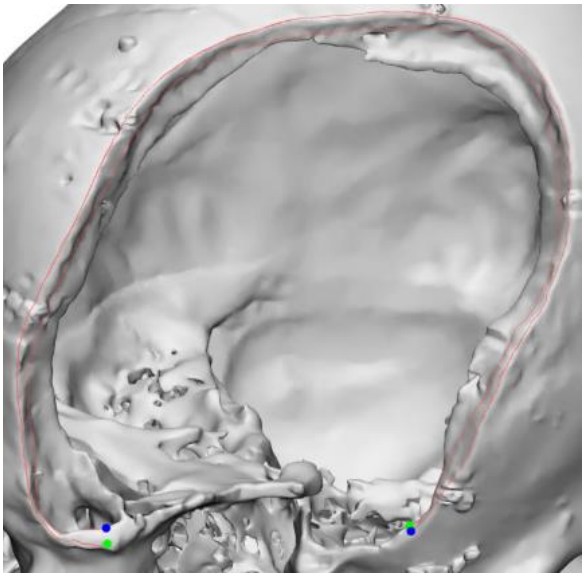

Figure 4. Inner and outer curve on postoperative skull in 3-Matic, anterolateral view left.

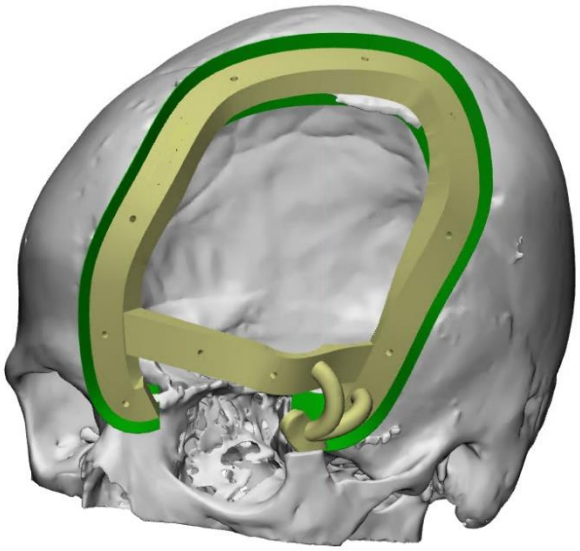

Figure 5. Defining preoperative osteotomy surface (green) in 3-Matic, anterolateral view left.

7.2 Appendix II: Matlab scripts for analysis

7.2.1 Patient-specific implant positioning

Transformation from realised PSI position to planned PSI position in craniofacial surgery, report version

```
% Larissa Nagtegaal
% Master Thesis, Technical Medicine
% "Evaluation of the positioning of virtually planned polyetheretherketone
% patient-specific implants and surgical guides in craniofacial surgery"

clc;
clear;
close all;
addpath(genpath('D:\Larissa_Nagtegaal\Documents\Technical_Medicine\Stages\TM3
MKA\Matlab\PEEK_STL'))
```

Preparation: fill in patient names here
In this script we worked with version 1 of the case names*

```
% Create arrays for names and translations
Name = ["PEEK_001";"PEEK_002";"PEEK_003";"PEEK_004";"PEEK_005";...
    "PEEK_006";"PEEK_007";"PEEK_008";"PEEK_010";"PEEK_011";"PEEK_012";...
    "PEEK_013";"PEEK_014";"PEEK_015";"PEEK_017";"PEEK_019";"PEEK_020";...
    "PEEK_021";"PEEK_022";"PEEK_026"];
Translation = zeros(length(Name),3);
% Create translation vector
trans_vector = [];

% Create arrays for names and rotations
Name_2 = ["PEEK_001";"";"";"PEEK_002";"";"";"PEEK_003";"";"";"PEEK_004";...
    "";"";"PEEK_005";"";"";"PEEK_006";"";"";"PEEK_007";"";"";"PEEK_008";...
    "";"";"PEEK_010";"";"";"PEEK_011";"";"";"PEEK_012";"";"";"PEEK_013";...
    "";"";"PEEK_014";"";"";"PEEK_015";"";"";"PEEK_017";"";"";"PEEK_019";...
    "";"";"PEEK_020";"";"";"PEEK_021";"";"";"PEEK_022";"";"";"PEEK_026";...
    "";""];
Rotation = zeros(length(Name_2),3);
% Create matrix for rotation around axes in degrees
Rotation_degrees = zeros(length(Name),3);
% Create axis-angle rotation array
axis_rot = [];

% Create arrays for names and transformations
Name_3 = ["PEEK_001";"";"";"";"PEEK_002";"";"";"";"PEEK_003";"";"";"";...
    "PEEK_004";"";"";"";"PEEK_005";"";"";"";"PEEK_006";"";"";"";...
    "PEEK_007";"";"";"";"PEEK_008";"";"";"";"PEEK_010";"";"";"";...
    "PEEK_011";"";"";"";"PEEK_012";"";"";"";"PEEK_013";"";"";"";...
    "PEEK_014";"";"";"";"PEEK_015";"";"";"";"PEEK_017";"";"";"";...
    "PEEK_019";"";"";"";"PEEK_020";"";"";"";"PEEK_021";"";"";"";...
    "PEEK_022";"";"";"";"PEEK_026";"";"";""];
Transformation = zeros(length(Name_3),4);
```

Read files and start transformations

```
for n = 1:length(Name)
```

Read STL files and convert into point clouds

```
    % Read STL file for each study name
    PEEK = Name(n);
    [Pre] = stlread(append("PEEK_STL\",PEEK,"\Preop_Implant.stl"));
    [Post] = stlread(append("PEEK_STL\",PEEK,"\Postop_Implant_corr.stl"));

    % Check whether STL models have same size, if not: display and skip
```

```
    if length(Pre.Points) ~= length(Post.Points)
        disp(append("STL dimensions ",PEEK," do not agree"))
        continue
    end

    % Create point clouds for pre-op and post-op
    % Point clouds contain x,y,z coordinates of all vertices of the models
    cloud_pre = pointCloud(Pre.Points);
    color_pre = zeros(cloud_pre.Count,3); color_pre(:,3) = 1;
    cloud_pre = pointCloud(Pre.Points,'color',color_pre);

    cloud_post = pointCloud(Post.Points);
    color_post = zeros(cloud_post.Count,3); color_post(:,2) = 1; ...
        color_post(:,3) = 1;
    cloud_post = pointCloud(Post.Points,'color',color_post);
```

1. Calculate translation between pre-op and post-op models

```
    % Centre of mass pre-op model
    x_pre = mean(cloud_pre.Location(:,1));
    y_pre = mean(cloud_pre.Location(:,2));
    z_pre = mean(cloud_pre.Location(:,3));
    origin_pre = [x_pre y_pre z_pre];
    % Centre of mass post-op model
    x_post = mean(cloud_post.Location(:,1));
    y_post = mean(cloud_post.Location(:,2));
    z_post = mean(cloud_post.Location(:,3));
    origin_post = [x_post y_post z_post];

    % Calculate translation centre of mass
    trans = origin_post - origin_pre;

    % Calculate size of translation vector
    trans_vector{n} = sqrt(trans(1)^2+trans(2)^2+trans(3)^2);
    save translation_vector.mat trans_vector
```

2. Calculate the rotation between pre-op and post-op models

```
    % 2.1 Translate post-op and pre-op to origin of coordinate system (0,0,0)
    % in order to calculate the rotation

    % Translate post-op to pre-op with translation found above
    post_trans = cloud_post.Location - trans;
    % Translate pre-op and post-op models to origin (0,0,0)
    post_trans_origin = post_trans - origin_pre;
    pre_trans_origin = cloud_pre.Location - origin_pre;
    % Create point clouds
    cloud_post_origin = pointCloud(post_trans_origin,'color',color_post);
    cloud_pre_origin = pointCloud(pre_trans_origin,'color',color_pre);

    % 2.2 Perform registration to obtain rotation matrix

    % Downsample point clouds to optimize registration
    positions_down = randperm(cloud_pre_origin.Count,10);

    pre_down = cloud_pre_origin.Location(positions_down,:);
    color_pre_down = zeros(10,1); color_pre_down(:,3) = 1;
    pre_down = pointCloud(pre_down,'color',color_pre_down);

    post_down = cloud_post_origin.Location(positions_down,:);
    color_post_down = zeros(10,1); color_post_down(:,2) = 1; ...
        color_post_down(:,3) = 1;
    post_down = pointCloud(post_down,'color',color_post_down);

    % Perform ICP algorithm to obtain rotation in transformation matrix with
    % pre-op as fixed and post-op as moving
    [tform] = pcregistericp(post_down,pre_down);
```

```
    % Check whether transformation was correct: translation must be 0 (or
    % something like <...e-3)
    if tform.Translation(:) >= 1e-3
        disp(append('Transformation for ',PEEK, ' is incorrect'));
    end
```

Fill up arrays with translation and rotation

```
    % Fill up translation and rotation arrays
    Translation(n,:) = trans;
    Rotation(n*3-2:n*3,:) = tform.Rotation';
    % Fill up axis-angle rotation array
    axis_rot(n,:) = rotm2axang(tform.Rotation');
    axis_rot(n,4) = rad2deg(axis_rot(n,4));
    % Fill up rotation array after converting to degrees
    Rotation_degrees(n,:) = rad2deg(rotm2eul(Rotation(n*3-2:n*3,:),'ZYX'));
end
```

Boxplot translation

```
% Convert translation vector into cranial and orbital vectors
trans_vector = [trans_vector(1:11),trans_vector(13:20)]';
trans_vector = cell2mat(trans_vector);
save translation_vector.mat trans_vector
trans_cranial = cat(1,trans_vector(3:5),trans_vector(7),trans_vector(10:12),...
    trans_vector(16:19));
trans_orbital = cat(1,trans_vector(1:2),trans_vector(6),trans_vector(8:9),...
    trans_vector(13:15));
trans_box = [trans_cranial;trans_orbital];

% Group the two categories
g1 = repmat({'Cranial'},11,1); g2 = repmat({'Orbital'},8,1); g = [g1; g2];

% Create boxplot
figure;
boxplot(trans_box,g,'OutlierSize',1,'Width',0.2,'Symbol','k',...
    'LabelOrientation','horizontal');
xlabel('Type of implant')
ylabel('Translation vector length [mm]')
hold on;

% Create scatter on boxplot
x1=ones(length(trans_cranial),1);
scatter(x1(:),trans_cranial(:),'filled','MarkerFaceAlpha',0.6,'jitter','on'...
    ,'jitterAmount',0.15);
x2=ones(length(trans_orbital),1)+1;
scatter(x2(:),trans_orbital(:),'filled','MarkerFaceAlpha',0.6,'jitter','on'...
    ,'jitterAmount',0.15);

% Plot means
plot(1,mean(trans_cranial),'+r');
SD_trans_cr = std(trans_cranial);
plot(2,mean(trans_orbital),'+r');
SD_trans_orb = std(trans_orbital);
```

Boxplot axis-angle rotation

```
% Convert rotataion into cranial and orbital rotation
axis_angle = cat(1,axis_rot(1:11,4),axis_rot(13:20,4));
axis_angle_cra = cat(1,axis_angle(3:5),axis_angle(7),axis_angle(10:12),...
    axis_angle(16:19));
axis_angle_orb = cat(1,axis_angle(1:2),axis_angle(6),axis_angle(8:9),...
    axis_angle(13:15));
axis_angle_box = [axis_angle_cra;axis_angle_orb];

% Create boxplot
figure;
boxplot(axis_angle_box,g,'OutlierSize',1,'Width',0.2,'Symbol','k',...
```

```
    'LabelOrientation','horizontal');
xlabel('Type of implant')
ylabel('Rotation around fixed axis [degrees]')
hold on;

% Create scatter on boxplot
scatter(x1(:),axis_angle_cra(:),'filled','MarkerFaceAlpha',0.6','jitter',...
    'on','jitterAmount',0.15);
scatter(x2(:),axis_angle_orb(:),'filled','MarkerFaceAlpha',0.6','jitter',...
    'on','jitterAmount',0.15);

% Plot means
plot(1,mean(axis_angle_cra),'+r');
SD_cr = std(axis_angle_cra);
plot(2,mean(axis_angle_orb),'+r');
SD_orb = std(axis_angle_orb);
```

Published with MATLAB® R2021a

7.2.2 Osteotomies, 1 curve

Difference between realised osteotomy and planned osteotomy in craniofacial surgery, report version

Contours consisting of 1 curve

```
% Larissa Nagtegaal
% Master Thesis, Technical Medicine
% "Evaluation of the positioning of virtually planned polyetheretherketone
% patient-specific implants and surgical guides in craniofacial surgery"

clc;
clear;
close all;
addpath(genpath('D:\Larissa_Nagtegaal\Documents\Technical_Medicine\Stages\TM3
MKA\Matlab\Osteotomies_STL'))
```

Preparation

Depending on image processing in 3-Matic the contours exist of 1 or 2 curves: fill in patient names of osteotomies with one curve here

In this script we worked with version 1* of the case names

```
% Create array for names
list = ["PEEK_001";"PEEK_003";"PEEK_004";"PEEK_005";"PEEK_010";...
    "PEEK_011";"PEEK_012";"PEEK_020";"PEEK_021"];

% Create empty arrays to fill later on
dist_out = []; dist_in = [];
curve_out = []; curve_in = [];
surf_out = []; surf_in = [];
all_out = []; all_in = [];
```

Read files and start analysis

```
for k = 1:length(list)
```

Read xml files from curves on skull and get x,y,z coordinates

```
    % Read xml files for each study name, inner & outer curve
    PEEK = list(k);
```

```
    info_out_skull =
fullfile(append('D:\Larissa_Nagtegaal\Documents\Technical_Medicine\Stages\TM3
MKA\Matlab\Osteotomies_STL\',PEEK,'\Outside_skull.xml'));
    info_in_skull =
fullfile(append('D:\Larissa_Nagtegaal\Documents\Technical_Medicine\Stages\TM3
MKA\Matlab\Osteotomies_STL\',PEEK,'\Inside_skull.xml'));
    import matlab.io.xml.dom.*
    xDoc_out_skull = parseFile(Parser,info_out_skull);
    xDoc_in_skull = parseFile(Parser,info_in_skull);
    % Get string array with coordinates
    list_out_skull = getElementsByTagName(xDoc_out_skull,'Point');
    list_in_skull = getElementsByTagName(xDoc_in_skull,'Point');
    % Convert string array to num array with coordinates
    points_out_skull = str2num(list_out_skull.TextContent);
    points_in_skull = str2num(list_in_skull.TextContent);

    % Create 3-column array with x,y,z coordinates for outside curve
    out_skull = zeros(length(points_out_skull)/3,3);
    for n = 1:length(out_skull)
        out_skull(n,1) = points_out_skull(n*3-2);
        out_skull(n,2) = points_out_skull(n*3-1);
        out_skull(n,3) = points_out_skull(n*3);
    end

    % Create 3-column array with x,y,z coordinates for inside curve
    in_skull = zeros(length(points_in_skull)/3,3);
    for i = 1:length(in_skull)
        in_skull(i,1) = points_in_skull(i*3-2);
        in_skull(i,2) = points_in_skull(i*3-1);
        in_skull(i,3) = points_in_skull(i*3);
    end
```

Convert curves into point clouds and downsample

```
    % Create point clouds
    cloud_out_skull = pointCloud(out_skull);
    cloud_in_skull = pointCloud(in_skull);

    % Downsample point clouds of osteotomy curves to correct for groups of
    % points lying close to each other, affecting the mean
    gridStep = 0.5;
    down_out = pcdownsample(cloud_out_skull,'gridAverage',gridStep);
    down_in = pcdownsample(cloud_in_skull,'gridAverage',gridStep);

    % Fill up arrays with coordinates of downsampled curves
    curve_out{k} = down_out.Location;
    curve_in{k} = down_in.Location;
```

Read STL file osteotomy

```
    [Ost] =
stlread(append('D:\Larissa_Nagtegaal\Documents\Technical_Medicine\Stages\TM3
MKA\Matlab\Osteotomies_STL\',PEEK,'\Osteotomy_plane.stl'));
```

Point2trimesh algorithm: surface distance calculation[41]

```
    % Daniel Frisch (2021). point2trimesh( ) – Distance Between Point and
    % Triangulated Surface (https://www.mathworks.com/matlabcentral/...
    % fileexchange/52882-point2trimesh-distance-between-point-and-...
    % triangulated-surface), MATLAB Central File Exchange.

    % Surface distance for outside curve
    [distances_out,surface_points_out] = point2trimesh('Faces', ...
        Ost.ConnectivityList, 'Vertices', Ost.Points, 'QueryPoints', ...
        down_out.Location);
    % Fill up arrays for distances and surface points outer curve
    dist_out{k} = distances_out;
    surf_out{k} = surface_points_out;
```

```
    % Calculate absolute min, max and mean distances from planned osteotomies
    all_out{1,k} = max(abs(distances_out));
    all_out{2,k} = min(abs(distances_out));
    all_out{3,k} = mean(abs(distances_out));
    all_out{4,k} = std(abs(distances_out));
    all_out{5,k} = max(distances_out);
    all_out{6,k} = min(distances_out);
    all_out{7,k} = mean(distances_out);
    all_out{8,k} = std(distances_out);

    % Surface distance for inside curve
    [distances_in,surface_points_in] = point2trimesh('Faces', ...
        Ost.ConnectivityList, 'Vertices', Ost.Points, 'QueryPoints', ...
        down_in.Location);
    % Fill up arrays for distances and surface points inner curve
    dist_in{k} = distances_in;
    surf_in{k} = surface_points_in;

    % Calculate absolute min, max and mean distances from planned osteotomies
    all_in{1,k} = max(abs(distances_in));
    all_in{2,k} = min(abs(distances_in));
    all_in{3,k} = mean(abs(distances_in));
    all_in{4,k} = std(abs(distances_in));
    all_in{5,k} = max(distances_in);
    all_in{6,k} = min(distances_in);
    all_in{7,k} = mean(distances_in);
    all_in{8,k} = std(distances_in);

    % Calculate combined min, max and mean distances from planned
    % osteotomies for inner & outer
    all_in_out{1,k} = max(abs(cat(1,distances_in, distances_out)));
    all_in_out{2,k} = min(abs(cat(1,distances_in, distances_out)));
    all_in_out{3,k} = mean(abs(cat(1,distances_in, distances_out)));
    all_in_out{4,k} = std(abs(cat(1,distances_in, distances_out)));
    all_in_out{5,k} = max(cat(1,distances_in, distances_out));
    all_in_out{6,k} = min(cat(1,distances_in, distances_out));
    all_in_out{7,k} = mean(cat(1,distances_in, distances_out));
    all_in_out{8,k} = std(cat(1,distances_in, distances_out));

    % Visualize inside and outside curves together with osteotomy with
    % coordinates of inside curve in blue and coordinates of outside skull
    % in green.
    figure;
    patch('Faces',Ost.ConnectivityList,'Vertices', Ost.Points,'FaceAlpha',...
        .5); xlabel('x'); ylabel('y'); zlabel('z'); title(append...
        ('Curves skull ',PEEK)); axis equal; hold on
    plot3M = @(XYZ,varargin) plot3(XYZ(:,1),XYZ(:,2),XYZ(:,3),varargin{:});
    plot3M(down_in.Location,'.b')
    plot3M(down_out.Location,'.g')
    plot3M(surface_points_in,'.k')
    plot3M(surface_points_out,'.k')
    plot3M(reshape([shiftdim(down_in.Location,-1);shiftdim(...
        surface_points_in,-1);shiftdim(down_in.Location,-1)*NaN],[],3),'k')
    plot3M(reshape([shiftdim(down_out.Location,-1);shiftdim(...
        surface_points_out,-1);shiftdim(down_out.Location,-1)*NaN],[],3),'k')
end
```

Export to excel file

```
filename = 'Osteotomies.xlsx';
writecell(dist_out',filename,'Sheet','Outer curve');
writecell(dist_in',filename,'Sheet','Inner curve');
writecell(all_out',filename,'Sheet','Outer means');
writecell(all_in',filename,'Sheet','Inner means');
writecell(all_in_out',filename,'Sheet','Combined means');
```

Export data for plots in script 2 curves

```
% Mean & SD
in_mean = cell2mat(all_in(7,:)');
out_mean = cell2mat(all_out(8,:)');
in_sdmean = cell2mat(all_in(7,:)');
out_sdmean = cell2mat(all_out(8,:)');
save full_curve_mean_sd.mat in_mean out_mean in_sdmean out_sdmean

% Absolute mean
abs_in_mean = cell2mat(all_in(3,:)');
abs_out_mean = cell2mat(all_out(3,:)');
save full_curve_absmean.mat abs_in_mean abs_out_mean

% SD
in_sd = cell2mat(all_in(4,:)');
out_sd = cell2mat(all_out(4,:)');
save sd.mat in_sd out_sd
```

Published with MATLAB® R2021a

7.2.3 Osteotomies, 2 curves

Difference between realised osteotomy and planned osteotomy in craniofacial surgery, report version

Contours consisting of 2 curves

```
% Larissa Nagtegaal
% Master Thesis, Technical Medicine
% "Evaluation of the positioning of virtually planned polyetheretherketone
% patient-specific implants and surgical guides in craniofacial surgery"

clc;
clear;
close all;
addpath(genpath('D:\Larissa_Nagtegaal\Documents\Technical_Medicine\Stages\TM3
MKA\Matlab\Osteotomies_STL'))
```

Preparation

Depending on image processing in 3-Matic the contours exist of 1 or 2 curves: fill in patient names of osteotomies with two curves here (names version 1*)

```
% Create array for names
list = ["PEEK_008";"PEEK_017";"PEEK_019"];

% Create empty arrays to fill later on
dist_out = []; dist_in = [];
curve_out = []; curve_in = [];
surf_out = []; surf_in = [];
all_out = []; all_in = [];
```

Read files and start analysis

```
for k = 1:length(list)
```

Read xml files from curves on skull and get x,y,z coordinates

```
    % Read xml files for each study name, inner & outer curve
    PEEK = list(k);
    info_out_skull_1 =
fullfile(append('D:\Larissa_Nagtegaal\Documents\Technical_Medicine\Stages\TM3
MKA\Matlab\Osteotomies_STL\',PEEK,'\Outside_skull_1.xml'));
```

```
    info_out_skull_2 =
fullfile(append('D:\Larissa_Nagtegaal\Documents\Technical_Medicine\Stages\TM3
MKA\Matlab\Osteotomies_STL\',PEEK,'\Outside_skull_2.xml'));
    info_in_skull_1 =
fullfile(append('D:\Larissa_Nagtegaal\Documents\Technical_Medicine\Stages\TM3
MKA\Matlab\Osteotomies_STL\',PEEK,'\Inside_skull_1.xml'));
    info_in_skull_2 =
fullfile(append('D:\Larissa_Nagtegaal\Documents\Technical_Medicine\Stages\TM3
MKA\Matlab\Osteotomies_STL\',PEEK,'\Inside_skull_2.xml'));
    import matlab.io.xml.dom.*
    xDoc_out_skull_1 = parseFile(Parser,info_out_skull_1);
    xDoc_out_skull_2 = parseFile(Parser,info_out_skull_2);
    xDoc_in_skull_1 = parseFile(Parser,info_in_skull_1);
    xDoc_in_skull_2 = parseFile(Parser,info_in_skull_2);
    % Get string array with coordinates of curves
    list_out_skull_1 = getElementsByTagName(xDoc_out_skull_1,'Point');
    list_out_skull_2 = getElementsByTagName(xDoc_out_skull_2,'Point');
    list_in_skull_1 = getElementsByTagName(xDoc_in_skull_1,'Point');
    list_in_skull_2 = getElementsByTagName(xDoc_in_skull_2,'Point');
    % Convert string array to num array with coordinates
    points_out_skull_1 = str2num(list_out_skull_1.TextContent);
    points_out_skull_2 = str2num(list_out_skull_2.TextContent);
    points_in_skull_1 = str2num(list_in_skull_1.TextContent);
    points_in_skull_2 = str2num(list_in_skull_2.TextContent);

    % Create 3-column arrays with x,y,z coordinates for outside curve
    out_skull_1 = zeros(length(points_out_skull_1)/3,3);
    out_skull_2 = zeros(length(points_out_skull_2)/3,3);
    for n = 1:length(out_skull_1)
        out_skull_1(n,1) = points_out_skull_1(n*3-2);
        out_skull_1(n,2) = points_out_skull_1(n*3-1);
        out_skull_1(n,3) = points_out_skull_1(n*3);
    end
    for n = 1:length(out_skull_2)
        out_skull_2(n,1) = points_out_skull_2(n*3-2);
        out_skull_2(n,2) = points_out_skull_2(n*3-1);
        out_skull_2(n,3) = points_out_skull_2(n*3);
    end
    out_skull = cat(1,out_skull_1,out_skull_2); % concatenate two curves to one

    % Create 3-column arrays with x,y,z coordinates for inside curve
    in_skull_1 = zeros(length(points_in_skull_1)/3,3);
    in_skull_2 = zeros(length(points_in_skull_2)/3,3);
    for i = 1:length(in_skull_1)
        in_skull_1(i,1) = points_in_skull_1(i*3-2);
        in_skull_1(i,2) = points_in_skull_1(i*3-1);
        in_skull_1(i,3) = points_in_skull_1(i*3);
    end
    for i = 1:length(in_skull_2)
        in_skull_2(i,1) = points_in_skull_2(i*3-2);
        in_skull_2(i,2) = points_in_skull_2(i*3-1);
        in_skull_2(i,3) = points_in_skull_2(i*3);
    end
    in_skull = cat(1,in_skull_1,in_skull_2); % concatenate two curves to one
```

Convert curves into point clouds and downsample

```
    % Create point clouds
    cloud_out_skull = pointCloud(out_skull);
    cloud_in_skull = pointCloud(in_skull);

    % Downsample point clouds of osteotomy curves to correct for groups of
    % points lying close to each other, affecting the mean
    gridStep = 0.5;
    down_out = pcdownsample(cloud_out_skull,'gridAverage',gridStep);
    down_in = pcdownsample(cloud_in_skull,'gridAverage',gridStep);

    % Fill up arrays with coordinates of downsampled curves
```

```
    curve_out{k} = down_out.Location;
    curve_in{k} = down_in.Location;
```

Read STL file osteotomy

```
    [Ost] =
stlread(append('D:\Larissa_Nagtegaal\Documents\Technical_Medicine\Stages\TM3
MKA\Matlab\Osteotomies_STL\',PEEK,'\Osteotomy_plane.stl'));
```

Point2trimesh algorithm: surface distance calculation[41]

```
    % Daniel Frisch (2021). point2trimesh( ) – Distance Between Point and
    % Triangulated Surface (https://www.mathworks.com/matlabcentral/...
    % fileexchange/52882-point2trimesh-distance-between-point-and-...
    % triangulated-surface), MATLAB Central File Exchange.

    % Surface distance for outside curve
    [distances_out,surface_points_out] = point2trimesh('Faces', ...
        Ost.ConnectivityList, 'Vertices', Ost.Points, 'QueryPoints', ...
        down_out.Location);
    % Fill up arrays for distances and surface points outer curve
    dist_out{k} = distances_out;
    surf_out{k} = surface_points_out;

    % Calculate absolute min, max and mean distances from planned osteotomies
    all_out{1,k} = max(abs(distances_out));
    all_out{2,k} = min(abs(distances_out));
    all_out{3,k} = mean(abs(distances_out));
    all_out{4,k} = std(abs(distances_out));
    all_out{5,k} = max(distances_out);
    all_out{6,k} = min(distances_out);
    all_out{7,k} = mean(distances_out);
    all_out{8,k} = std(distances_out);

    % Surface distance for inside curve
    [distances_in,surface_points_in] = point2trimesh('Faces', ...
        Ost.ConnectivityList, 'Vertices', Ost.Points, 'QueryPoints', ...
        down_in.Location);
    % Fill up arrays for distances and surface points inner curve
    dist_in{k} = distances_in;
    surf_in{k} = surface_points_in;

    % Calculate absolute min, max and mean distances from planned osteotomies
    all_in{1,k} = max(abs(distances_in));
    all_in{2,k} = min(abs(distances_in));
    all_in{3,k} = mean(abs(distances_in));
    all_in{4,k} = std(abs(distances_in));
    all_in{5,k} = max(distances_in);
    all_in{6,k} = min(distances_in);
    all_in{7,k} = mean(distances_in);
    all_in{8,k} = std(distances_in);

    % Calculate combined min, max and mean distances from planned
    % osteotomies for inner & outer
    all_in_out{1,k} = max(abs(cat(1,distances_in, distances_out)));
    all_in_out{2,k} = min(abs(cat(1,distances_in, distances_out)));
    all_in_out{3,k} = mean(abs(cat(1,distances_in, distances_out)));
    all_in_out{4,k} = std(abs(cat(1,distances_in, distances_out)));
    all_in_out{5,k} = max(cat(1,distances_in, distances_out));
    all_in_out{6,k} = min(cat(1,distances_in, distances_out));
    all_in_out{7,k} = mean(cat(1,distances_in, distances_out));
    all_in_out{8,k} = std(cat(1,distances_in, distances_out));

    % Visualize inside and outside curves together with osteotomy with
    % coordinates of inside curve in blue and coordinates of outside skull
    % in green.
    figure;
    patch('Faces',Ost.ConnectivityList,'Vertices', Ost.Points,'FaceAlpha',...
```

```
        .5); xlabel('x'); ylabel('y'); zlabel('z'); title(append(...
        'Curves skull ',PEEK)); axis equal; hold on
    plot3M = @(XYZ,varargin) plot3(XYZ(:,1),XYZ(:,2),XYZ(:,3),varargin{:});
    plot3M(down_in.Location,'.b')
    plot3M(down_out.Location,'.g')
    plot3M(surface_points_in,'.k')
    plot3M(surface_points_out,'.k')
    plot3M(reshape([shiftdim(down_in.Location,-1);shiftdim(...
        surface_points_in,-1);shiftdim(down_in.Location,-1)*NaN],[],3),'k')
    plot3M(reshape([shiftdim(down_out.Location,-1);shiftdim(...
        surface_points_out,-1);shiftdim(down_out.Location,-1)*NaN],[],3),'k')
end
```

Export to excel file

```
filename = 'Osteotomies_2curves.xlsx';
writecell(dist_out',filename,'Sheet','Outer curve');
writecell(dist_in',filename,'Sheet','Inner curve');
writecell(all_out',filename,'Sheet','Outer means');
writecell(all_in',filename,'Sheet','Inner means');
writecell(all_in_out',filename,'Sheet','Combined means');
```

Visualization of mean for all patients, case names version 2*

```
% Create empty arrays to fill for mean and SD of all osteotomy cases (both
% contours consisting of 1 and 2 curves)
mean_in_all = zeros(12,1); mean_out_all = zeros(12,1);
mean_in_allsd = zeros(12,1); mean_out_allsd = zeros(12,1);

% Import mean and SD from contours consisting of 1 curve '1_curve'
load full_curve_mean_sd.mat

% Convert cells from 2-curve contours into arrays
in_v1 = cell2mat(all_in(7,:)'); out_v1 = cell2mat(all_out(7,:)'); % mean
in_v1sd = cell2mat(all_in(8,:)'); out_v1sd = cell2mat(all_out(8,:)'); % SD

% !!! NEW ORDER: patient names from version 1 to version 2 !!!
% Fill up arrays for all patients, both 1 and 2 curves

% Inner curves, mean
mean_in_all(1:3) = in_mean(2:4); mean_in_all(4:7) = in_mean(6:9); ...
    mean_in_all(8) = in_mean(1); mean_in_all(9) = in_v1(1); ...
    mean_in_all(10) = in_mean(5); mean_in_all(11:12) = in_v1(2:3);
% Outer curves, mean
mean_out_all(1:3) = out_mean(2:4); mean_out_all(4:7) = out_mean(6:9);...
    mean_out_all(8) = out_mean(1); mean_out_all(9) = out_v1(1); ...
    mean_out_all(10) = out_mean(5); mean_out_all(11:12) = out_v1(2:3);
% Inner curves, SD
mean_in_allsd(1:3) = in_sdmean(2:4); mean_in_allsd(4:7) = in_sdmean(6:9); ...
    mean_in_allsd(8) = in_sdmean(1); mean_in_allsd(9) = in_v1sd(1); ...
    mean_in_allsd(10) = in_sdmean(5); mean_in_allsd(11:12) = in_v1sd(2:3);
% Outer curves, SD
mean_out_allsd(1:3) = out_sdmean(2:4); mean_out_allsd(4:7) = out_sdmean(6:9);...
    mean_out_allsd(8) = out_sdmean(1); mean_out_allsd(9) = out_v1sd(1);...
    mean_out_allsd(10) = out_sdmean(5); mean_out_allsd(11:12) = out_v1sd(2:3);

% Plot errorbar with mean and SD
figure;
errorbar(1:12,mean_in_all,mean_in_allsd,'LineStyle','none','Marker','x');
hold on;
errorbar(1.4:1:12.4, mean_out_all,mean_out_allsd,'LineStyle','none',...
    'Color','k','Marker','x');
% Plot line at zero
nul = zeros(14,1); plot(0:13,nul,'--k');

names = ["1";"2";"3";"5";"6";"7";"8";"9";"10";"11";"12";"13"];
xlim([0.5 13]); ylim([-5 9]);
set(gca,'xtick',1.2:12.2,'xticklabel',names);
```

```
grid on;
legend('Inner curve','Outer curve','Location','north');
xticklabels(names);
xlabel('Case'); ylabel('Mean distance [mm]')
```

Visualization of absolute mean for all patients, case names version 2*

```
% Create empty arrays to fill for absolute mean and SD of all osteotomy
% cases (both contours consisting of 1 and 2 curves)
meanabs_in_all = zeros(12,1); meanabs_out_all = zeros(12,1);
in_sd_all = zeros(12,1); out_sd_all = zeros(12,1);

% Import absolute mean and SD from contours consisting of 1 curve '1_curve'
load full_curve_absmean.mat
load sd.mat

% Convert cells from 2-curve contours into arrays
inabs_v1 = cell2mat(all_in(3,:)'); outabs_v1 = cell2mat(all_out(3,:)');
in_sd_v1 = cell2mat(all_in(4,:)'); out_sd_v1 = cell2mat(all_out(4,:)');

% !!! NEW ORDER: patient names from version 1 to version 2 !!!
% Fill up arrays for all patients, both 1 and 2 curves

% Inner curves, absolute mean
meanabs_in_all(1:3) = abs_in_mean(2:4); meanabs_in_all(4:7) = abs_in_mean(6:9);...
    meanabs_in_all(8) = abs_in_mean(1); meanabs_in_all(9) = inabs_v1(1);...
    meanabs_in_all(10) = abs_in_mean(5); meanabs_in_all(11:12) = inabs_v1(2:3);
% Outer curves, absolute mean
meanabs_out_all(1:3) = abs_out_mean(2:4); meanabs_out_all(4:7) =
abs_out_mean(6:9);...
    meanabs_out_all(8) = abs_out_mean(1); meanabs_out_all(9) = outabs_v1(1);...
    meanabs_out_all(10) = abs_out_mean(5); meanabs_out_all(11:12) = outabs_v1(2:3);
% Inner curves, SD
in_sd_all(1:3) = in_sd(2:4); in_sd_all(4:7) = in_sd(6:9); in_sd_all(8) =
in_sd(1);...
    in_sd_all(9) = in_sd_v1(1); in_sd_all(10) = in_sd(5); in_sd_all(11:12) = ...
    in_sd_v1(2:3);
% Outer curves, SD
out_sd_all(1:3) = out_sd(2:4); out_sd_all(4:7) = out_sd(6:9); out_sd_all(8) = ...
    out_sd(1); out_sd_all(9) = out_sd_v1(1); out_sd_all(10) = out_sd(5);...
    out_sd_all(11:12) = out_sd_v1(2:3);

% Plot errorbar with absolute mean and SD
figure;
errorbar(1:12,meanabs_in_all,in_sd_all,'LineStyle','none','Marker','x');
hold on;
errorbar(1.4:1:12.4, meanabs_out_all,out_sd_all,'LineStyle','none',...
    'Color','k','Marker','x');

names = ["1";"2";"3";"5";"6";"7";"8";"9";"10";"11";"12";"13"];
xlim([0.5 13]); ylim([0 9]);
set(gca,'xtick',1.2:12.2,'xticklabel',names);
grid on;
legend('Inner curve','Outer curve','Location','north');
xticklabels(names);
xlabel('Case'); ylabel('Absolute mean distance [mm]')
```

Scatter plot & regression of absolute mean and translation vector length

```
% Import translation vectors from transformation script
load translation_vector.mat;
% Create array with translation vector of cases with resection
trans_scatter = cat(1,trans_vector(1),trans_vector(3:5),trans_vector(8:11),...
    trans_vector(14:17));

% !!! NEW ORDER: patient names from version 1 to version 2 !!!
trans_vector_new = zeros(12,1);
trans_vector_new(1:3) = trans_scatter(2:4); trans_vector_new(4:5) = ...
```

```
    trans_scatter(7:8); trans_vector_new(6:7) = trans_scatter(11:12);...
    trans_vector_new(8) = trans_scatter(1); trans_vector_new(9:10) = ...
    trans_scatter(5:6); trans_vector_new(11:12) = trans_scatter(9:10);

% Fill array with absolute mean over inner and outer curves
abs_mean_all = zeros(12,2);
abs_mean_all(:,1) = meanabs_in_all;
abs_mean_all(:,2) = meanabs_out_all;
abs_mean = zeros(12,1);
for g = 1:12
    abs_mean(g) = mean(abs_mean_all(g,:))
end

% Scatter plot
figure;
scatter(abs_mean,trans_vector_new); hold on;
xlim([0 5]); ylim([0 8]);
set(gca,'xtick',1:1:5,'ytick',1:1:8);
xlabel('Absolute mean distance [mm]');
ylabel('Translation vector [mm]');
% Regression line
x = 0:5;
y1 = 0.343 + 1.247*x;
plot(x,y1);
```

Published with MATLAB® R2021a

*Version 1 of the case names regard the names that were initially given to the cases. However, for better interpretation, the order and names were adjusted later on to use in the report. The table below specifies the alterations.

Version 1	1	2	3	4	5	6	7	8	10	11	12	14	15	17	19	20	21	22	26
Version 2	9	17	1	2	3	18	4	10	11	5	6	14	19	12	13	7	8	15	16

7.3 Appendix III: Patient-specific implant positioning

7.3.1 Translation from the realised patient-specific implant position to the planned patient-specific implant position

Translation in x, y and z-direction and the length of the translation vector in millimetres from the corrected postoperative PSI position to the preoperative PSI position. Numbers were rounded off to one decimal.

Translation [mm]				
Case	**x**	**y**	**z**	**Vector length**
1	2.0	0.7	1.4	2.5
2	0.0	-0.5	0.0	0.5
3	1.1	0.9	-0.1	1.4
4	-0.7	-1.1	1.8	2.3
5	-1.4	2.3	-0.2	2.7
6	1.1	-0.6	1.0	1.6
7	-0.7	-0.8	-0.8	1.3
8	0.2	0.4	0.8	0.9
9	-1.1	0.7	1.0	1.6
10	-2.3	5.0	3.8	6.7
11	0.6	1.6	5.1	5.4
12	1.4	4.6	1.3	5.0
13	-1.3	2.6	-3.1	4.3
14	-0.0	0.2	-1.2	1.2
15	-0.6	0.6	0.7	1.1
16	-0.9	0.3	-0.4	1.1
17	-1.7	5.2	-1.6	5.7
18	3.4	2.5	-0.2	4.2
19	2.1	4.4	2.5	5.4

7.3.2 Rotation from the realised patient-specific implant position to the planned patient-specific implant position

Rotation around the x, y and z-axes in degrees from the corrected postoperative PSI position to the preoperative PSI position. Numbers were rounded off to one decimal.

Case	Rotation [degrees]		
	x-axis	y-axis	z-axis
1	4.6	8.6	3.5
2	1.5	-0.6	0.0
3	2.2	-10.8	7.8
4	-0.2	4.9	-0.7
5	-1.3	1.2	1.3
6	0.9	-1.0	-3.2
7	10.3	-5.1	0.5
8	2.0	-1.7	-0.6
9	10.4	0.3	3.7
10	-13.6	-10.9	1.2
11	1.3	1.4	3.4
12	2.4	3.9	-4.0
13	4.6	-9.3	5.0
14	-0.6	-1.8	0.1
15	1.0	-1.3	0.7
16	0.8	0.6	0.0

Rotation around a specific axis in degrees from the corrected postoperative PSI position to the preoperative PSI position. Numbers were rounded off to one decimal.

Case	Rotation around fixed axis [degrees]	Unit vector v representing fixed axis		
		v1	v2	v3
1	10.2	0.4	0.9	0.3
2	1.6	0.9	-0.4	0.0
3	13.6	0.2	-0.8	0.6
4	4.9	0.0	1.0	-0.1
5	2.2	-0.6	0.5	0.6
6	3.4	0.3	-0.3	-0.9
7	11.5	0.9	-0.4	0.1
8	2.7	0.7	-0.6	-0.2
9	11.0	0.9	0.1	0.3
10	17.4	-0.8	-0.6	0.0
11	3.9	0.3	0.4	0.9
12	6.2	0.4	0.6	-0.7
13	11.6	0.4	-0.8	0.5
14	1.9	-0.3	-1.0	0.1
15	1.8	0.6	-0.7	0.4
16	0.9	0.8	0.6	0.0

7.4 Appendix IV: Osteotomies

7.4.1 Difference between the realised inner curves and planned osteotomies

Difference between the inner curve, representing the realised osteotomy, and the planned osteotomy. The minimum, maximum, mean (SD) and absolute mean (SD) in millimetres are reported. Numbers were rounded off to one decimal.

Case	Minimum	Maximum	Mean (SD)	Absolute mean (SD)
1	-4.9	0.9	-2.2 (1.7)	2.3 (1.5)
2	-2.1	14.1	1.7 (3.8)	2.1 (3.6)
3	-4.6	3.0	0.2 (2.0)	1.7 (1.1)
5	-1.2	2.2	-0.1 (0.9)	0.7 (0.5)
6	-3.0	1.4	-0.6 (1.4)	1.3 (0.8)
7	-2.4	0.4	-0.5 (0.7)	0.6 (0.6)
8	-1.9	4.1	1.0 (1.5)	1.4 (1.2)
9	-1.8	1.4	0.2 (0.9)	0.8 (0.4)
10	-1.3	9.4	3.2 (2.3)	3.2 (2.2)
11	-0.2	8.4	4.0 (2.2)	4.0 (2.2)
12	-3.5	6.8	-0.5 (2.4)	2.1 (1.2)
13	-3.4	4.9	-0.1 (2.6)	2.4 (1.1)

7.4.2 Difference between the realised outer curves and the planned osteotomies

Difference between the outer curve, representing the realised osteotomy, and the planned osteotomy. The minimum, maximum, mean (SD) and absolute mean (SD) in millimetres are reported. Numbers were rounded off to one decimal.

Case	Minimum	Maximum	Mean (SD)	Absolute mean (SD)
1	-0.9	3.5	0.5 (1.1)	0.8 (0.9)
2	0.0	16.8	3.4 (4.3)	3.4 (4.3)
3	-3.4	4.3	1.2 (2.0)	2.0 (1.1)
5	-0.6	2.2	0.6 (0.8)	0.8 (0.6)
6	-1.6	1.6	0.2 (1.0)	0.9 (0.5)
7	-2.2	1.8	0.4 (0.7)	0.7 (0.4)
8	-1.9	3.9	1.2 (1.2)	1.3 (1.1)
9	-1.5	1.7	0.5 (1.0)	1.1 (0.4)
10	0.3	10.2	4.9 (2.6)	4.9 (2.6)
11	-3.0	8.3	3.7 (2.6)	4.1 (1.9)
12	-3.5	8.8	-0.1 (3.1)	2.6 (1.6)
13	-4.0	6.9	0.7 (3.1)	2.7 (1.7)

7.4.3 Difference between the realised inner & outer curves and the planned osteotomies

Difference between the inner and outer curve, representing the realised osteotomy, and the planned osteotomy. Absolute mean (SD) in millimetres is reported. Numbers were rounded off to one decimal.

Case	Absolute mean (SD)
1	1.6 (1.1)
2	2.7 (4.0)
3	1.8 (1.1)
5	0.8 (0.6)
6	1.1 (0.7)
7	0.6 (0.5)
8	1.4 (1.1)
9	0.9 (0.5)
10	4.1 (2.6)
11	4.1 (2.1)
12	2.4 (1.4)
13	2.5 (1.4)

7.5 Appendix V: Individual patient cases

Individual results for all patients include

- Translation in x, y and z-direction in millimetres from the corrected postoperative PSI position to the planned PSI position
- Length of translation vector in millimetres from the corrected postoperative PSI position to the planned PSI position
- Rotation around the x, y and z-axes in degrees from the corrected postoperative PSI position to the planned PSI position
- Rotation around a specific axis, defined by [v1 v2 v3], in degrees from the corrected postoperative PSI position to the preoperative PSI position

Individual results for patients with preceding resection include

- Difference between the realised outer curves and planned osteotomies
    - mean (SD), absolute mean (SD) and minimum and maximum in millimetres
- Difference between the realised inner curves and planned osteotomies
    - mean (SD), absolute mean (SD) and minimum and maximum in millimetres
- Difference between the realised inner & outer curve and the planned osteotomy
    - Absolute mean (SD) in millimetres

Numbers were rounded off to one decimal.

Visualization

Orientation of the models is visualized on top. This was imported from 3-Matic, causing left and right to be flipped with respect to the patient.

Planned PSI position is visualized in dark blue, whereas corrected postoperative PSI position is visualized in light blue.

Planned osteotomies are visualized in red and realised osteotomies are presented as red curves on the postoperative skull. The surgical guide is visualized in yellow.

Finally, Matlab output for osteotomy analysis presents the osteotomy in grey, the realised outer curves in green and the realised inner curves in blue.

Case 1 | Hemangioma | Zygoma, left | Resection

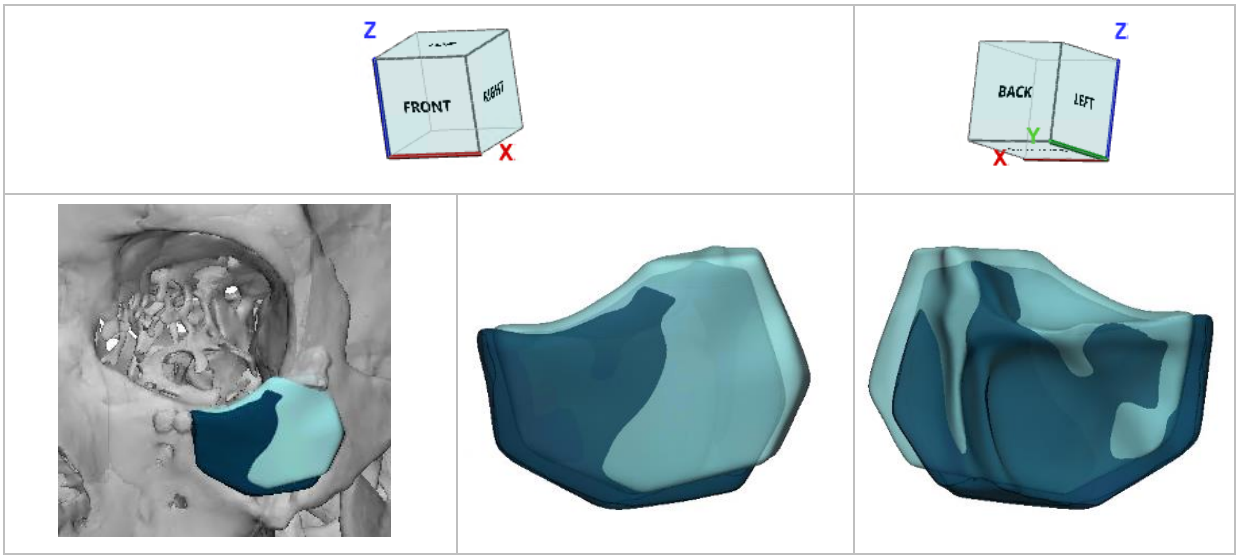

PSI

	Translation [mm]				Rotation [degrees]		
Case	**x**	**y**	**z**	**Vector length**	**x-axis**	**y-axis**	**z-axis**
1	2.0	0.7	1.4	2.5	4.6	8.6	3.5

Rotation around fixed axis [degrees]	Unit vector v representing fixed axis		
	v1	**v2**	**v3**
10.2	0.4	0.9	0.3

Osteotomy

Outer curve				Inner curve				Combined
Mean (SD)	**Absolute mean (SD)**	**Min**	**Max**	**Mean (SD)**	**Absolute mean (SD)**	**Min**	**Max**	**Absolute mean (SD)**
0.5 (1.1)	0.8 (0.9)	-0.9	3.5	-2.2 (1.7)	2.3 (1.5)	-4.9	0.9	1.6 (1.1)

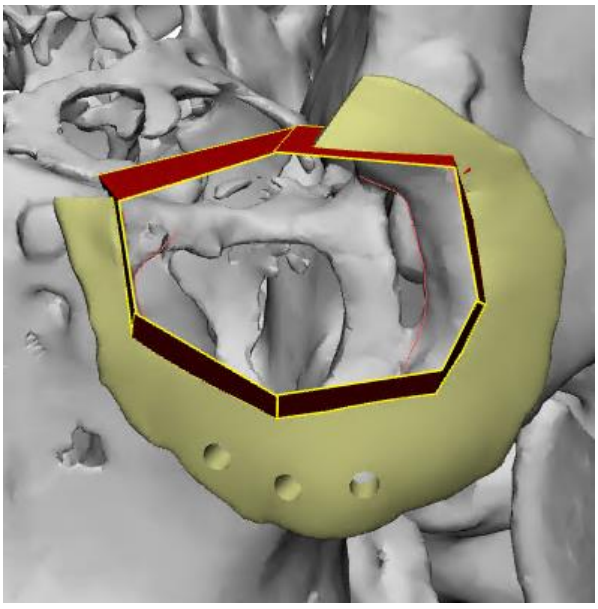

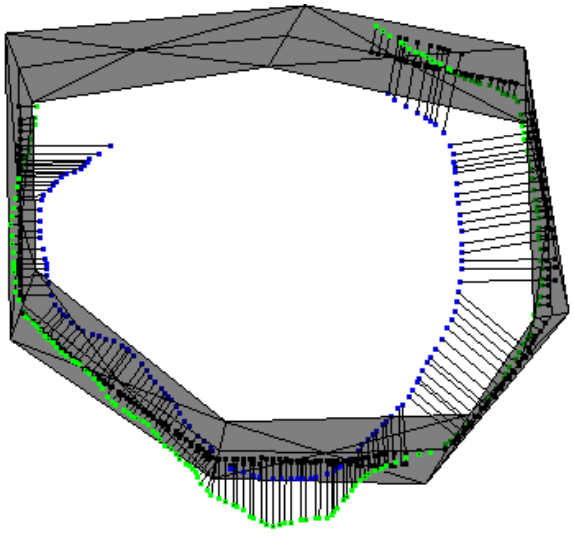

Case 2 | Meningioma | Frontal | Resection

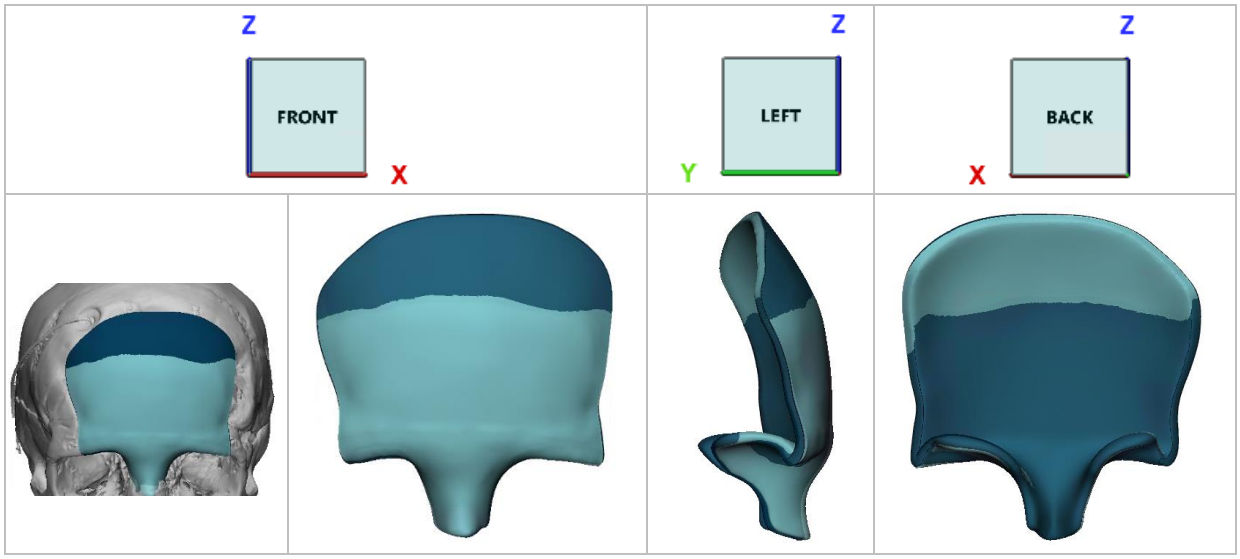

PSI

	Translation [mm]				Rotation [degrees]		
Case	**x**	**y**	**z**	**Vector length**	**x-axis**	**y-axis**	**z-axis**
2	0.0	-0.5	0.0	0.5	1.5	-0.6	0.0

Rotation around fixed axis [degrees]	Unit vector v representing fixed axis		
	v1	**v2**	**v3**
1.6	0.9	-0.4	0.0

Osteotomy

Outer curve				Inner curve				Combined
Mean (SD)	**Absolute mean (SD)**	**Min**	**Max**	**Mean (SD)**	**Absolute mean (SD)**	**Min**	**Max**	**Absolute mean (SD)**
3.4 (4.3)	3.4 (4.3)	0.0	16.8	1.7 (3.8)	2.1 (3.6)	-2.1	14.1	2.7 (4.0)

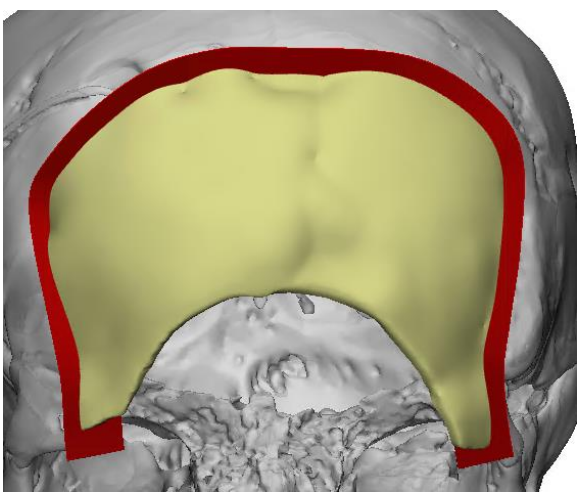

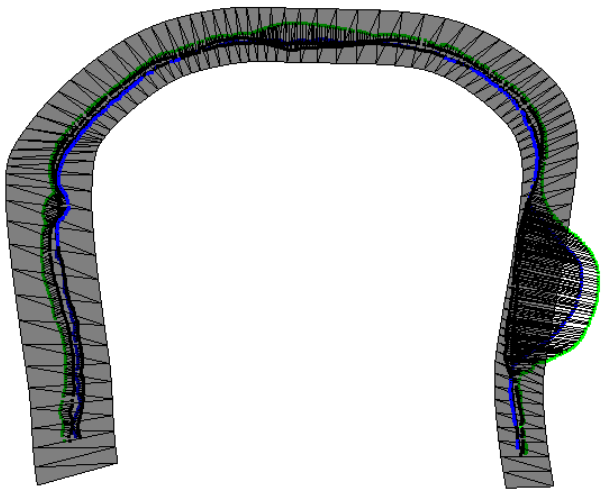

Case 3 | Meningioma | Frontal | Resection

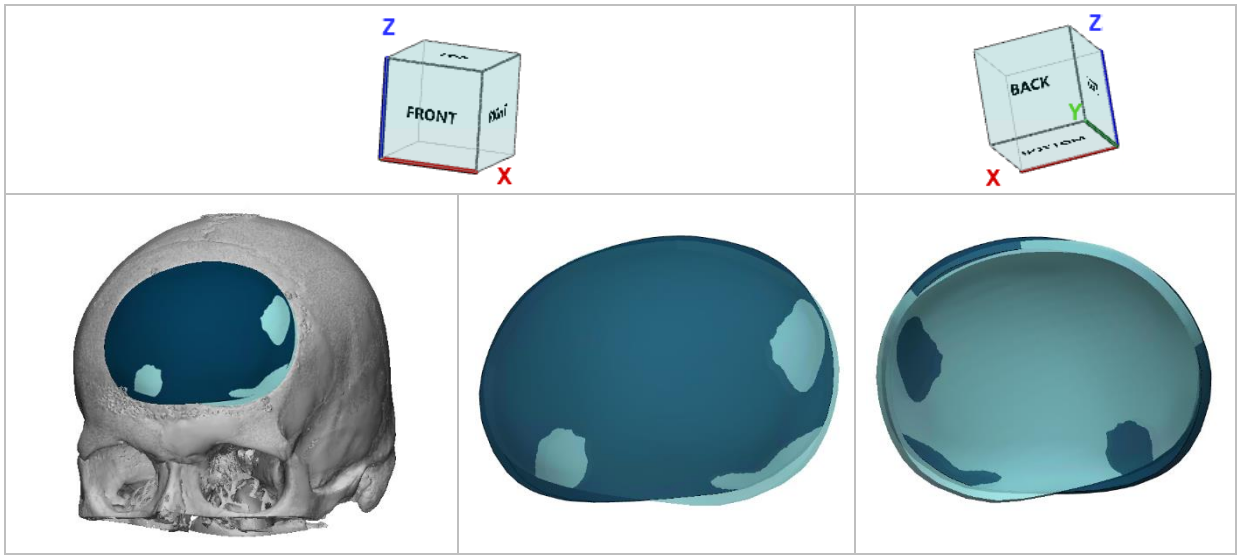

PSI

	Translation [mm]				Rotation [degrees]		
Case	**x**	**y**	**z**	**Vector length**	**x-axis**	**y-axis**	**z-axis**
3	1.1	0.9	-0.1	1.4	2.2	-10.8	7.8

Rotation around fixed axis [degrees]	Unit vector v representing fixed axis		
	v1	**v2**	**v3**
13.6	0.2	-0.8	0.6

Osteotomy

Outer curve				Inner curve				Combined
Mean (SD)	**Absolute mean (SD)**	**Min**	**Max**	**Mean (SD)**	**Absolute mean (SD)**	**Min**	**Max**	**Absolute mean (SD)**
1.2 (2.0)	2.0 (1.1)	-3.4	4.3	0.2 (2.0)	1.7 (1.1)	-4.6	3.0	1.8 (1.1)

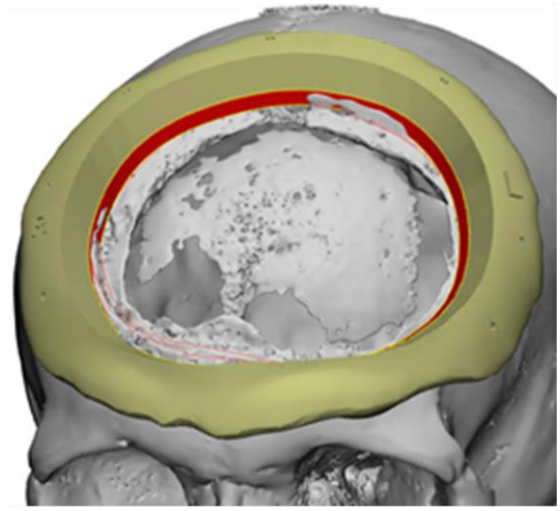

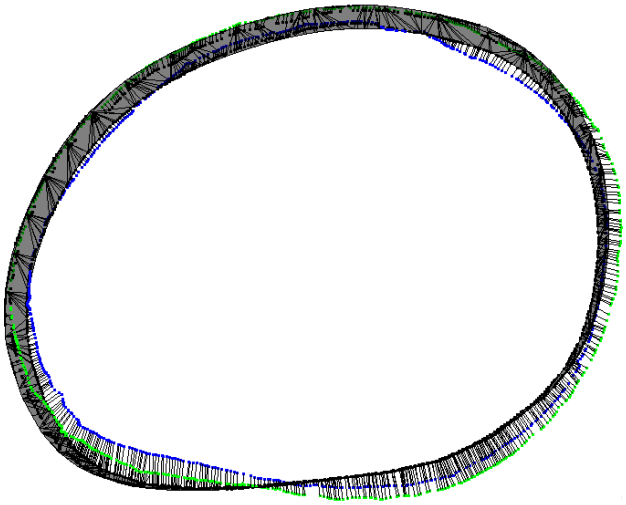

Case 4 | Meningioma | Frontal | Resection, but no osteotomy model available

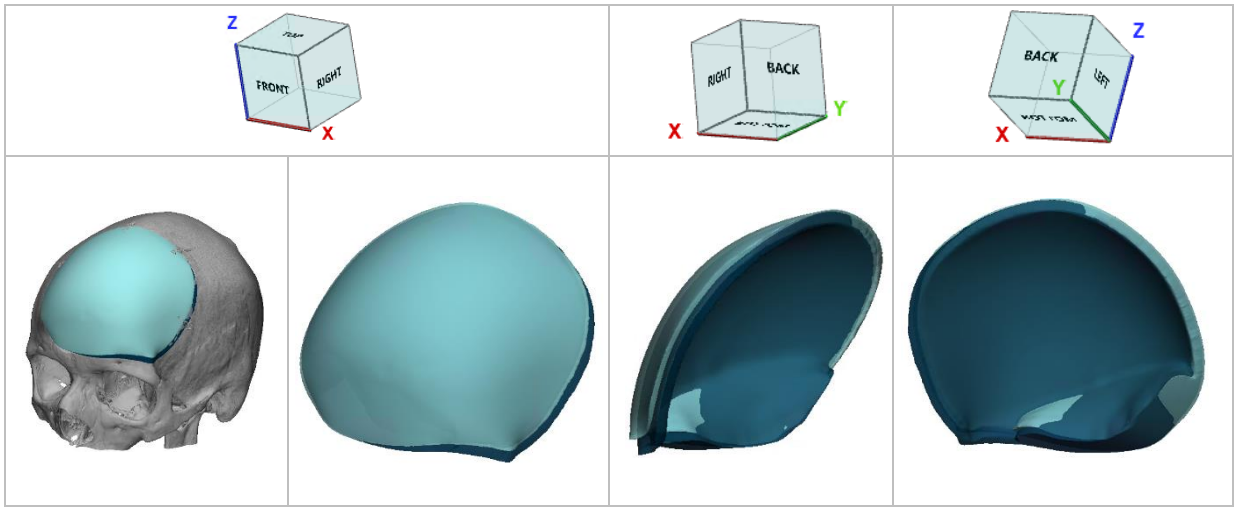

PSI

	Translation [mm]				Rotation [degrees]		
Case	**x**	**y**	**z**	**Vector length**	**x-axis**	**y-axis**	**z-axis**
4	-0.7	-1.1	1.8	2.3	-0.2	4.9	-0.7

Rotation around fixed axis [degrees]	Unit vector v representing fixed axis		
	v1	**v2**	**v3**
4.9	0.0	1.0	-0.1

Case 5 | Squamous cell carcinoma | Maxillary sinus, ethmoid, frontal sinus, right | Resection

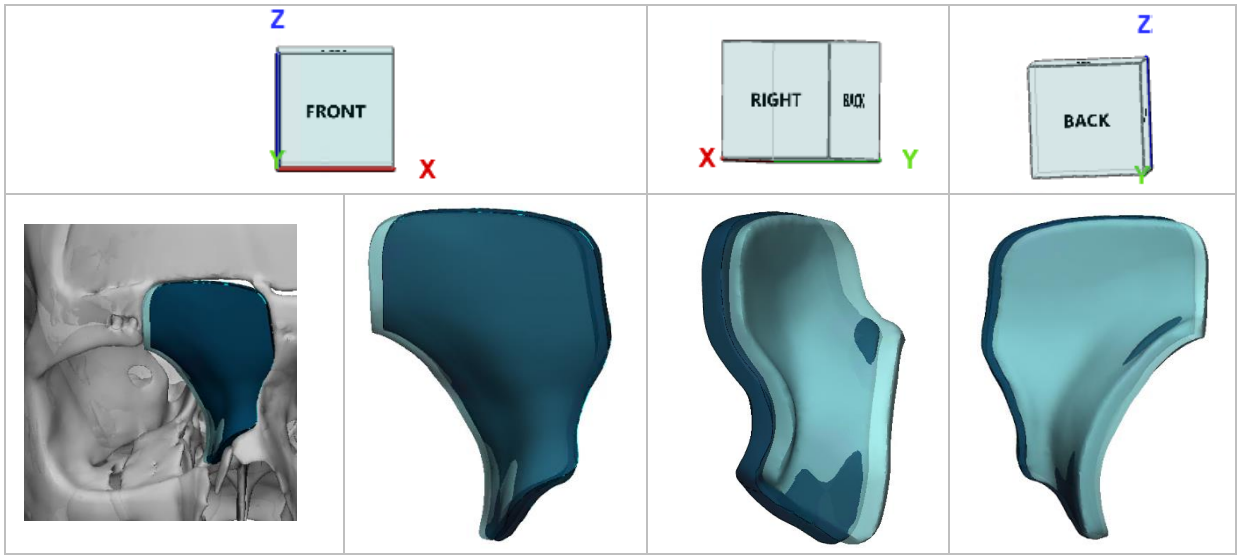

PSI

	Translation [mm]				Rotation [degrees]		
Case	**x**	**y**	**z**	**Vector length**	**x-axis**	**y-axis**	**z-axis**
5	-1.4	2.3	-0.2	2.7	-1.3	1.2	1.3

Rotation around fixed axis [degrees]	Unit vector v representing fixed axis		
	v1	**v2**	**v3**
2.2	-0.6	0.5	0.6

Osteotomy

Outer curve				Inner curve				Combined
Mean (SD)	**Absolute mean (SD)**	**Min**	**Max**	**Mean (SD)**	**Absolute mean (SD)**	**Min**	**Max**	**Absolute mean (SD)**
0.6 (0.8)	0.8 (0.6)	-0.6	2.2	-0.1 (0.9)	0.7 (0.5)	-1.2	2.2	0.8 (0.6)

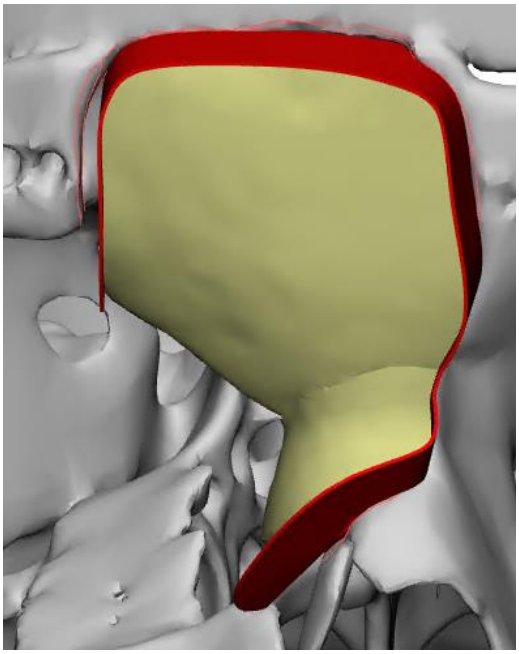

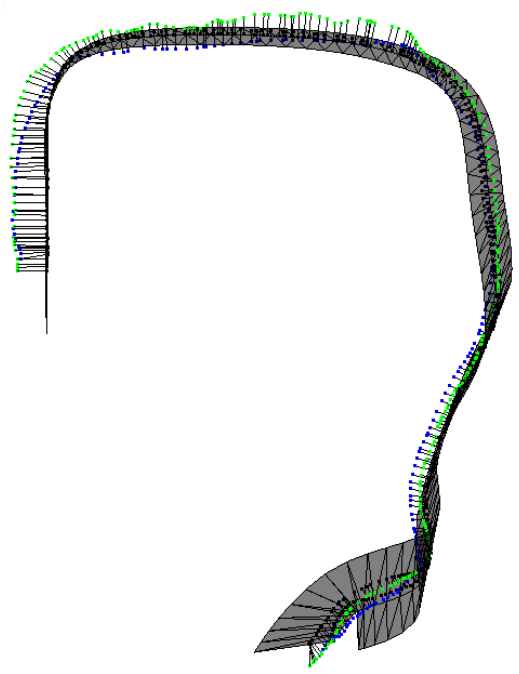

Case 6 | Hemangioma | Lateral wall frontal sinus, right | Resection

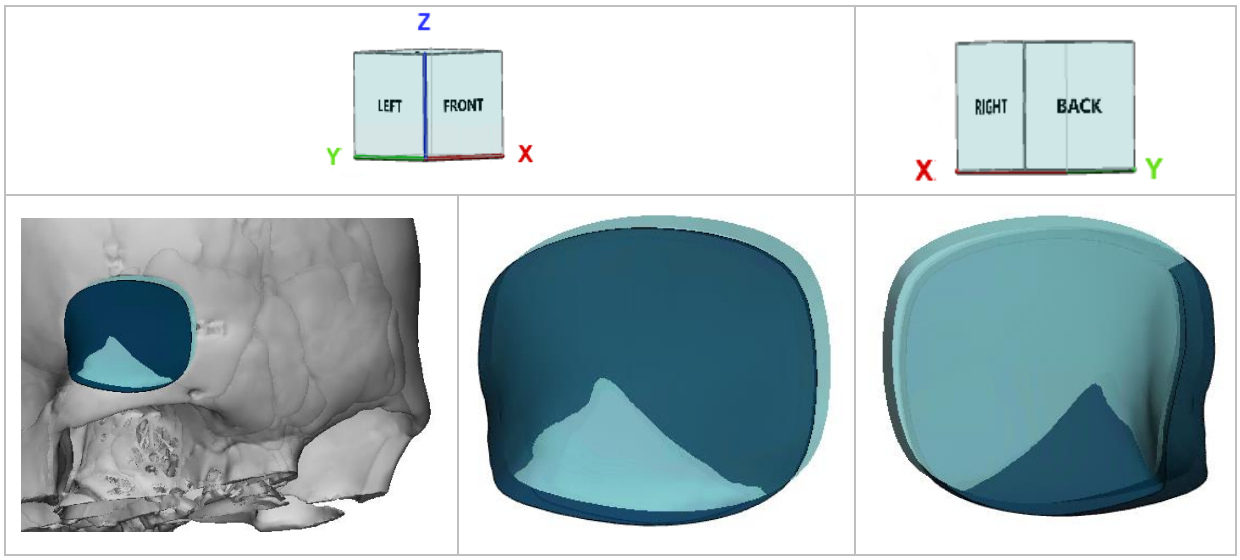

PSI

	Translation [mm]				Rotation [degrees]		
Case	**x**	**y**	**z**	**Vector length**	**x-axis**	**y-axis**	**z-axis**
6	1.1	-0.6	1.0	1.6	0.9	-1.0	-3.2

Rotation around fixed axis [degrees]	Unit vector v representing fixed axis		
	v1	**v2**	**v3**
3.4	0.3	-0.3	-0.9

Osteotomy

Outer curve				Inner curve				Combined
Mean (SD)	**Absolute mean (SD)**	**Min**	**Max**	**Mean (SD)**	**Absolute mean (SD)**	**Min**	**Max**	**Absolute mean (SD)**
0.2 (1.0)	0.9 (0.5)	-1.6	1.6	-0.6 (1.4)	1.3 (0.8)	-3.0	1.4	1.1 (0.7)

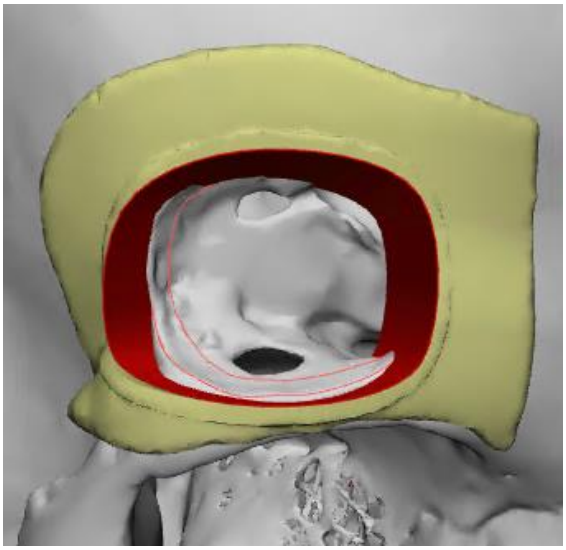

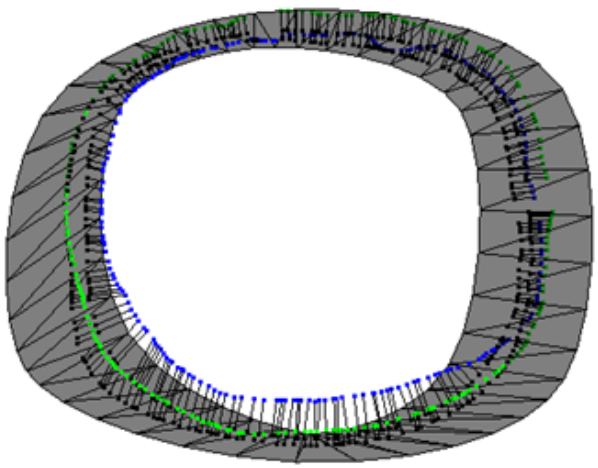

Case 7 | Juvenile psammomatoid ossifying fibroma (JPOF) | Frontal sinus | Resection

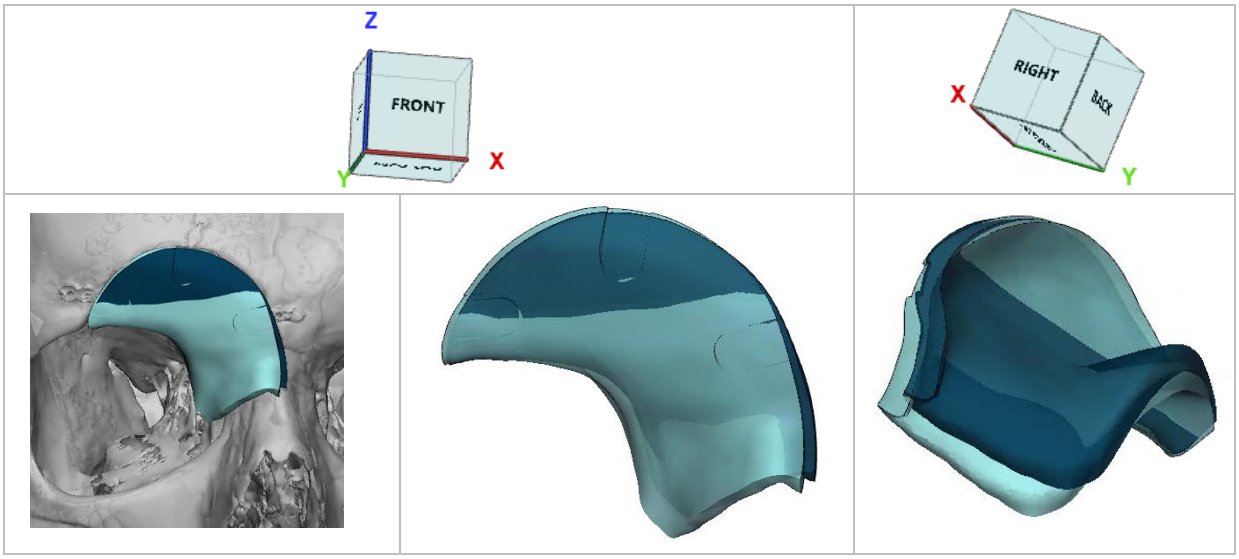

PSI

	Translation [mm]				Rotation [degrees]		
Case	**x**	**y**	**z**	**Vector length**	**x-axis**	**y-axis**	**z-axis**
7	-0.7	-0.8	-0.8	1.3	10.3	-5.1	0.5

Rotation around fixed axis [degrees]	Unit vector v representing fixed axis		
	v1	**v2**	**v3**
11.5	0.9	-0.4	0.1

Osteotomy

Outer curve				Inner curve				Combined
Mean (SD)	**Absolute mean (SD)**	**Min**	**Max**	**Mean (SD)**	**Absolute mean (SD)**	**Min**	**Max**	**Absolute mean (SD)**
0.4 (0.7)	0.7 (0.4)	-2.2	1.8	-0.5 (0.7)	0.6 (0.6)	-2.4	0.4	0.6 (0.5)

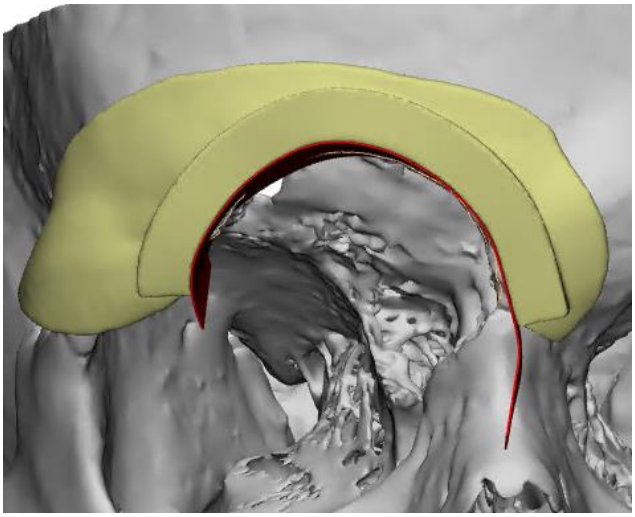

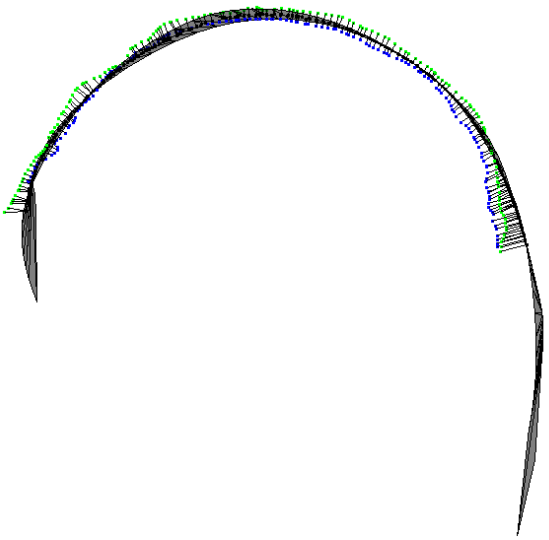

Case 8 | Meningioma | Frontal, left | Resection

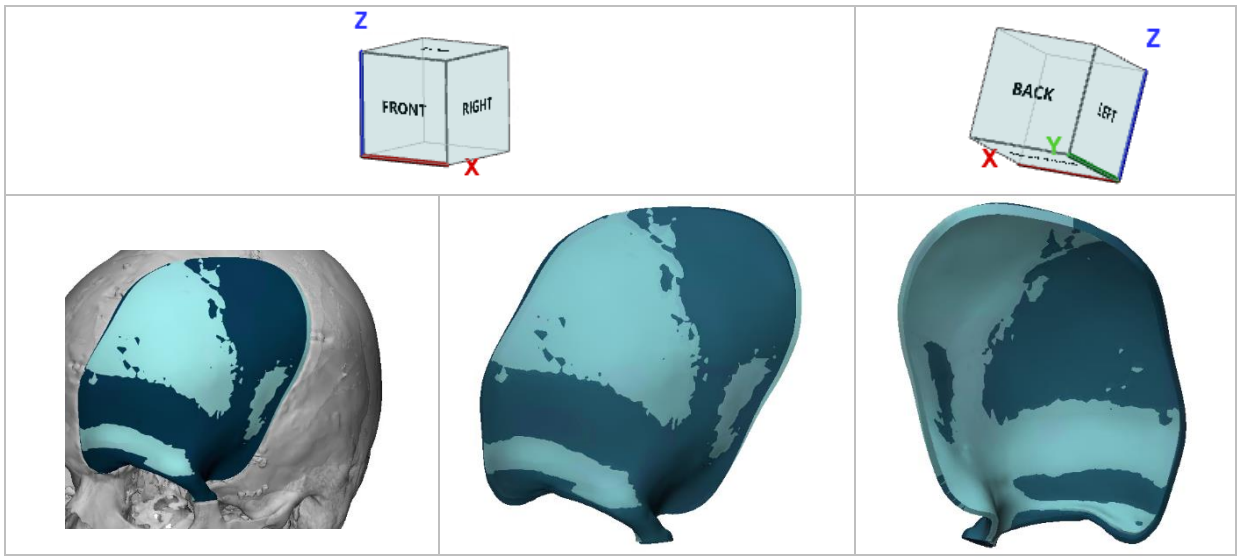

PSI

	Translation [mm]				Rotation [degrees]		
Case	**x**	**y**	**z**	**Vector length**	**x-axis**	**y-axis**	**z-axis**
8	0.2	0.4	0.8	0.9	2.0	-1.7	-0.6

Rotation around fixed axis [degrees]	Unit vector v representing fixed axis		
	v1	**v2**	**v3**
2.7	0.7	-0.6	-0.2

Osteotomy

Outer curve				Inner curve				Combined
Mean (SD)	**Absolute mean (SD)**	**Min**	**Max**	**Mean (SD)**	**Absolute mean (SD)**	**Min**	**Max**	**Absolute mean (SD)**
1.2 (1.2)	1.3 (1.1)	-1.9	3.9	1.0 (1.5)	1.4 (1.2)	-1.9	4.1	1.4 (1.1)

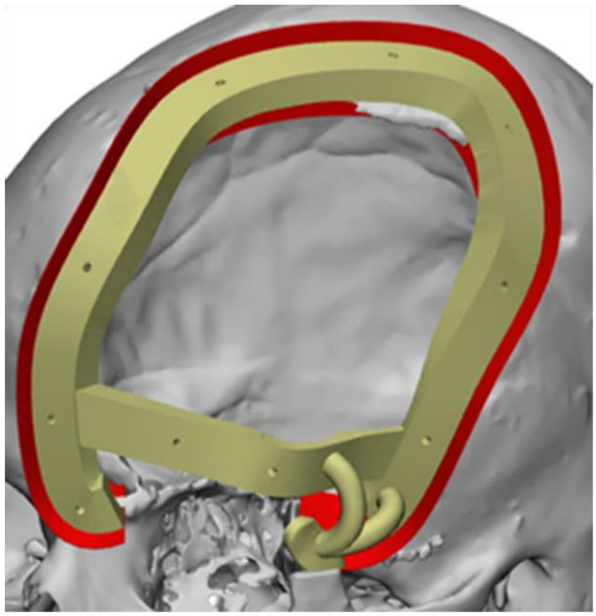

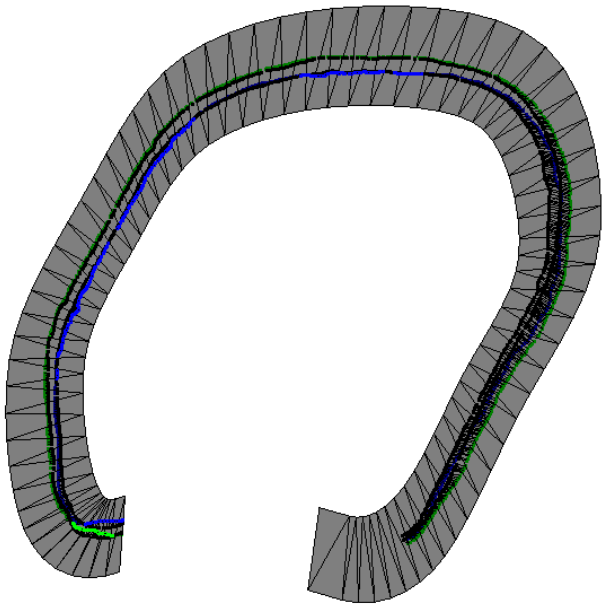

Case 9 | Hemangioma | Orbit wall, right | Resection

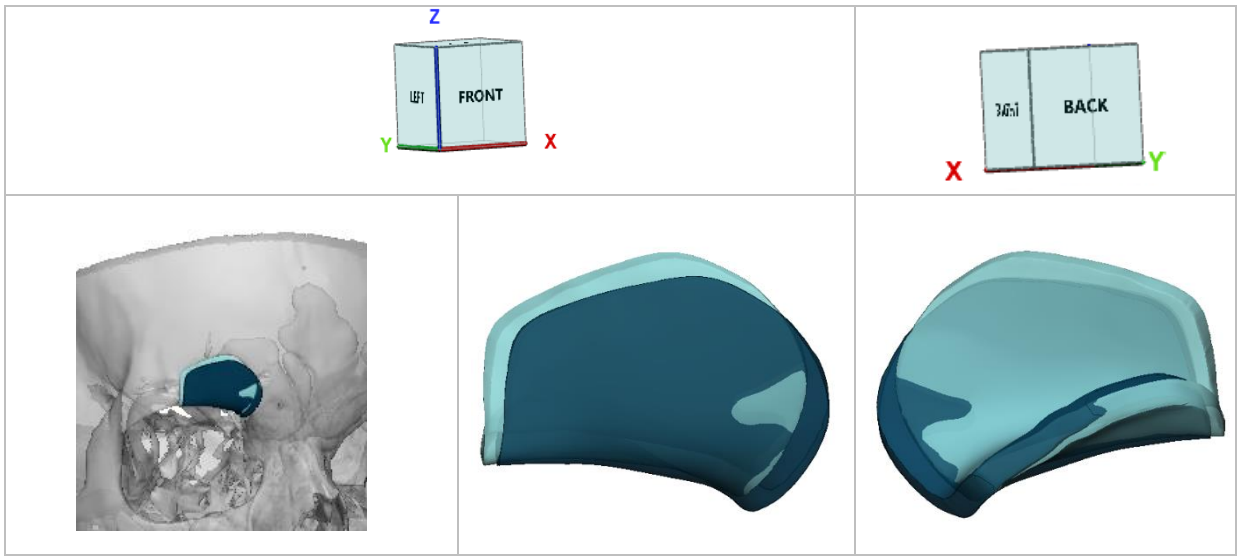

PSI

	Translation [mm]				Rotation [degrees]		
Case	**x**	**y**	**z**	**Vector length**	**x-axis**	**y-axis**	**z-axis**
9	-1.1	0.7	1.0	1.6	10.4	0.3	3.7

Rotation around fixed axis [degrees]	Unit vector v representing fixed axis		
	v1	**v2**	**v3**
11.0	0.9	0.1	0.3

Osteotomy

Outer curve				Inner curve				Combined
Mean (SD)	**Absolute mean (SD)**	**Min**	**Max**	**Mean (SD)**	**Absolute mean (SD)**	**Min**	**Max**	**Absolute mean (SD)**
0.5 (1.0)	1.1 (0.4)	-1.5	1.7	0.2 (0.9)	0.8 (0.4)	-1.8	1.4	0.9 (0.5)

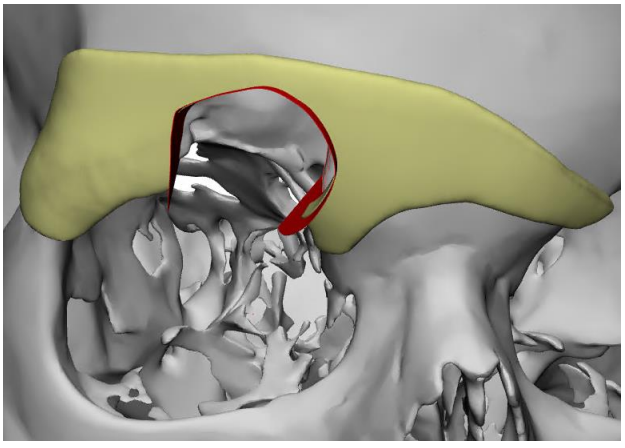

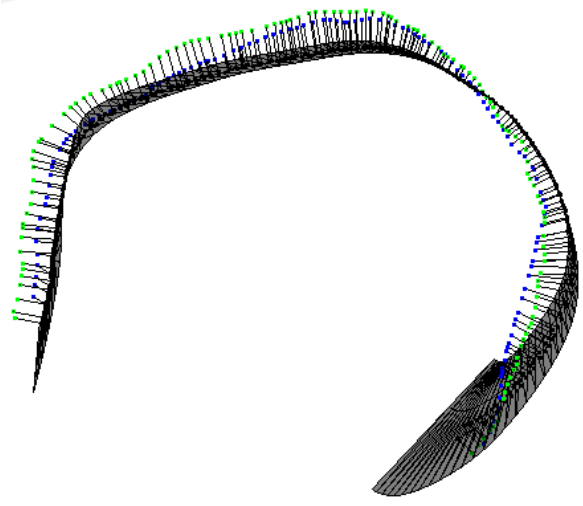

Case 10 | Meningioma | Spheno-orbital, right | Resection

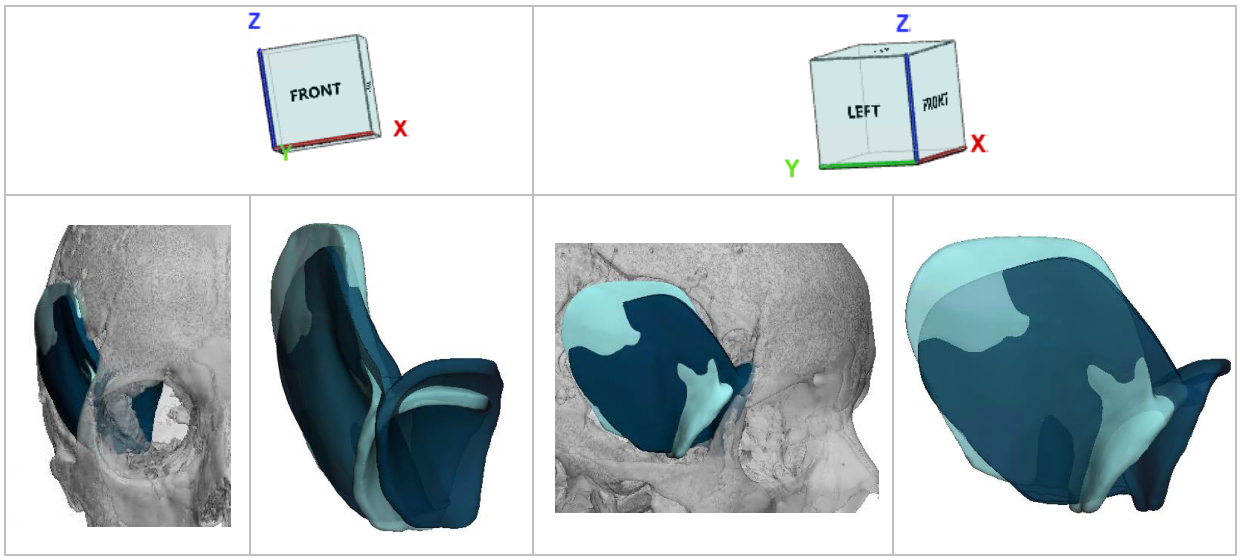

PSI

	Translation [mm]				Rotation [degrees]		
Case	**x**	**y**	**z**	**Vector length**	**x-axis**	**y-axis**	**z-axis**
10	-2.3	5.0	3.8	6.7	-13.6	-10.9	1.2

Rotation around fixed axis [degrees]	Unit vector v representing fixed axis		
	v1	**v2**	**v3**
17.4	-0.8	-0.6	0.0

Osteotomy

Outer curve				Inner curve				Combined
Mean (SD)	**Absolute mean (SD)**	**Min**	**Max**	**Mean (SD)**	**Absolute mean (SD)**	**Min**	**Max**	**Absolute mean (SD)**
4.9 (2.6)	4.9 (2.6)	0.3	10.2	3.2 (2.3)	3.2 (2.2)	-1.3	9.4	4.1 (2.6)

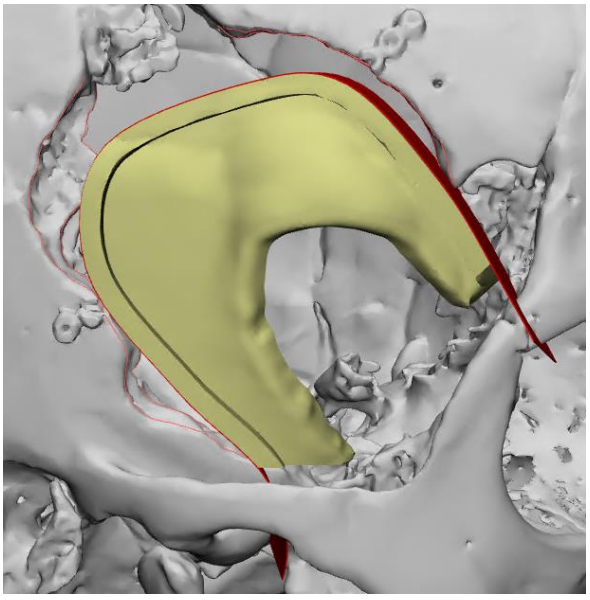

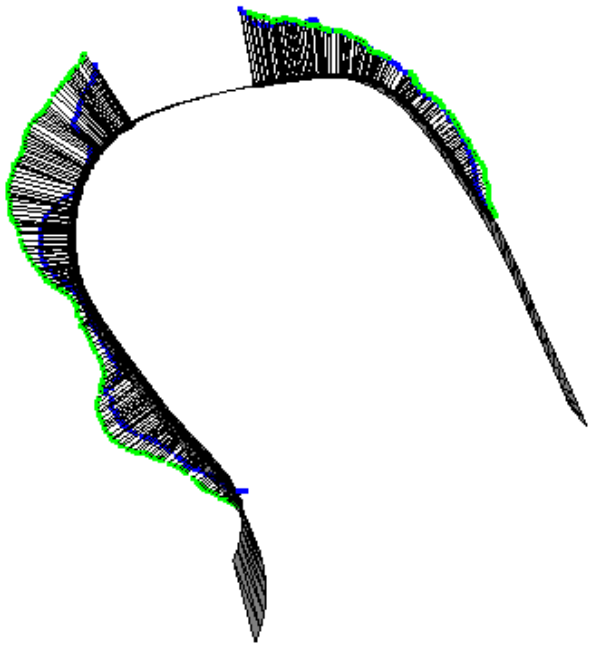

Case 11 | Meningioma | Spheno-orbital, left | Resection

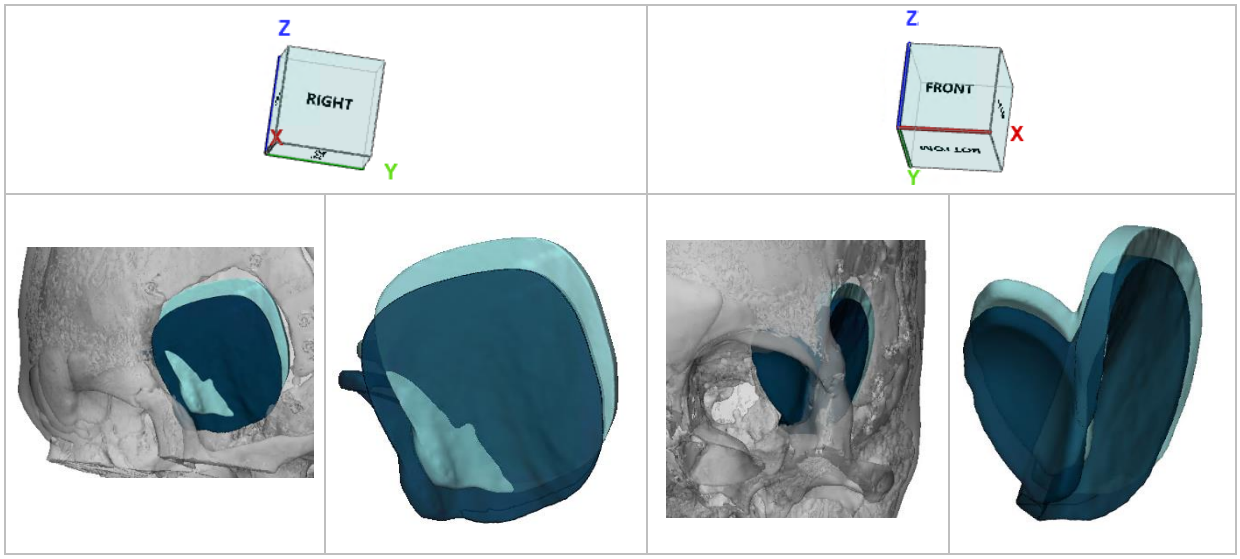

PSI

	Translation [mm]				Rotation [degrees]		
Case	**x**	**y**	**z**	**Vector length**	**x-axis**	**y-axis**	**z-axis**
11	0.6	1.6	5.1	5.4	1.3	1.4	3.4

Rotation around fixed axis [degrees]	Unit vector v representing fixed axis		
	v1	**v2**	**v3**
3.9	0.3	0.4	0.9

Osteotomy

Outer curve				Inner curve				Combined
Mean (SD)	**Absolute mean (SD)**	**Min**	**Max**	**Mean (SD)**	**Absolute mean (SD)**	**Min**	**Max**	**Absolute mean (SD)**
3.7 (2.6)	4.1 (1.9)	-3.0	8.3	4.0 (2.2)	4.0 (2.2)	-0.2	8.4	4.1 (2.1)

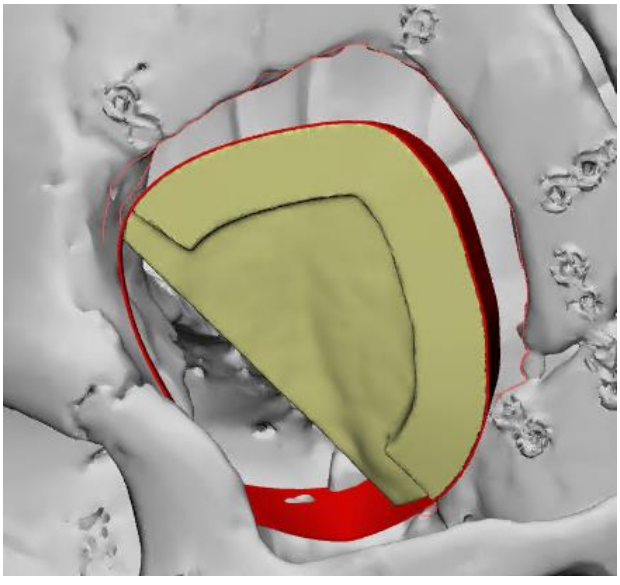

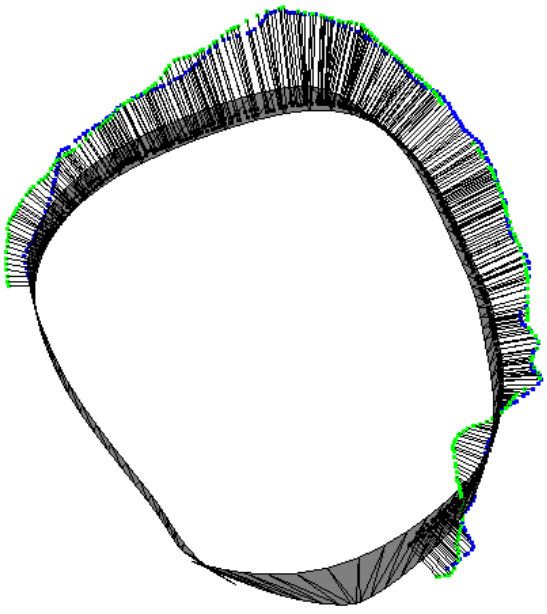

Case 12 | Meningioma | Spheno-orbital, left | Resection

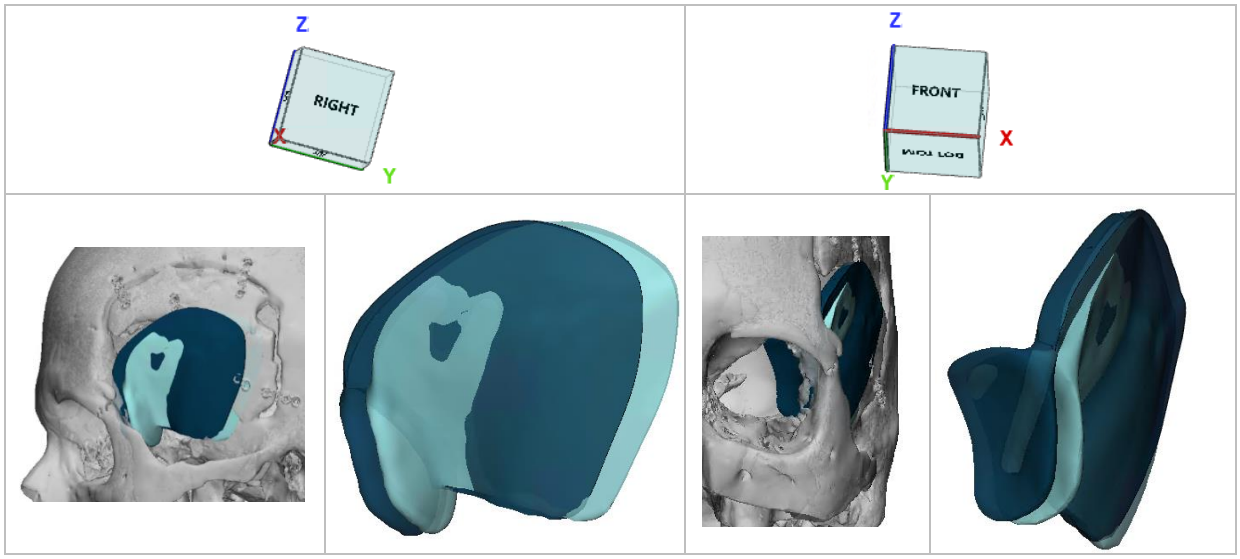

PSI

	Translation [mm]				Rotation [degrees]		
Case	**x**	**y**	**z**	**Vector length**	**x-axis**	**y-axis**	**z-axis**
12	1.4	4.6	1.3	5.0	2.4	3.9	-4.0

Rotation around fixed axis [degrees]	Unit vector v representing fixed axis		
	v1	**v2**	**v3**
6.2	0.4	0.6	-0.7

Osteotomy

Outer curve				Inner curve				Combined
Mean (SD)	**Absolute mean (SD)**	**Min**	**Max**	**Mean (SD)**	**Absolute mean (SD)**	**Min**	**Max**	**Absolute mean (SD)**
-0.1 (3.1)	2.6 (1.6)	-3.5	8.8	-0.5 (2.4)	2.1 (1.2)	-3.5	6.8	2.4 (1.4)

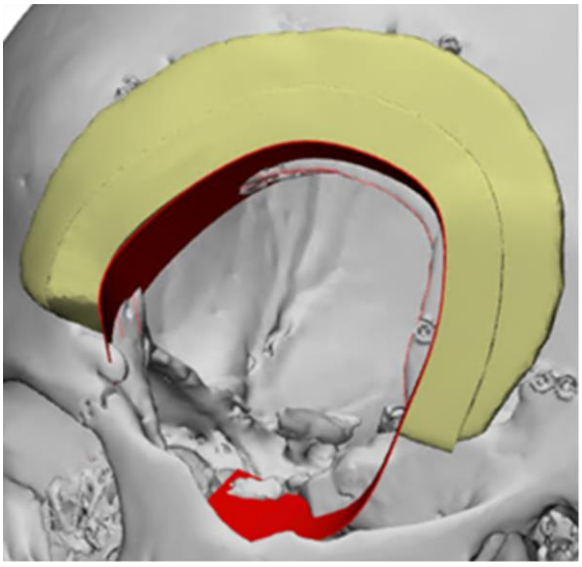

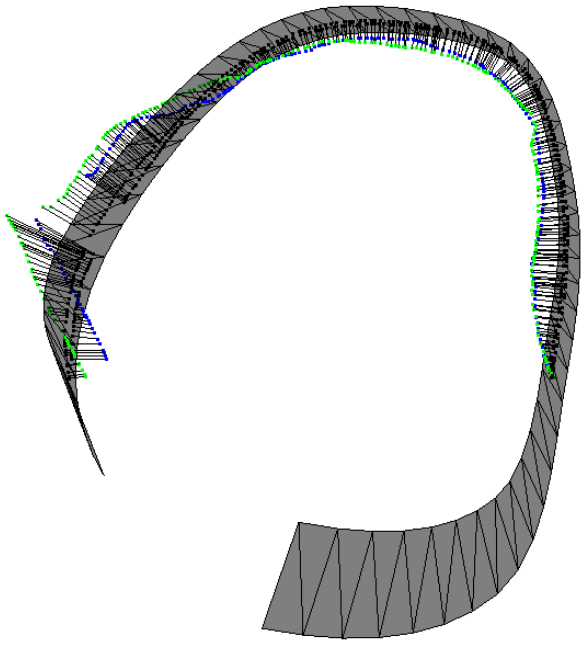

Case 13 | Meningioma | Spheno-orbital, right | Resection

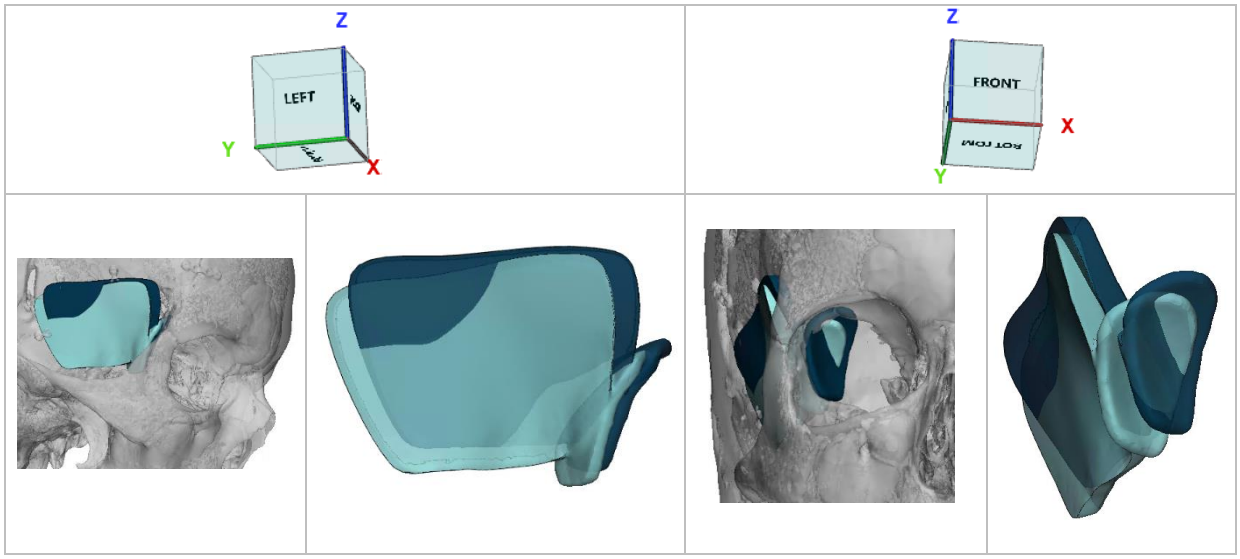

PSI

	Translation [mm]				Rotation [degrees]		
Case	**x**	**y**	**z**	**Vector length**	**x-axis**	**y-axis**	**z-axis**
13	-1.3	2.6	-3.1	4.3	4.6	-9.3	5.0

Rotation around fixed axis [degrees]	Unit vector v representing fixed axis		
	v1	**v2**	**v3**
11.6	0.4	-0.8	0.5

Osteotomy

Outer curve				Inner curve				Combined
Mean (SD)	**Absolute mean (SD)**	**Min**	**Max**	**Mean (SD)**	**Absolute mean (SD)**	**Min**	**Max**	**Absolute mean (SD)**
0.7 (3.1)	2.7 (1.7)	-4.0	6.9	-0.1 (2.6)	2.4 (1.1)	-3.4	4.9	2.5 (1.4)

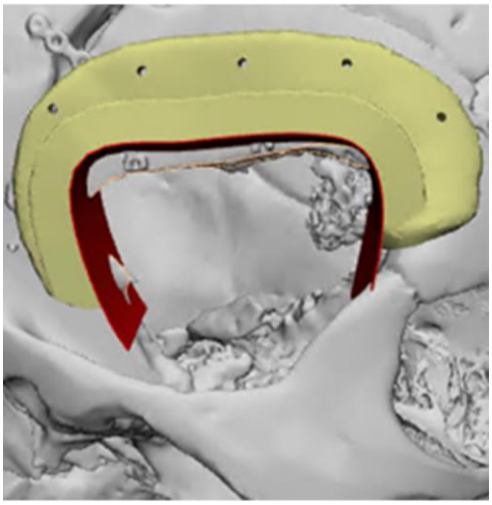

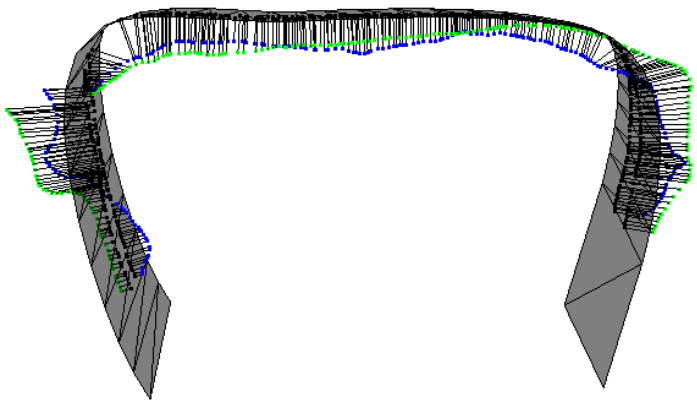

Case 14 | Decompressive craniectomy | Bifrontal | No resection

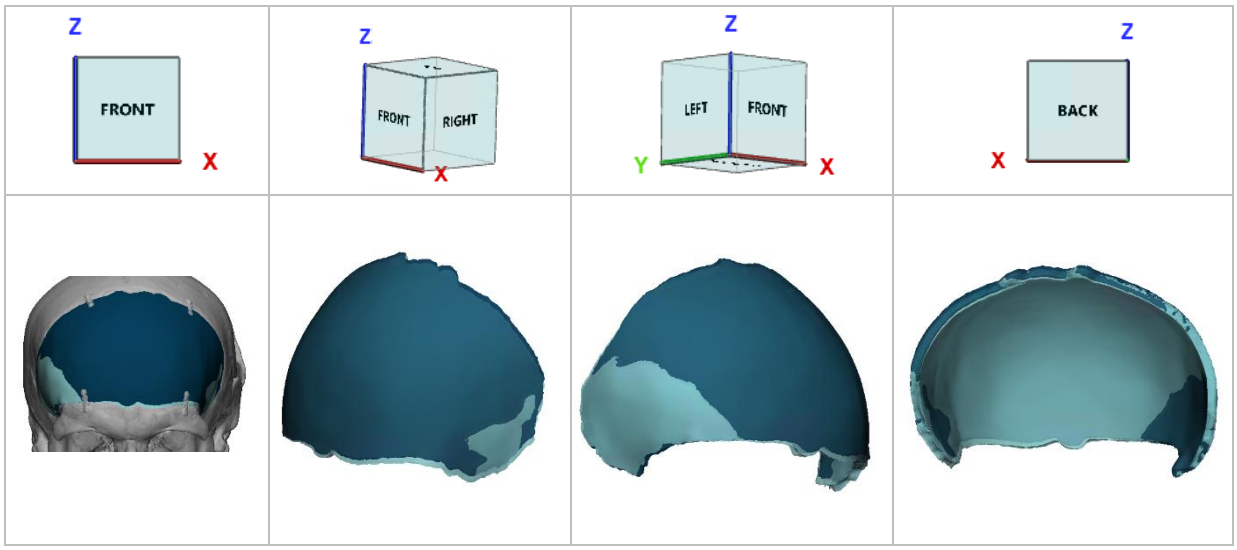

	Translation [mm]				Rotation [degrees]		
Case	x	y	z	Vector length	x-axis	y-axis	z-axis
14	-0.0	0.2	-1.2	1.2	-0.6	-1.8	0.1

Rotation around fixed axis [degrees]	Unit vector v representing fixed axis		
	v1	v2	v3
1.9	-0.3	-1.0	0.1

Case 15 | Bone flap removal due to infection | Cranium, right | No resection

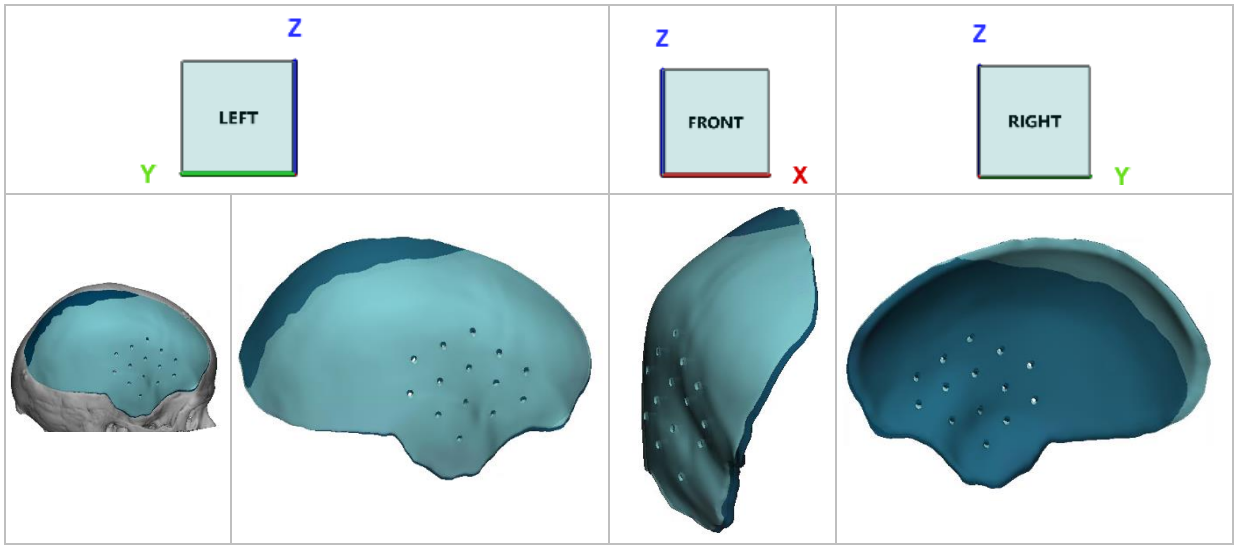

	Translation [mm]				Rotation [degrees]		
Case	x	y	z	Vector length	x-axis	y-axis	z-axis
15	-0.6	0.6	0.7	1.1	1.0	-1.3	0.7

Rotation around fixed axis [degrees]	Unit vector v representing fixed axis		
	v1	v2	v3
1.8	0.6	-0.7	0.4

Case 16 | Craniectomy for cerebral infarction | Cranium, left | No resection

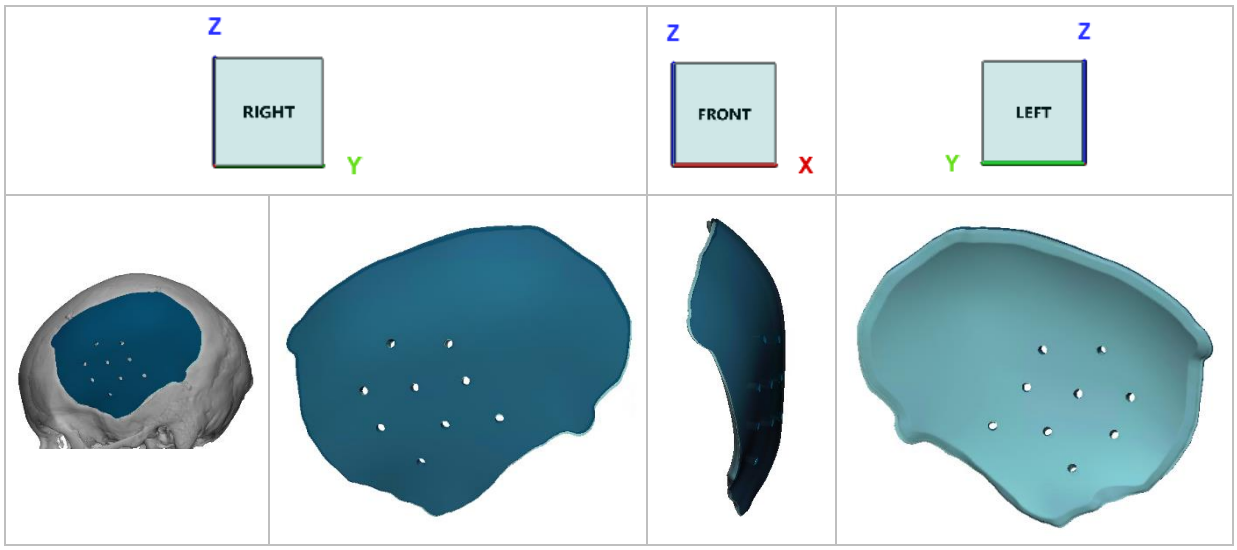

	Translation [mm]				Rotation [degrees]		
Case	x	y	z	Vector length	x-axis	y-axis	z-axis
16	-0.9	0.3	-0.4	1.1	0.8	0.6	0.0

Rotation around fixed axis [degrees]	Unit vector v representing fixed axis		
	v1	v2	v3
0.9	0.8	0.6	0.0

Case 17 | Meningioma | Spheno-orbital, right | No resection

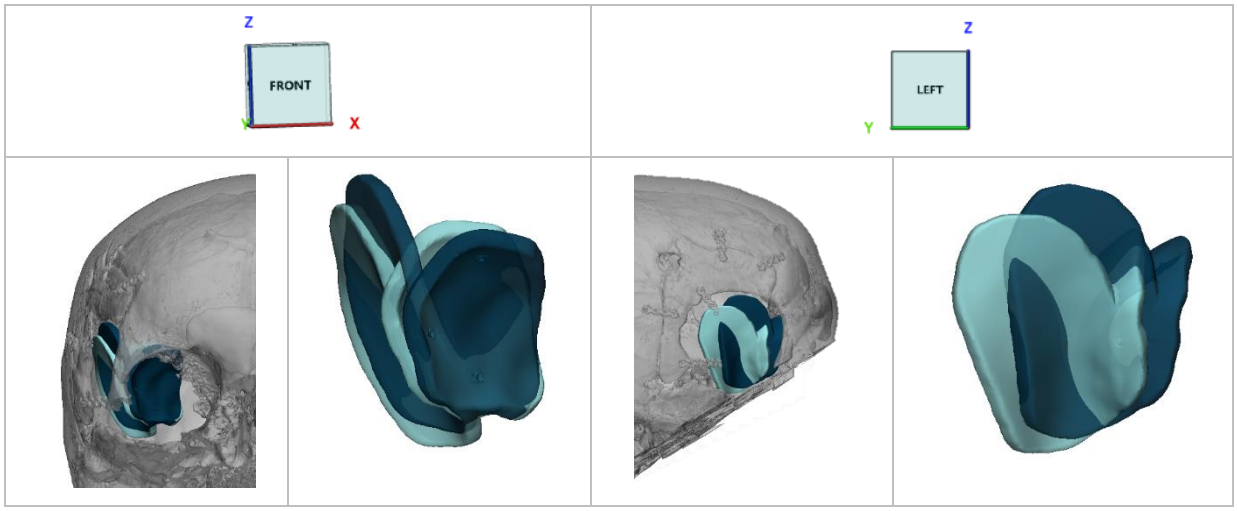

	Translation [mm]				Rotation [degrees]		
Case	x	y	z	Vector length	x-axis	y-axis	z-axis
17	-1.7	5.2	-1.6	5.7	11.8	7.1	8.0

Rotation around fixed axis [degrees]	Unit vector v representing fixed axis		
	v1	v2	v3
15.5	0.7	0.5	0.5

Case 18 | Meningioma | Spheno-orbital, left | No resection

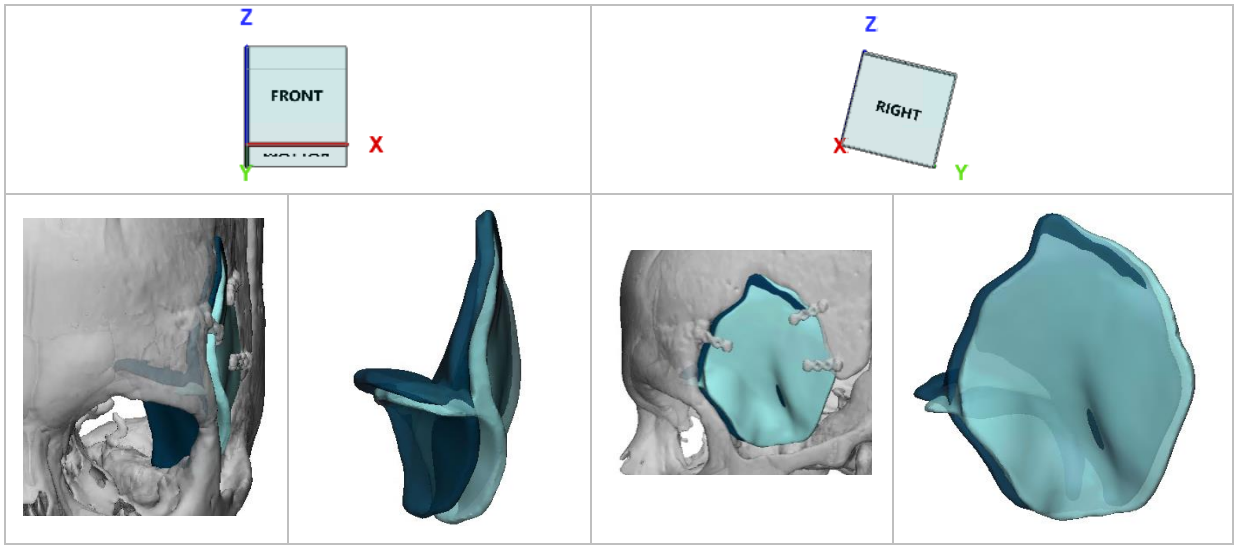

	Translation [mm]				Rotation [degrees]		
Case	x	y	z	Vector length	x-axis	y-axis	z-axis
18	3.4	2.5	-0.2	4.2	-3.1	6.6	-1.7

Rotation around fixed axis [degrees]	Unit vector v representing fixed axis		
	v1	v2	v3
7.4	-0.4	0.9	-0.2

Case 19 | Meningioma | Spheno-orbital, left | No resection

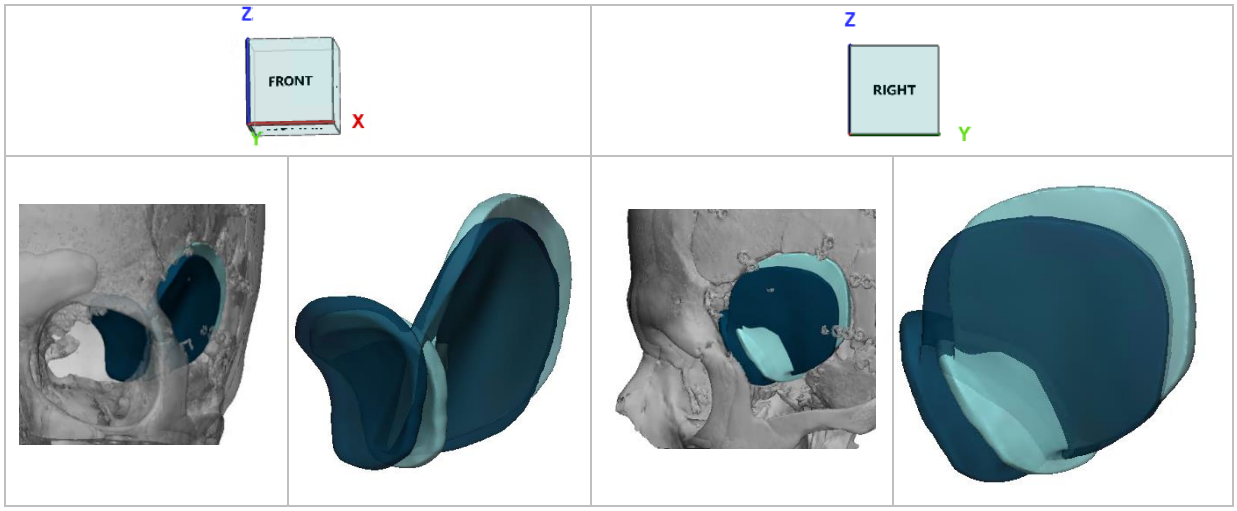

	Translation [mm]				Rotation [degrees]		
Case	x	y	z	Vector length	x-axis	y-axis	z-axis
19	2.1	4.4	2.5	5.4	-6.8	8.6	3.0

Rotation around fixed axis [degrees]	Unit vector v representing fixed axis		
	v1	v2	v3
11.4	-0.6	0.7	0.3